2014-01-01

Geochemical Studies Of Backfill Aggregates, Lake Sediment Cores And The Hueco Bolson Aquifer

Anita Thapalia
University of Texas at El Paso, athapalia@miners.utep.edu

GEOCHEMICAL STUDIES OF BACKFILL AGGREGATES, LAKE SEDIMENT CORES AND THE HUECO BOLSON AQUIFER

ANITA THAPALIA

Department of Geological Sciences

APPROVED:

David M. Borrok, Ph.D., Co-Chair

Diane I. Doser, Ph.D.,Co-Chair

Richard Langford, Ph.D.

Laura F. Serpa, Ph.D.

Soheil Nazarian, Ph.D.

Charles H. Ambler, Ph.D.
Dean of the Graduate School

Dedication

To my
Parents: Bodha Raj Thapalia and Sita Thapalia
and
Mother-in-law, Tara Budhathoki

GEOCHEMICAL STUDIES OF BACKFILL AGGREGATES, LAKE SEDIMENT CORES AND THE HUECO BOLSON AQUIFER

by

ANITA THAPALIA, M.S., M.Sc.

DISSERTATION

Presented to the Faculty of the Graduate School of

The University of Texas at El Paso

in Partial Fulfillment

of the Requirements

for the Degree of

DOCTOR OF PHILOSOPHY

Department of Geological Sciences

THE UNIVERSITY OF TEXAS AT EL PASO

December 2014

Acknowledgements

I wish to express deep gratitude to my advisor Dr David Borrok for untiring support and motivation to pursue PhD at UTEP. Your financial support and personal efforts has made my dream come true. I deeply respect you for all your tremendous efforts in teaching competent scientific writing and encouragement to work hard to achieve this success. I want to thank my advisor Dr Diane Doser for your patience while working with me in the final academic year at UTEP. Your motivating words have provided me strength to work in two industry internships as well as my final project with infant child next to me. My sincere appreciation goes to my committee members Dr Laura Serpa, Dr Soheil Nazarian, and Dr Richard Langford for your great support these years to accomplish this work.

I will be forever grateful to Peter Van Meter for providing U.S. lake sediment cores and age dates as well as USGS student contract grant while working at UTEP. I am thankful to Alfredo Ruiz and Eric bangs of El Paso Water Utilities for well log and water quality data. I wish to thank to Dr Mark Baker for discussions related to fluid flow and Galen Kaip for training the geophysical equipment. I especially thank to Carlos Montana for solving all computer related issues. I also like to thank Victor Avila (Yogi), Sandy Marrufo, and Pawan Budhathoki for your permission to use gravity and well cuttings data in this study.

There are no words to express my gratitude how my husband and dear friend, Pawan Budhathoki have stood by my side during the whole time. His emotional support, love, and understanding have always added enthusiasm even I was working in two projects at the same time. My son, Keidas, is a true blessing as he has added great motivation to finish this dissertation. My parents and brother have brought me in U.S. for higher studies and their encouragement for obtaining a doctorate degree. I share this degree and achievements with my lovely family.

I would like to thank staff of UTEP Geology department, Graduate School, and Office of International Programs for their kind cooperation throughout my program. My sincere thanks goes to Pam Hart and Tina Carrick in Department of Geological Sciences for their timely guidance. I wish to remember all the friends who have made this journey enjoyable with your caring support. Last not the least, I thank Geological Society of America research grant, International Association of Geochemistry

(IAGC) grant, American Association of Petroleum Geologist (AAPG) Foundation grant for supporting my ideas in these projects. In addition, the Southwest Section AAPG, the West Texas Geological Foundation, the Graduate school and the Society of Exploration Geophysicist for providing scholarships and travel grants in various national meetings.

Anita Thapalia

December 2014

Abstract

This dissertation comprises of three different researches that focuses on the application of geochemistry from aggregates, lake sediment cores and Hueco Bolson Aquifer. Each study is independent and presented in the publication format. The first chapter is already published and the second chapter is in revision phase. Overall, three studies measure the large scale (field) as well as bench scale (lab) water-rock interactions influenced by the climatic and anthropogenic factors spans from the field of environmental geology to civil engineering.

The first chapter of this dissertation addresses the chemical evaluation of coarse aggregates from six different quarries in Texas. The goal of this work is to find out the best geochemical methods for assessing the corrosion potential of coarse aggregates prior to their use in mechanically stabilized earth walls. Electrochemical parameters help to define the corrosion potential of aggregates following two different leaching protocols. Testing the coarse and fine aggregates demonstrate the chemical difference due to size-related kinetic leaching effects. Field fines also show different chemistry than the bulk rock indicating the weathering impact on carbonate rocks.

The second chapter investigates zinc (Zn) isotopic signatures from eight lake sediment cores collected both from pristine lakes and those impacted by urban anthropogenic contamination. Zinc from the natural weathering of rocks and anthropogenic atmospheric pollutants are transported to these lakes and the signatures are recorded in the sediments. Isotopic analysis of core samples provides the signature of anthropogenic contamination sources. Dated sediment core and isotopic analysis can identify Zn inputs that are correlated to the landuse and population change of the watersheds. Comparison of isotopic data from both pristine and urban lake sediment core also serves as an analog in other lake sediment cores in the world.

The third chapter studies on Hueco Bolson Aquifer that an important sources of water in the El Paso/Cd. Juraez metroplex. To delineate the boundary between fresh and brackish water from the northern Hueco Bolson Aquifer, we utilize an integrative geochemical, geophysical, and sedimentological approach. The goal of this study is to use geophysical well-log analysis and the water chemical analysis for identifying the changes in the quality of the groundwater. A detailed microgravity survey is utilized to explore the subsurface geological structures that control the conduits and/or barriers

of groundwater flow. A detailed geochemical analysis of aquifer samples provide salinity of groundwater that will complement to the subsurface structures obtained from the geophysical study. This fundamental research in developing methods from an integrated approach to estimate aquifer quality can be used as an analog for similar studies in other arid regions.

Table of Contents

List of Tables

List of Figures

SECTION 1

Assessment Of Corrosion Potential Of Coarse Backfill Aggregates For Mechanically Stabilized Earth Walls

(Paper in a journal)
Transportation Research Record: Journal of the Transportation Research Board, No. 2253, Transportation Research Board of the National Academies, Washington, D.C., 2011, pp. 63–72.
DOI: 10.3141/2253-07
A. Thapalia[1], D.M. Borrok[1], S. Nazarian[2] and J. Garibay[2]
[1]Department of Geological Sciences, University of Texas at El Paso, El Paso, TX 79968-0555
[2]Center for Transportation Infrastructure Systems, University of Texas at El Paso, El Paso, TX 79968-0555

1.1 Abstract

The service life of mechanically stabilized earth walls depends on the rate of corrosion of the metallic reinforcements used in their construction. Assessment of corrosion potential requires the accurate evaluation of pH, resistivity, and sulfate and chloride concentrations of aqueous solutions in contact with the surrounding aggregate. There is a tendency among highway agencies to utilize larger-size aggregates that contain only a small amount of fine material (passing No. 40 sieve) in the backfill. Evaluation of the electrochemical parameters of coarse aggregates is challenging because traditional methods utilize only fine material. We tested the effectiveness of traditional soil characterization techniques for use with coarse aggregates by performing leaching experiments with coarse limestone and dolomite aggregates from six quarries in Texas. Chemical differences were isolated from size-related kinetic leaching effects by comparing results from the same-sized material collected in the field versus material derived from the crushing of larger (≥ 3/8") aggregates in the laboratory. Testing demonstrated that the fines collected from the field were enriched in chemicals that when exposed to water decreased pH and resistivity and increased sulfate concentrations relative to the bulk rock. This is likely the result of sulfur compounds in the atmosphere reacting with carbonate rocks to produce reactive surface layers that are mechanically abraded into fines. This phenomenon can bias traditional soil

testing results and therefore the assessment of corrosion potential. We demonstrate that a more accurate assessment of the electrochemical parameters can be obtained by crushing the coarse material to meet testing size specifications.

1.2 Introduction

Mechanically Stabilized Earth (MSE) walls consist of layers of compacted aggregate backfill reinforced mostly by galvanized steel strips or meshes. The service life of MSE walls depends largely on the corrosion rate of the metallic reinforcements. Accelerated corrosion of the metallic reinforcements can cause sudden and catastrophic failures of MSE structures (*1*). Corrosion rates for metallic reinforcements are directly linked to the electrochemical properties of the compacted aggregate. Hence, it is crucial to effectively evaluate the corrosive potential of the aggregate prior to construction.

Most state Departments of Transportation (DOTs) specify acceptable ranges for the electrochemical characteristics of backfill aggregates as a surrogate for potential corrosivity of backfill. These parameters and their acceptable ranges, which are generally adapted or modified from those provided by the **American Association of State Highway and Transportation Officials (**AASHTO) or the American Society for Testing and Materials (ASTM), include pH, resistivity, chloride (Cl) concentration, sulfate (SO_4) concentration and total organic content. Many of these methods specify the use of materials that are finer than either No. 10 (2mm) or No. 40 (425µm) sieve. This size limitation poses a significant problem when coarse backfills like the Texas Department of Transportation (TxDOT) Type A (50-100% retained on 1/2" sieve and 85-100% retained on No 40 sieve) or Type D (85-100% retained on 3/8" sieve) are used for MSE construction. In many cases these coarse backfills contain only a few percent finer than No. 10 sieve materials. Hence, these tests focus on only a small subset of the aggregates in the backfill, with the assumption that the fines are chemically representative of the bulk rock. This assumption has not been adequately tested and it remains unclear whether fine-grained-based testing methods are adequate for predominantly coarse aggregate backfills. Because the chemical

test results directly impact whether an aggregate is accepted or rejected for MSE construction, the financial consequences of improper characterization of aggregates may be serious. The unnecessary rejection of a backfill as the result of ineffective or biased testing methodologies may result in significant financial losses. Conversely, erroneously accepting a backfill that has a high potential for causing corrosion can reduce the service life of MSE walls and possibly result in catastrophic failure. In this investigation leaching experiments were used to directly test whether traditional fine-grained testing methodologies designed to assess corrosive potential are adequate for coarse aggregates.

1.3 Methodology

1.3.1 Collection, Classification And Preparation Of Backfills

TxDOT provides four different acceptable gradations (Type A through Type D) for the backfill of MSE walls under its Item (ftp://ftp.dot.state.tx.us/pub/txdot-info/des/specs/specbook.pdf) (*2*). The so-called rock backfills (i.e. Types A and D), which are being used more frequently, contain more than 85% retained on No. 4 sieve. A survey of 25 TxDOT districts revealed that 44% of MSE walls are backfilled with Type A (30%) or D (14%) with the main constituents of more than 73% of the backfill materials being limestone. The concern of TxDOT is whether the traditional electrochemical tests are applicable to these freely-drainable coarse backfills. To address this concern, Type A or D backfills from six different representative quarries throughout Texas were collected. All six materials were sampled from the stockpiles being actively used in construction of MSE walls.

As reflected in Table 1.1, five of the backfills were limestone and one dolomite. The gradation curves for the six backfills along with the specification limits for the Types A and D are presented in Figure 1, and summarized in Table 1.1. Quarries A, C, D, and F meet "Type D" gradation specifications and quarries B and E are "Type A" backfills. The distribution of the backfills represents the practical uses of the materials statewide well. The plasticity index (PI) of each backfill is shown in Table 1.1. Material from quarries B, C, and D were determined to be

non-plastic while material from quarries A, E, and F all had a PI of about 4. TxDOT specification does not specify a minimum regarding PI, but it does specify a maximum of 30.

Three alternative means of assessing the hardness of the aggregates are also presented in Table 1.1, the wet ball mill, aggregate crushing value (ACV, British Standard 812) and aggregate impact value (AIV, British Standard 812) tests. The most crush susceptible materials are from quarries A, E, and F.

Finally, the optimum moisture content (OMC) and the maximum dry density (MDD) for each material obtained are shown in Table 1.1. It was impossible to develop moisture-density curves for the backfill materials from quarries D, B, and C. These materials would not absorb any water and the compacted specimens would crumble as soon as they were extracted. Material from quarries A, E, and F exhibited the highest crushing potential and yielded reasonable moisture-density curves because the coarse aggregates severely crushed to finer materials during compaction. In practical terms, even though the materials from these districts specified and delivered as a Type A or D backfill, they look and behave like a finer backfill material after compaction.

The geochemical characterization using the standard TxDOT methodologies is summarized in Table 1.2. Although the TxDOT methods can be linked to their AASHTO counterparts (also listed in Table 1.2), some modifications do exist and are discussed in the appropriate sections below. According to TxDOT's specifications, most of the materials would not have passed the chloride or sulfate concentration criteria and the samples from quarries A, C, E, and F also fail the resistivity criterion. The pH for all samples was within the 5.5-10 window for acceptability.

1.3.2 LEACHING TESTS

In order to characterize more representative specimens of the backfills, we chose to employ the U.S. Geological Survey's Field Leach Test (USGS FLT). The FLT has been shown to be effective for evaluating the geochemical properties of leachate from a variety of soils and

rocks and FLT results are comparable to those obtained using the Environmental Protection Agency's synthetic precipitation leaching procedure (USEPA 1312 SPLP) (*3*) and the European "shake test" recently standardized by the Comité Européen de Nomialisation (EN-12457-3) (*4*). The advantages of the USGS FLT are that it is rapid, inexpensive, has no aggregate size restrictions, and produces enough leachate for any number of additional analytical tests. Briefly, the FLT method utilizes a 50 g sample of soil or rock that is added to 1000 mL of distilled water in a 1L plastic bottle. The solution is shaken vigorously for 5 minutes, and after settling for 30 minutes, the pH and resistivity of the fluid are measured in-situ and filtered (0.45μm) samples are collected for laboratory analysis (*3*). We slightly modified the FLT method by increasing the mass of the rock to 100 g and by continuing the duration of some tests for days or weeks with intermittent sampling. The increase in sample mass from 50 to 100 g was necessary to accommodate the largest pieces of rock without additional crushing. This solid-to-liquid ratio (100 g to 1L) is identical to that used for the European "shake test" (EN-12457-3) and the TxDOT Tex-620-J method for measuring Cl and SO_4 concentrations, respectively. An ExTech™ EC 500 instrument was used to measure the pH and resistivity of FLT samples and Cl and SO_4 analyses were performed using a Metrohm™ ion chromatograph.

To evaluate the impact of the aggregate size on the results, the sieved backfill materials were divided into six bins shown in Table 3.

To obtain most of the geochemical results under current specifications, an exorbitant amount of backfill has to be sieved to obtain adequate quantities of required materials. In most applications, this process may be impractical. To evaluate a more practical approach, the aggregates retained on 3/8" sieve from each quarry were crushed in the laboratory using a Massco™ crusher and sieved to obtain adequate materials for the same six size bins as for the field samples. These samples will be referred to as "lab-crushed samples," while the samples collected and sieved directly from the quarries will be referred to as "field samples." Because the lab-crushed samples were directly obtained from mechanical crushing of large pieces of rock, they are considered more homogeneous in composition and representative of the true chemistry

of the aggregate. On the other hand, the field samples are subject to natural weathering and degradation processes and the different size fractions may not be chemically homogeneous. The purpose of preparing two sample sets of the same sized materials, one collected from the field and the other collected from crushing of larger rock, was to isolate the chemical differences by eliminating size-related kinetic leaching affects. Chemicals typically leach into solution more rapidly from smaller-sized aggregates because surface to volume ratios increase with decreasing size.

1.4 Results and Discussion

1.4.1 pH

Figure 2 presents pH measurements for different size fractions of the field and lab-crushed samples obtained using the FLT method. The pH of the leachate ranged from 8.5 to 10.1, which is typical of carbonate rock; however, there was significant variation in pH among different sized materials and between lab-crushed and field samples. Size-dependent variation in pH is probably attributable to kinetic leaching affects, whereas the differences between the lab-crushed and field samples when compared at the same sieve size are primarily attributable to chemical differences. The aggregates sieved from the field samples exhibit a lower pH than the lab-crushed aggregates by as much as 0.8 log units and the magnitude of this difference is generally greatest for the smallest size fractions (finer than No. 40 sieve).

Figure 3 presents pH measurements for different size fractions of Quarry A collected as a function of leaching time during FLT experiments. Again, the pH of the samples sieved in the field is lower than that for the lab-crushed samples of the same size fraction. The magnitude of the pH difference is greatest for the smaller size fractions and becomes insignificant for the larger size fractions (4 and 3/8”). Although pH generally decreases toward an equilibrium value for the carbonate rock system of around 8.3 as a function of time, the magnitude of the pH difference between field and lab-crushed samples persists over the more than 200 hr duration of

the experiments (Figure 3). This further supports the interpretation that the lab-crushed and field samples are chemically different, particularly for the finer than No. 40 sieve fractions.

The pH for each quarry was additionally evaluated using method Tex-128-E, which calls for leaching of the soil at 45º to 60ºC. This is a modification from the corresponding AASHTO T-289 and ASTM G-51 methods (and the FLT method employed here) where pH is determined from leaching of soil at room temperature. The Tex-128-E results, shown as dashed lines in Figure 2, range from pH of about 8 to 9, but are consistently lower than those measured using the FLT method. The reason for this discrepancy is that the higher temperature employed in the TxDOT method accelerates leaching, moving the system toward equilibrium more rapidly. The FLT pH measurements begin to converge with the TxDOT values if the leaching time is increased to 48 hours. However, a possible pitfall when utilizing the TxDOT method is that the activity of hydrogen (and thus pH) changes with temperature. The pH measured at 60ºC is about 0.4 log units less than the pH at 25ºC. This fact requires a correction of the pH measured at higher temperature to avoid an underestimation of the pH of likely field conditions.

1.4.2 RESISTIVITY

Figure 4 presents the resistivity values recorded in the FLT solutions for the six different bins for each of the backfills. Resistivity is a reflection of the total ion concentration of the solution and more resistive samples correspond to lower ion concentrations. Variations in resistivity among the lab-crushed size fractions for aggregates from an individual quarry are reflective of differences in leaching rates attributable to size. The smallest lab-crushed fractions are less resistive than the larger lab-crushed fractions because more ions had leached into solution by the time the samples were measured. With only one exception (Quarry B), the finer than Bin 40 field samples are less resistive than the corresponding lab-crushed samples. Hence, the finer than Bin 40 field fractions are characterized by a greater quantity of rapidly-leachable material than the corresponding lab-crushed fractions. The resistivity values measured using the FLT method are not comparable to those measured using traditional soil-box methods (e.g.,

AASHTO T-288; ASTM G-187; Tex-129-E), because the liquid to volume ratios and the spacing and geometries of the electrodes are method-specific parameters.

1.4.3 SULFATE AND CHLORINE CONTENT

Figures 5 and 6 respectively represent the results of SO_4 and Cl analyses of FLT leachates from different bins. The SO_4 concentrations of the fine field samples were always greater than those for the corresponding lab-crushed samples. In some cases leachate from the field samples contained more than three times as much SO_4 as the lab-crushed samples. The SO_4 concentrations of the larger size fractions (coarser than Bin 40) of the field material more closely matched those of the lab-crushed material (Figure 5). This demonstrates that SO_4 was enriched in the finer field samples relative to SO_4 in the bulk rock. In general, the Cl contents of the field and lab-crushed samples were similar with the exceptions of quarries E and F (Figure 6). This demonstrates that in limited cases Cl was enriched in the finer field samples in excess of Cl in the bulk rock. Many of the finer field samples were additionally enriched in nitrate relative to the bulk rock (data not shown).

For quarries A, B, and C, there was virtually no difference among SO_4 concentrations measured for the finest size fractions using the FLT method (lab-crushed samples) when compared to the Tex-620-J method (dashed line in Figure 5). Unlike the pH and resistivity methods, the Tex-620-J method utilizes lab-crushed material. This is also a deviation from the root AASHTO T-290 and ASTM C-1580 methods for evaluating the SO_4 content of soils in that these methods utilize materials collected from the field. Sulfate concentrations from Tex-620-J were much greater than FLT values for quarries D and E. This discrepancy is likely attributable to the fact that the Tex-620-J method involves aggressive leaching at elevated temperature (40º to 60ºC), while the FLT, AASHTO, and ASTM methods are performed at room temperature. Higher temperatures typically result in anomalously high concentrations of chloride and sulfate relative to other testing methods. Similar results were observed for chloride concentrations in that the values obtained using Tex-620-J were either similar to or greater than those obtained

using the FLT for all quarries except F. For Quarry F both SO_4 and Cl concentrations measured using Tex-620-J were less than those measured using the FLT method. This suggests that the higher temperature induced some chemical and/or physical changes that were not observed at room temperature.

1.5 Processes Leading to Chemical Differences between Fine and Coarse Aggregate

The pH, resistivity, and chemical data demonstrate that the fine (passing No. 4 sieve) aggregates collected at the quarry sites are not electrochemically representative of the bulk rocks. The fines are enriched in easily-leachable chemical species that when exposed to water decrease pH, decrease resistivity, and increase SO_4 concentrations relative to the bulk rock. This is most likely the result of a chemical weathering phenomenon related to atmospheric acid deposition (*5-7*). SO_x and NO_x compounds in the atmosphere react with carbonate rocks to produce reactive surface layers (typically of soluble sulfate minerals and dry acids) that are easily mechanically abraded and easily chemically leached (*8,9*). Emissions from heavy equipment (loaders, dozers, trucks, etc.) typically used in quarries can substantially add to SO_x and NO_x emissions, compounding the problem. The reactive surface layers are likely ground off and mechanically abraded during transport and movement of the coarse aggregate thereby biasing the chemistry of the fines. This chemical weathering process is probably limited to carbonate-rich rocks because of their surface reactivity (*10*). An alternate, but less likely, explanation is that excess sulfate is attributable to the oxidative weathering and physical breakdown of sulfide minerals like pyrite (FeS_2) in these rocks. However in this case none of the carbonate aggregates contained visible sulfide minerals and none were detected through X-ray diffraction.

1.6 Implications for the Assessment of Corrosive Potential using Traditional Soil Testing Methods

This work demonstrates that for coarse, carbonate-rich aggregates (like the TxDOT Type A and D materials investigated here) the fines that develop in the field often comprise only a few

percent of the total rock mass (Figure 1) and can be chemically different than the bulk rock (Figures 2-6). This fact can bias traditional AASHTO, ASTM, and TxDOT soil testing methodologies that call for the use of material collected directly from the field and specify the use of fines. For example, the TxDOT methods for the assessment of pH, resistivity, and SO_4 and Cl call for the testing of material passing the No. 40 sieve, while the AASHTO methods for the same parameters call for the testing of material passing the No. 10 sieve. Presumably this testing bias would begin to disappear as aggregate sizes decrease and fines passing these sieve sizes begin to comprise more of the total rock mass.

As an illustration of the importance of this testing bias, Figure 7 presents the results for resistivity testing of field and lab-crushed material from six of the selected quarries using Tex-129-E (similar to AASHTO T-288), a traditional soil-box resistivity testing method used by many state DOTs. The material tested using this method must have a resistivity greater than 3000 Ω-cm to be used for construction of MSE walls in Texas. Going by this criterion, the lab-crushed material from five of the six quarries would be acceptable (i.e., > 3000 Ω-cm), but material from quarries C, E, and F would additionally be rejected based on the resistivity of the field fines (which is what is specified by the method). In cases like these where field fines represent less than about 5% of the bulk rock material by mass, we suggest that only lab-crushed materials be used for the assessment of corrosive potential. In these specific cases, the true electrochemical properties of the bulk rock are better reflected in the lab-crushed material than in the field fines. We base this suggestion on the assumption that long-term corrosion rates for metallic reinforcements in MSE walls are best correlated with the average chemical properties of the bulk rock and not with the heterogeneous field fines. Additional work in our laboratory with bench-scale percolation tests of Type A and D material that has been cyclically saturated with water (2 days) and dried (5 days) has demonstrated that any chemical impact of the fines is ephemeral. After just a few cycles the pore water chemistry is similar to the chemistry obtained from the lab-crushed chemical testing. Further work will focus on correlating corrosion rates of metallic

coupons (embedded within the packed aggregates used for the percolation tests) with the electrochemical properties discussed here.

The use of lab-crushed material in cases where fines represent less than about 5% of the bulk rock may require changes to several of the current AASHTO, ASTM, and TxDOT methodologies that specify the use of field fines. These standard methods were developed and calibrated for assessing the corrosion potential of "soils" and fine-grained materials. The problems posed by the use of coarse rock fragments for MSE construction were not considered. Hence, modification of the existing methods for these special cases may be appropriate. Moreover, in many cases simplistic leaching tests that use representative sample sizes like the FLT may be equally (or more) effective when compared to traditional AASHTO, ASTM, or TxDOT methods for the assessment of the Cl and SO_4 concentrations of coarse aggregates. However, as recently pointed out by Thornly et al. (*11*) in an investigation of the rapid corrosion of metallic reinforcements within a set of MSE walls in Nevada, bulk leaching methods are not be comparable to traditional soil box testing for the evaluation of resistivity. The soil box methodologies employ specific electrode geometries for the direct measurement of resistivity in saturated aggregate. Bulk leaching methods "over-saturate" the aggregate because they use higher liquid to volume ratios. This can lead to artificial increases in the measured resistivity of the liquid for batch leaching tests.

1.7 Acknowledgments

The authors wish to gratefully acknowledge the support of the Texas Department of Transportation project no 0-6259. Anita is funded as a research assistant (2008-2009) and research associate (2009-2011) through Center of Transportation Infrastructure Systems on this project. Thapalia acknowledges additional support through a Geological Society of America research grant, 2009.

References

Baedeker, P. A., M. M., Reddy, K. J., Reimann, and C. A ., Sciammarella. Effects of Acidic Deposition on the Erosion of Carbonate Stones - Experimental Results from the U.S. National Acid Precipitation Assessment Program (NAPAP). *Atmospheric Environment. Part B. Urban Atmosphere*, Vol. 26, Issue 2, 1992, pp. 147-158.

Bell, F. G. Durability of Carbonate Rock as Building Stone with Comments on its Preservation. *Environmental Geology*, Vol. 21,1993, pp.187-200.

Elias, V. *Corrosion/Degradation of Soil Reinforcements for Mechanically Stabilized Earth Walls and Reinforced Soil Slopes*. Publication FHWA-NHI-00-044, National Highway Institute, Federal Highway Administration, Washington, D.C., 2000.

Hage J. L.T. and E. Mulder. Preliminary Assessment of Three New European Leaching Tests. *Waste Management*, Vol. 24, 2004, pp. 165-172.

Hageman P. L. *U.S. Geological Survey Field Leach Test for Assessing Water Reactivity and Leaching Potential of Mine Wastes, Soils, and Other Geologic and Environmental Materials*. U.S. Geological Survey Techniques and Methods, 2007.

Johansson, L.G., O., Lindqvist, and R.E. , Mangio. Corrosion of Calcareous Stones in Humid Air Containing SO_2 and NO_2. *Durability of Building Materials*, Vol. 5,1988, pp. 439-449.

Olaru, M., M., Aflori, B., Simionescu, F., Doroftei, and L., Stratulat. Effect of SO_2 Dry Deposition on Porous Dolomitic Limestones. *Materials*, Vol.*3*, 2010, pp. 216-231. doi:10.3390/ma3010216

Reddy, M. M. and S. D. Leith. Dry deposition of Sulfur to Limestone and Marble. Preliminary evaluation of a process based model: Proceedings of the 3rd International Symposium for Conservation of Monuments in the Mediterranean Basin, Venice, Italy. June 22-25, 1994, pp.185-187.

Spiker, E. C., V. J., Comer, R. P., Hosker, and S. I., Sherwood. Dry Deposition of SO2 on Limestone and Marble: Role of Humidity. In *7th International Congress on Deterioration and Conservation of Stone*, Lisbon,1992; Delgado Rodrigues, J., Henriques, F., Telmo, Jeremias, F., Eds., 1992, pp. 397- 406.

Texas Department of Transportation: Standard Specifications for Construction and Maintenance of Highways, Streets, and Bridges, 2004.

Thornley, J. D., R. V., Siddharthan, B., Luke, and J. M., Salazar. Investigation and implications of MSE wall corrosion in Nevada. *89th Annual Meeting Compendium of papers DVD*, TRB, Washington, DC, TRB paper # 10-0480. http://docs.trb.org/prp/10-0480.pdf

Table 1.1: Material Constituent of Backfill Materials

Parameter		A	B	C	D	E	F
Rock Source		Limestone	Limestone	Limestone	Dolomite	Limestone	Limestone
Classification		Type D	Type A	Type D	Type D	Type A	Type D
Gradation*	**Gravel**	94	79	100	99	80	93
	Coarse Sand	3	15	0	1	9	2
	Fine Sand	2	5	0	0	5	4
	Fines	1	2	0	0	6	0
Atterberg Limits	**Liquid Limit**	16	Non-plastic	Non-plastic	Non-plastic	15	22
	Plasticity Index	3				4	4
Hardness of Aggregates	**Wet Ball Mill (%)**	11	6	1	1	NA	30
	Aggregate Impact Value	19	11	13	9	25	28
	Aggregate Crushing Value	29	22	26	16	37	34
Moisture Density Properties	**Opt. Moisture Content, %**	9.0	N/A	N/A	N/A	6.0	8.3
	Maximum Dry Unit Weight, pcf	130	108	95	122	129	123

*** Gravel = Retained on No. 4, Coarse Sand = retained on No.40 and passing No. 4, Fine Sand= Retained on No. 200 and passing No. 40, Fines = passing No. 200**

Table 1.2: Resistivity, pH, and Cl/SO_4 Contents of Backfill Materials

Backfill Material	**Resistivity** Tex-129-E (AASHTO T-288) Ω-cm	**pH** Tex-128-E (AASHTO T-289)	**Chloride** Tex-620-J (AASHTO T-291) mg/kg	**Sulfate** Tex-620-J (AASHTO T-290) mg/kg
A	**2322**	7.92	**116.8**	**309.6**
B	8815	8.79	**326.0**	151.6
C	**1871**	7.93	**349.8**	**751.5**
D	7740	8.69	**611.3**	**460.7**
E	**2365**	8.54	**204.7**	**238.9**
F	**1967**	8.14	91.5	64.7
TxDOT Limits	**≥3000**	**5.5-10**	**≤ 100**	**≤ 200**

Shaded cells represent failure of TxDOT criteria for acceptability of corrosion potential.

Table 1.3: Bin Sizes for the Sieved Material

Bin Designation	Passing Sieve	Retained on Sieve
Pan	No. 200	
200	No. 100	No. 200
100	No. 40	No. 100
40	No. 4	No. 40
4	3/8 in.	No. 4
3/8 in.		3/8 in.

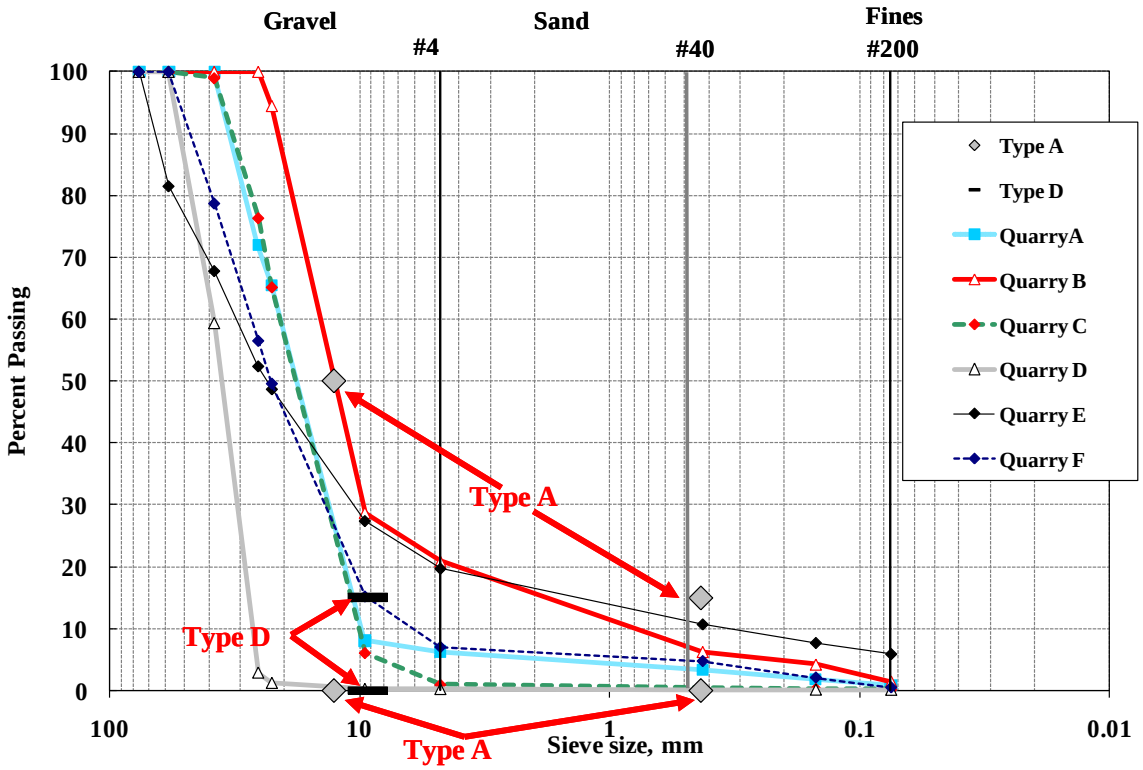

Figure 1.1: Grain Size Distribution of the Selected Backfill

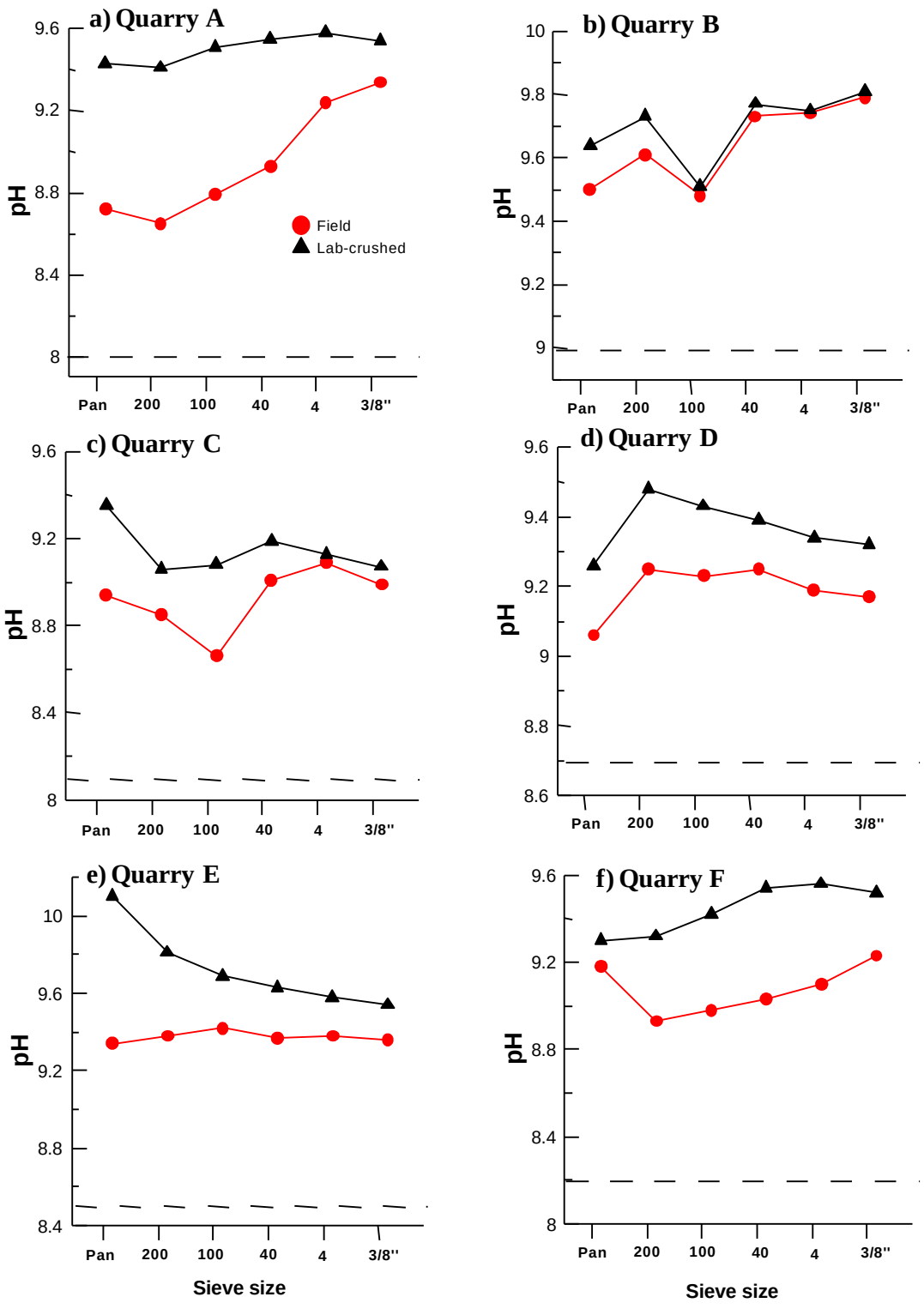

Figure 1.1: In-situ pH measurements from FLT tests (similar to AASTO T-289) completed using different sizes of field and lab-crushed aggregate from Quarries A-F. Dashed lines represent results using Tex-129-E.

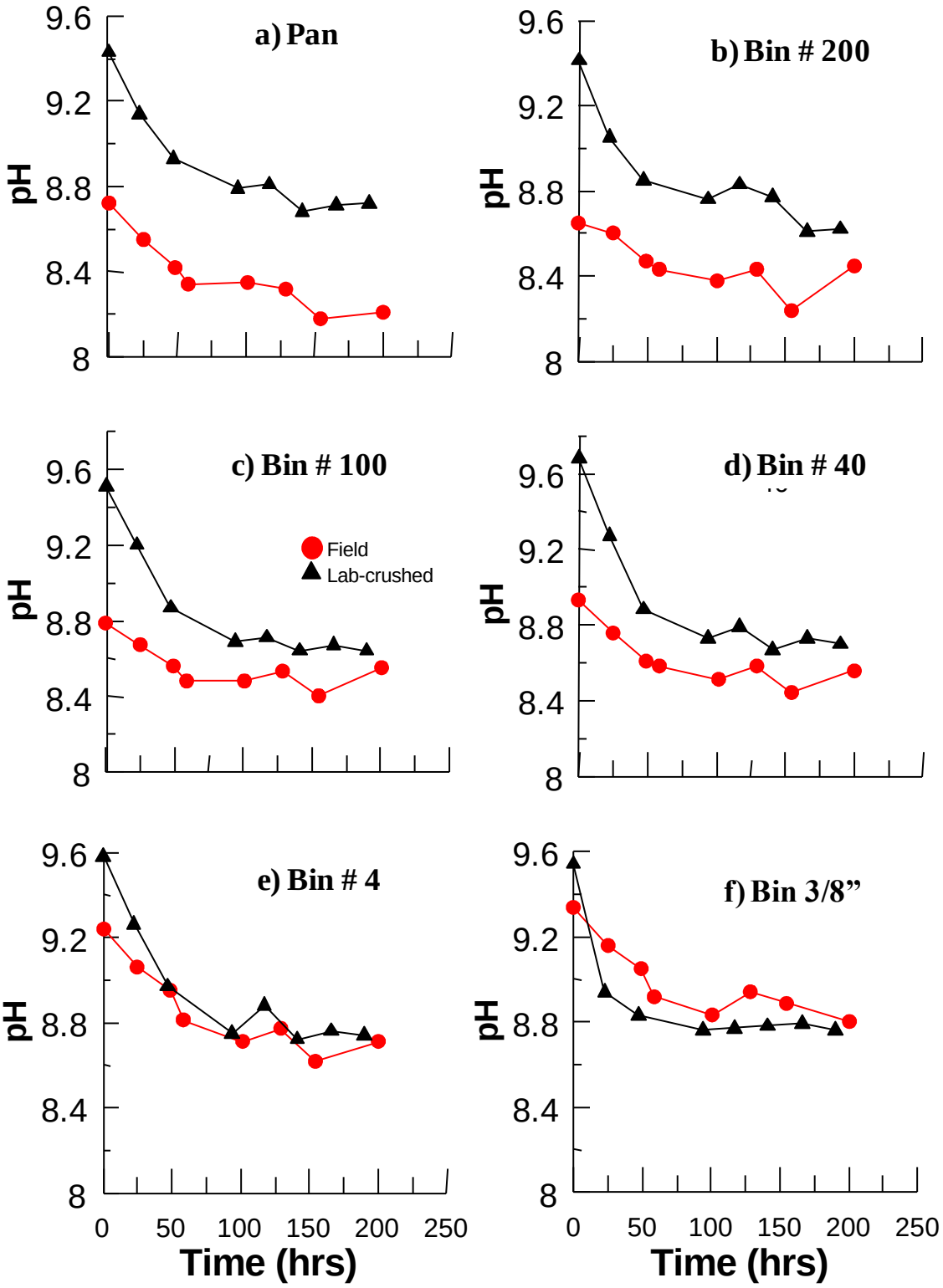

Figure 1.2: pHs for field and lab-crushed aggregate from Quarry A collected during FLT experiments as a function of leaching time

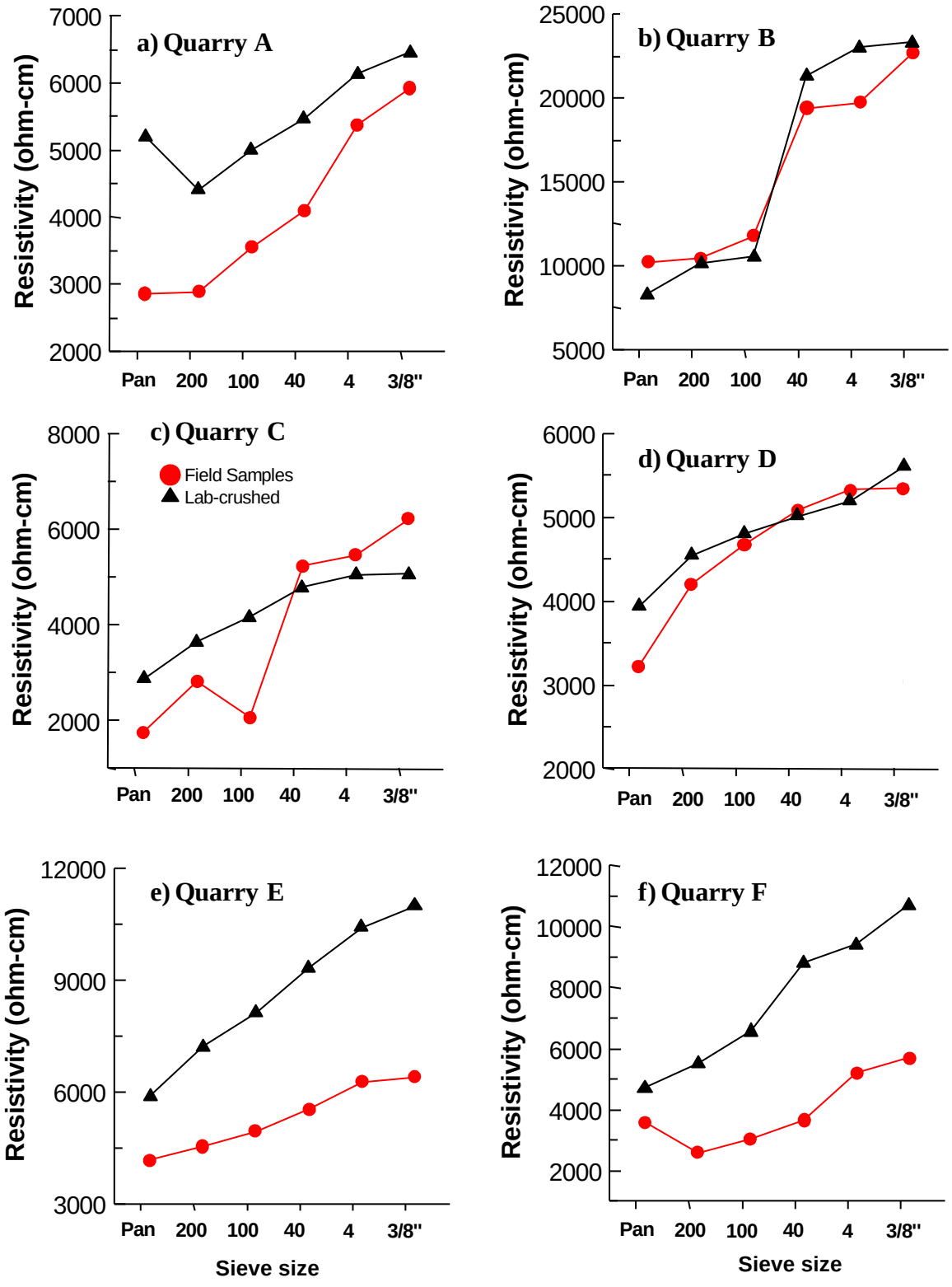

Figure 1.3: Resistivity measured during FLT experiments of different sized field and lab-crushed aggregates or each of the tested materials.

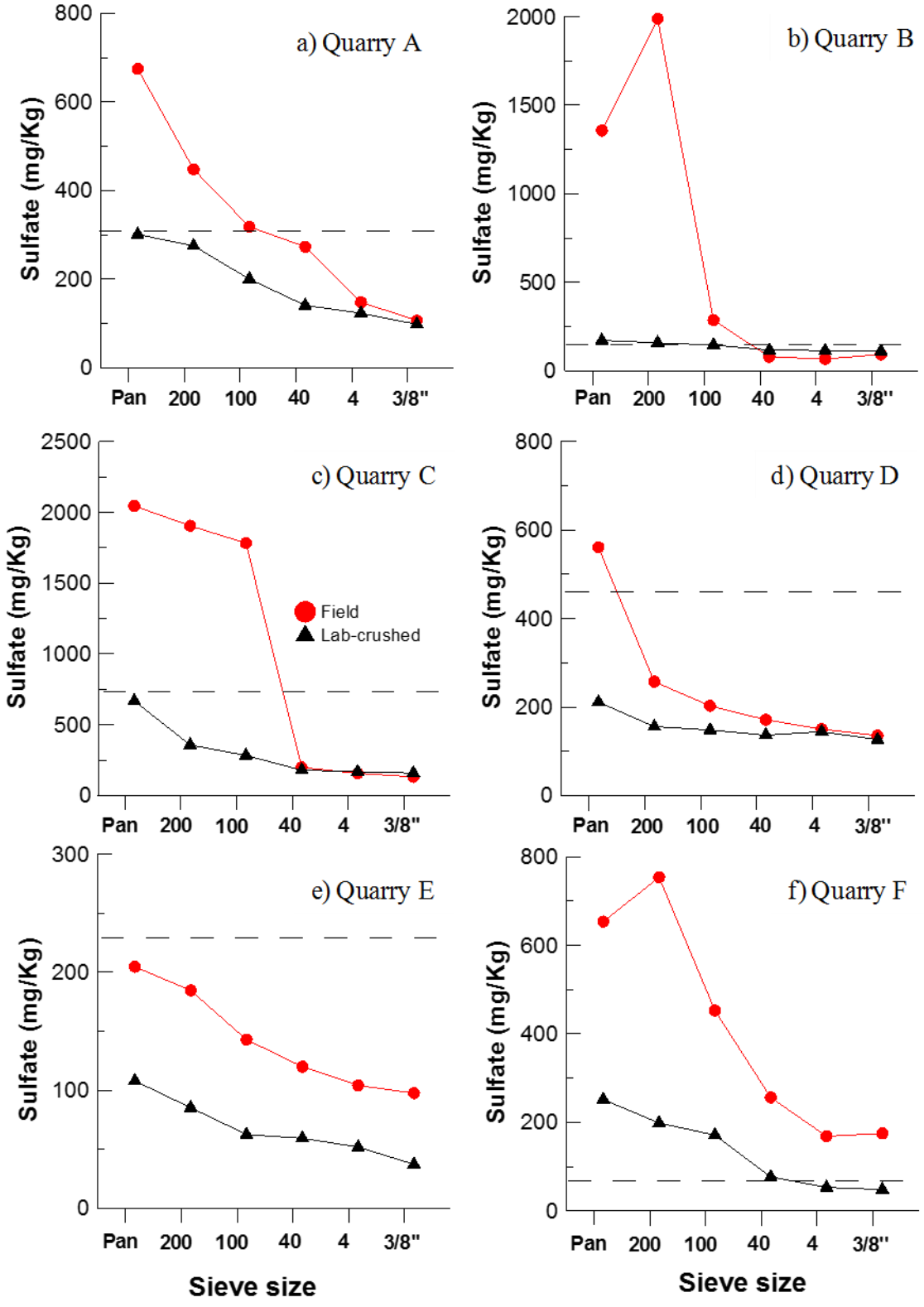

Figure 1.4: SO4 concentrations of FLT leachate for field and lab-crushed aggregate for each of the tested materials (similar to AASHTO T-290). The dashed line represents values measured using Tex-620-J.

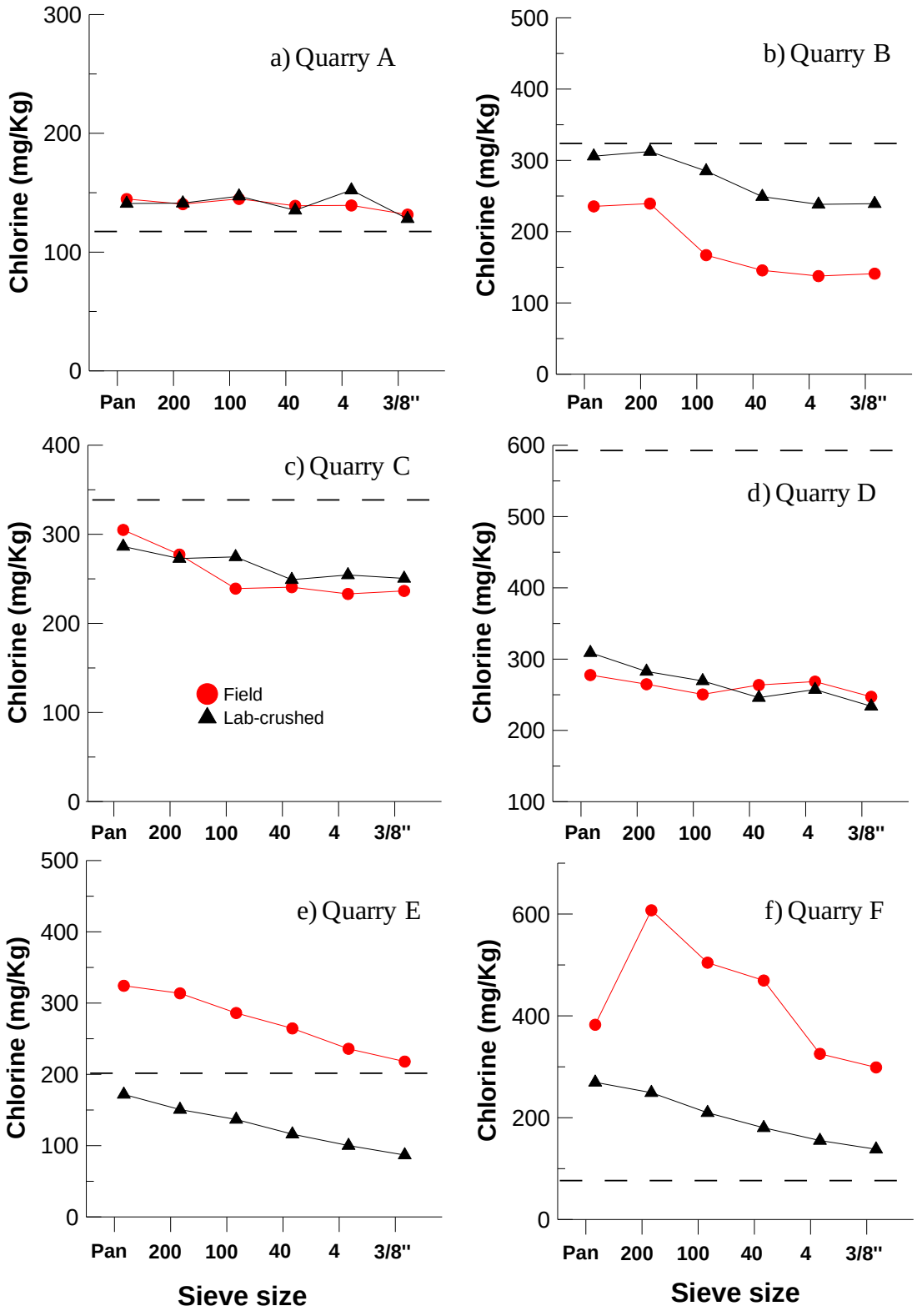

Figure 1.5: Chloride concentrations of FLT leachate for field and lab-crushed aggregate for each of the tested materials (similar to AASHTO T-291). The dashed lines represent measurements using Tex-620-J.

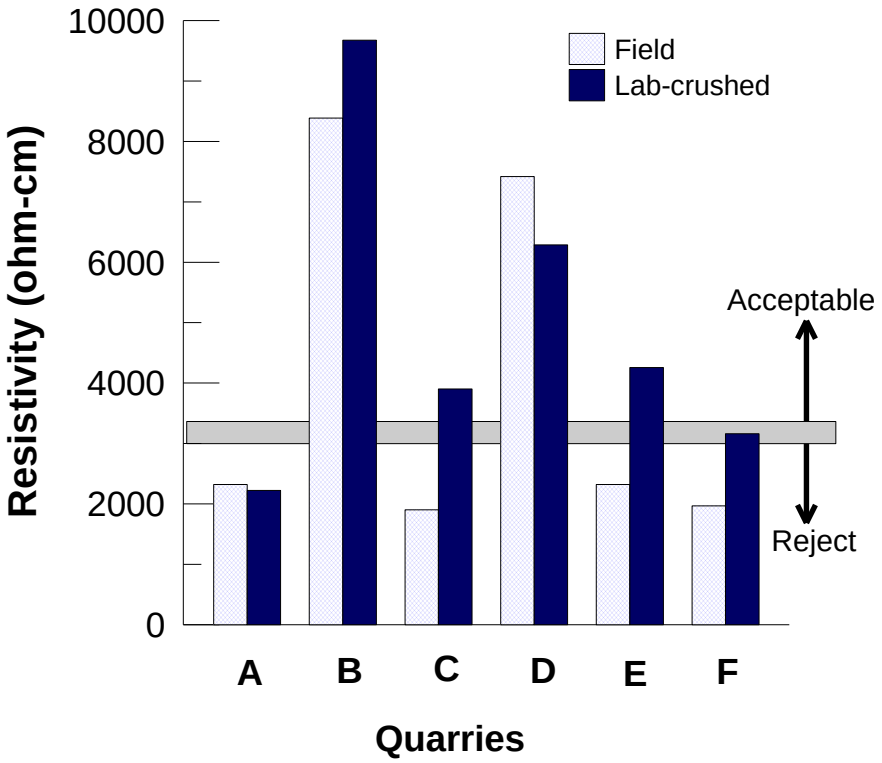

Figure 1. 6: Resistivity measurements for lab-crushed and field material from selected quarries obtained using method Tex-129-E (AASHTO T-288)

Date: Dec 10, 2014

Dear Ms. Thapalia:

The Transportation Research Board grants permission to use your paper, "Assessment of Corrosion Potential of Coarse Backfill Aggregates for Mechanically Stabilized Earth Walls," coauthored with D. Borrok, S. Nazarian, and J. Garibay in your dissertation, as identified in your request of November 11, 2014, subject to the following conditions:

1. Please cite the publication in *Transportation Research Record: Journal of the Transportation Research Board, No. 2253*, pp. 63-72, Washington, D.C., 2011.
2. Please acknowledge that the material from your paper is reproduced with permission of the Transportation Research Board.
3. None of this material may be presented to imply endorsement by TRB of a product, method, practice, or policy.

Every success with your dissertation. Please let me know if you have any questions.

Sincerely,

Javy Awan
Director of Publications
Transportation Research Board

Phyllis Barber
Transportation Research Board
Publications Office
202 334-2972 phone
202 334-3495 fax
pbarber@nas.edu

SECTION 2

Zinc Isotopic Signatures In Lake Sediment Cores From Across The United States

(Paper in revision in ES&T)

Anita Thapalia[1], David M. Borrok[1], Peter C. Van Metre[2], Jennifer Wilson[2]
[1]Department of Geological Sciences, University of Texas at El Paso, El Paso, TX 79968-0555
[2] USGS 8027 Exchange Drive, Austin, TX 78754

2.1 Abstract

Zinc is an important trace element pollutant in urban environments; however, the extent of Zn contamination and the sources of urban Zn pollution are often unclear. We measured Zn concentrations and isotopes (relative to JMC-3-0749-L) in sediment cores collected from eight lakes and reservoirs across the United States. We were able to pair the historical records of land use within each watershed with the Zn isotope data to determine Zn isotopic compositions for natural (+0.32 ±0.07‰, n = 29) and urban (+0.13 ±0.06‰, n = 15) lake sediments. Using the outer bounds of the natural and urban distributions, we estimated the respective source end-member compositions to be +0.43 and +0.05, respectively. The urban end-member is consistent with Zn pollution from automobile tire wear and emissions. Aan isotope mixing model was created using these end-member values that indicates large anthropogenic inputs of Zn to even the medium and low-density urban lakes.

2.2 Introduction

More than three million metric tons of Zn is released into the atmosphere annually (Graedal et al., 2005), affecting even remote locations such as Greenland and Antarctica (Candelone et al., 1995; Planchon et al., 2002). Sources of Zn contamination include waste-burning, power generation, refining, and the manufacturing and disposal of products such as

galvanized steel, rubber, cement, fertilizers, medicines, and cosmetics (Spliethoff and Hemond 1996; Hornberger, et al., 1999; Sonke et al., 2002; Gordon et al., 2003; Cloquet et al., 2006; John et al., 2007; Borrok et al., 2010). Zinc also is concentrated in automobile exhaust and leaches into the environment from the wearing of tires and brakes (e.g., Councell et al., 2004; Giere et al., 2006; Gioia et al., 2008; Thapalia et al., 2010).

Sediment cores obtained from long-standing bodies of water can record the depositional history of Zn (and other elements) derived from natural weathering and human activities (Carignan and Nriagu, 1985; Birch et al., 1996). Investigations of lake sediment cores from across the U.S. have demonstrated that Zn concentrations have substantially increased in urban locations over the last 2 or more decades. The increase in Zn concentration in lake sediments is especially notable when compared to other metals, as the concentrations of elements like Pb and As have decreased on average over the last several decades in response to environmental regulations such as the Clean Air Act (Mahler et al, 2006). Hence, it is becoming increasingly important to identify, track, and understand the distributions of anthropogenic Zn in natural environments.

The stable isotope ratios of Zn have been used as an environmental tracer to track the sources of atmospheric and industrial pollution in waters and soils (e.g., Borrok et al., 2010; Giere et al., 2006; Cloquet et el., 2006; Dolgopolova et al., 2006; Weiss et al., 2007; Chen et al., 2008; Sonke et al., 2008; Sivry et al., 2008; Mattielli et al., 2009; Shiel et al., 2010). In a previous study, we used Zn isotopes to investigate Zn contamination recorded in a sediment core from an urban lake, Lake Ballinger, in Seattle, Washington (Thapalia et al., 2010). Using zinc isotopes in the core collected from Lake Ballinger, we were able to distinguish among natural and anthropogenic Zn sources, including metal smelting and urban runoff (Thapalia et al., 2010).

In this study, we expand on this earlier work by analyzing Zn concentrations and isotopic compositions in sediment cores collected from eight lakes and reservoirs across the United States. The combination of urban and reference lakes provided an opportunity to pair Zn isotope changes with known changes in land usage within the watersheds. Using the percentage of urban land use in each watershed as a guide, we were able to calculate mean Zn isotope signatures for natural background and anthropogenic Zn inputs. An end-member mixing model was used to determine, to a first approximation, the relative input of anthropogenic Zn in a given watershed.

2.3 Methods

2.3.1 SAMPLE COLLECTION AND AGE DATING OF SEDIMENT CORE

The lakes chosen for this investigation were previously sampled as part of the U.S. Geological Survey's (USGS) National Water Quality Assessment (NAWQA) program (Mahler et al., 2006). Eight lakes and reservoirs, distributed widely throughout the USA and representing a range in land use and development history, were selected for Zn isotopic analyses (Figure 2.1). The locations and recent land-use characteristics of the watersheds are summarized in Table 2.1.

Sediment cores were collected using a 6.3 cm diameter free-fall gravity corer (Lakes Berkeley, Lake in the Hills, Newbridge Pond, Palmer, Tanasbrook, and Wheeler) or a 14 x14 cm box corer (Lakes Panola and Table Rock) from depositional areas of the lake or reservoir (Van Metre et al., 2004). Cores were vertically extruded, sectioned into 1-4 cm intervals and freeze-dried for further preparation and analysis. Activities of cesium-137 (^{137}Cs), radium-226 (^{226}Ra), and lead-210 (^{210}Pb) were measured by counting freeze-dried sediments in fixed geometry with a high-resolution, intrinsic germanium detector gamma spectrometer; the method of analysis was similar to that reported by other studies (e.g., Baskaran and Naidu, 1994; Fuller et al., 1999). Age dates of the sediment core intervals were estimated using the ^{137}Cs peak (1964) and reservoir construction

date as date-depth markers and assuming constant sediment mass accumulation rates for intervening layers; in some cases, ^{210}Pb profiles were used as supporting information for dating (Van Metre et al., 2004; Appleby and Oldfield, 1992).

2.3.1.1 Analytical procedures

Sediment core samples were digested and analyzed for their Zn concentrations prior to preparation for Zn isotopic analysis. Savillex digestion vessels, syringes, test tubes and collection bottles were acid washed in 10% sub-boiling HCl for 24 hours and rinsed with pure (18.2 MΩ) water three times prior to use. Dried sediment splits from the lake core samples were digested in a mixture of concentrated ultra-pure hydrochloric, nitric, and hydrofluoric (HCl-HNO_3-HF) acids at a volumetric ratio of (2:3:1). One hundred milligrams of sediment was added to the acid mixture in Savillex vials. The vials were capped and placed on a hotplate at 85^{o} C for 7 days (Lamothe et al., 2002). After the digestion period, the sample lids were removed and the material was evaporated to dryness. The material was re-dissolved in 5% HCl and then filtered using a pre-washed 0.45-μm nylon filter to remove any possible residual un-digested silicate material. These solutions were then analyzed for their Zn concentrations using a Perkin Elmer™ Optima 5300DV Inductively Coupled Plasma-Optical Emission Spectrometer (ICP-OES) at the University of Texas at El Paso (UTEP). The ICP-OES was calibrated using multi-element ICP standards. Analytical uncertainty was less than ± 5% for all the samples. The calculated recoveries of Zn for the individual digests were compared with the Zn concentration data originally measured for the same sample intervals by the USGS (Van Metre et al., 2004). All of our Zn recoveries were within ±10% of the original USGS values (data not shown). We also performed replicate digestions for all but one of the lake sediment samples (Supporting Information, Table S-1). The relative percent difference in Zn concentration among replicates

varied from 2-14% and averaged 5%. All digestion blanks contained less than 5 nanograms of Zn, which was less than 1% of the total Zn in the samples.

Samples for Zn isotopic analysis were prepared in a class 100 clean room using anion-exchange column chromatography (Borrok et al., 2007). An aliquot of the dissolved sample that provided about 2 to 4 μg Zn was dissolved in 1 mL of 10M ultra-pure HCl. The acidified sample was then loaded onto a column with pre-cleaned 100-200 mesh AG MP-1 resin (Bio-Rad). Additional aliquots of 10M, 5M, and 1M HCl were added to the column to elute matrix elements, while Zn remained on the column as an anionic Zn-chloride complex. The separation procedure was completed by adding 4 mL of ultra-pure water to elute the Zn fraction. This fraction was evaporated to dryness and re-dissolved in 2% HNO_3. All column blanks contained less than 10 ng of Zn, which was less than 1% of the total Zn.

Zinc isotopes were analyzed using a Nu Instruments™ Multicollector Inductively Coupled Plasma - Mass Spectrometer (MC-ICP-MS) at the Center for Earth and Environmental Isotope Research at UTEP. Among the five stable isotopes of Zn, the four most abundant isotopes ^{64}Zn, ^{66}Zn, ^{67}Zn, and ^{68}Zn were measured simultaneously. A desolvating nebulizer system (Nu DSN 100) was used to introduce the samples into the instrument at a concentration of ~150μg/L. The standard-sample-standard bracketing approach was used to correct for mass bias (Borrok et al., 2007, 2009, 2010; Thapalia et al., 2010; Albarede and Beard, 2004). Because the mass bias was stable over individual analytical sessions, the addition of an internal dopant of Cu did not improve precision. Isotopic changes were referenced to Johnson Matthey standard solution JMC 3-0749-L. Quality assurance samples, including column blanks and duplicates from the acid digestions, were integrated into the isotopic preparation and analysis protocol. The isotopic data are presented using standard delta notation (Eq.1).

$$^{66}Zn = \left[\frac{(^{66}Zn/^{64}Zn)_{sample}}{(^{66}Zn/^{64}Zn)_{JMCaverage}} - 1 \right] \times 1000$$

Eq. 1.

The delta notation expresses the ratio of isotope abundances ($^{66}Zn/^{64}Zn$ in this case) in a sample relative to the ratio of isotope abundances in a designated reference material (in parts per thousand, or per mil). The majority of the individual samples were replicated 3 or 4 times over multiple analytical sessions spanning a period of about 18 months (Table S-1). The average 2σ uncertainty for all samples was ±0.06‰. For all discussions and figures herein, we report the measured 2σ uncertainty. These include the uncertainties associated with replications of the digestion procedure and column exchange process (Table S-1). Mass dependency plots of $\delta^{68}Zn$ and $\delta^{67}Zn$ versus $\delta^{66}Zn$ demonstrated that spectral interferences were not present for these masses (Supporting Information, Figure S-1).

2.4 Results and Discussion

The concentrations of Zn and corresponding $\delta^{66}Zn$ for the lake sediment core samples are plotted as a function of estimated deposition date for the individual lakes in Figure 2.2. Deposition dates of the core samples varied substantially based on when the cores were collected, lake sedimentation rates, age of the reservoir, and the availability of archived core material. Concentrations of Zn ranged from 37.2 mg/kg in Lake Wheeler to 984 mg/kg in Newbridge Pond and varied substantially within and among lakes as a function of land use and time (Figure 2.2). The $\delta^{66}Zn$ varied from +0.07‰ to +0.45‰ among all the lakes (Figure 2.2; Table S-1). This variation is about 6 times greater than the average analytical uncertainty of the Zn isotope measurements.

Present day land use varied substantially among the studied watersheds, ranging from pristine conditions (Table Rock Reservoir) to dense urbanization (Newbridge Pond, Table 2.1).

Except for the two reference watersheds (Table Rock Reservoir and Lake Panola), historical trends in land use followed a pattern of increasing urbanization over time. Using available site history data we grouped land use in the studied watersheds into the following time periods: (1) *pre-urban* (0 to ~5% urban land use); (2) *transitional* (~5 to 70% urban land use), and (3) *urban* (70 to 100% urban land use; Table 2.2). Although there are some uncertainties associated with estimating historical land use patterns, we believe that we have reasonably captured the prevalent land-use distributions during the corresponding times.

2.4.1 Zn concentration and isotope data

2.4.1.1 Berkeley Lake

Berkeley Lake was constructed in 1948 and is located in suburban Atlanta, Georgia, 34 km north of the city center (Figure1). The Zn concentrations of the available sediment core samples from Berkeley Lake ranged from 286 mg/kg in 1978 to 541 mg/kg in 1995 (Figure 2.2a; Table S1). The δ^{66}Zn for the Berkeley Lake sediments varied from +0.11‰ to +0.27‰ (Figure 2.2a). The population density in 2006 was 640 people per km^2 and urban land use was 66% (Table 2.1). Because land use in the watershed was always greater than 5% and never reached above 70% in the sampled time periods, we classify all samples (1977 to 2000) as transitional (17). The mean δ^{66}Zn for the core was +0.17 ± 0.07‰; n=10 (Table 2.2).

2.4.1.2 Lake in the Hills

Lake in the Hills, also known as Woods Creek Reservoir, is located in suburban northwest Chicago, Illinois (Figure 2.1). This reservoir was constructed in 1923 in the village of Lake in the Hills. Residential areas were developed around the lake in the late 1940s (Groschen et al., 2004). There was an increase in Zn concentration from 50.5 mg/kg in the 1939 sample to 105 mg/kg in the 1947 sample (Figure 2b). In spite of rapid and more extensive urban

development of the watershed since the 1990s, after the initial increase in the 1940s the concentrations of Zn remained relatively stable, varying from 101 to 139 mg/kg but not showing any systematic trend (Figure 2.2b). From its inception in 1923 until 1970, the Lake in the Hills watershed can be classified as pre-urban (0 to around 5% urban land use). From 1970 through the mid-1990's more urban development took place in the watershed, with 14% residential land use occurring by 1990 and 21% residential land use occurring in the late 1990s (Vogelmann et al., 2001). The watershed was more rapidly urbanized since 2000, with classifications of 66% and 80% urban in 2001 and 2006, respectively (Table 2.1). Based on this evidence we classify the land use from 1970 to 2001 as the transitional period and land use after 2001 as urban. The δ^{66}Zn of the pre-urban period (pre-1970) was +0.30 ± 0.05‰; n=4, the δ^{66}Zn of the transitional period was +0.26 ± 0.08 ‰; n=5, and the δ^{66}Zn of the urban period was +0.22 ± 0.06 ‰; n=3 (Table 2.2).

2.4.1.3 Newbridge Pond

Newbridge Pond is located on Long Island east of New York City (Figure 2.1), and was constructed in 1895 to supply water to the city (Long et al., 2003). Development of the 12.96 km^2 watershed for this lake started in the early 1900s and the entire watershed was urbanized by the late 1940s (Long et al., 2003). As of 2006, the area was 99.6% urban (17, 34; Table 2.1). Core intervals from Newbridge Pond that were available for this study span an estimated range of dates from 1959 to 1996, therefore, all of the samples were classified as urban (>70% urban land use). The concentration of Zn in the Newbridge core ranged from 363 mg/kg in 1959 to 984 mg/kg in 1985 (Figure 2.2c). The elevated Zn concentrations have been attributed to industrial activities and to the presence of two major highways that cross the watershed (Spliethoff and Hemond, 1996; Long et al., 2003). Despite a large increase in Zn concentrations over time, the

consistency of the Zn isotope data, ranging from +0.09‰ to +0.15‰, suggest that the source (or sources) of Zn have not changed appreciably since 1959. The mean δ^{66}Zn for the urban period (i.e., all the Zn isotope data for this lake) is +0.09 ± 0.07‰; n=9 (Figure 2.2c).

2.4.1.4 Palmer Lake

Palmer Lake is located 24 km north of Minneapolis, Minnesota (Figure 2.1). The Zn concentration in Palmer Lake increased from 182 mg/kg in 1970 to 299 mg/kg in 2002 (Figure 2.2d). The change in Zn concentration corresponds to the rapid urbanization of the watershed starting in the 1970s. The watershed was 29.6% urban in 1970, 51.9% urban in the 1990s, and 77% urban in 2006 (Mahler et al., 2006; Van Metre et al., 2000; Table 2.1). The consistency of Zn concentrations near the top of the core suggests that land use and population growth stabilized by the late-1990's. Based on census data from 1970 and land cover digital data from 1990, we estimate that the Palmer Lake watershed was pre-urban before 1975, transitional between 1975 and 2000, and urban after 2000 (Rohe, 2011; U.S. Geological Survey, 1990; Stark et al., 2000). The δ^{66}Zn of the Palmer Lake sediment core samples changed from +0.37‰ at the bottom of the sediment core (1970) to +0.09‰ at the top of the core (2005) (Figure 2.2d). Using the classification scheme presented above, the mean δ^{66}Zn for core in the pre-urban, transitional, and urban periods was +0.35 ± 0.07‰ (n=2), +0.24 ± 0.06‰ (n=5), and +0.09 ± 0.06‰ (n=3), respectively (Table 2.2).

2.4.1.5 Lake Panola

Lake Panola, constructed in 1946, is located 24 km southeast of Atlanta, Georgia, in a forested state park with very little urban influence in the watershed, but in an area that is surrounded by extensive suburban development. The available sediment core from Lake Panola spans an estimated date range from 1959 to 1998. The concentrations of Zn in the sediment core

were relatively constant, ranging from 143 mg/kg in 1995 to 194 mg/kg in 1959 (Figure 2.2e). The watershed was characterized as 1.1% urban in the 1990s and 5.5% urban in 2001 and 2006 (Mahler et al., 2006; Table 2.1). Based on the available land use data, we categorized all of the sediment samples except for the 1998 sample as pre-urban. We classified the 1998 core sample as transitional because urban land use was greater than 5% a few years later in 2001. The δ^{66}Zn for the sediment samples varied from +0.13‰ to +0.27‰ (Figure 2.2e), with a mean of +0.21 ± 0.06‰; n=7. The δ^{66}Zn of the pre-urban period (pre-1998) was +0.23 ± 0.06‰; n=6 and the δ^{66}Zn of the transitional period was +0.13 ± 0.06 ‰; n=1. The Zn concentrations (all of which are above the median Zn concentration in US reference lakes of 134 mg/kg (17) and δ^{66}Zn values (the average of which is lower than all other pre-urban averages for lakes studied here [Table 2.2]) suggest some input of anthropogenic Zn, possibly from atmospheric deposition from the city of Atlanta and surrounding suburbs (Frick et al., 1998).

2.4.1.6 Table Rock Reservoir

Table Rock Reservoir drains a 39.24 Km^2 area of the Southern Blue Ridge Escarpment of northwestern South Carolina (Figure 2.1). The reservoir has been servicing the Greenville Water System since its construction in 1930. The watershed is protected with no public access (Van Metre et al., 2009; Austin and Krueger, 2014). Currently there is no residential, commercial, agricultural or industrial land use in the watershed (Table 2.1). This reference lake setting means that the entire core can be classified as pre-urban. The concentrations of Zn in the sampled core reached a maximum of 143 mg/kg in 1968, remained relatively stable in the 100-120 mg/kg range for the next 3 decades, and decreased after 2000 to 71 mg/kg in 2007 (Figure 2.2f). It is unclear what might have caused the recent decrease in Zn concentrations, although lacking any watershed sources, a change in atmospheric deposition is implied. The δ^{66}Zn of the Table Rock

Reservoir sediments varied from +0.28‰ to +0.45‰. Changes in Zn isotopes did not appear to correlate with Zn concentration or the estimated ages of the samples (Figure 2.2f). The average δ^{66}Zn of the pre-urban sediment was +0.36 ± 0.08‰; n=13 (Table 2.2).

2.4.1.7 Tanasbrook Pond

Tanasbrook Pond is located 16 km east of Portland, Oregon, and has a 10.49 km^2 watershed dominated by suburban development (Figure 2.1; Wentz et al., 1998). The concentration of Zn in the oldest Tanasbrook sediment sample (1970) was 143 mg/kg (Figure 2.2g). The Zn concentration in the sediment core increased after 1970, stabilizing at around 300 mg/kg in the late 1990s. These changes in Zn concentration are consistent with the urbanization of the watershed since the 1970s. Prior to 1973, the Tanasbrook Pond watershed area consisted of farmland and beginning in the mid-1970s, the watershed developed rapidly. By 2006, 65% of the watershed was categorized as urban (Wentz et al., 1998; Table 2.1). Based on our classification scheme, the 1970 core sample was assigned to the pre-urban category, while the remaining samples were considered to be transitional. The δ^{66}Zn for the sole pre-urban sample was +0.30, while the transitional signal (post-1978) averaged +0.17 ± 0.05‰; n=8 (Figure 2.2g).

2.4.1.8 Lake Wheeler

Lake Wheeler, constructed in 1950, is located 10 km south of Raleigh, North Carolina, in the Albemarle-Pamlico Drainage Basin (Figure 2.1; Spruill et al., 1998). The concentration of Zn in Lake Wheeler sediment increased from 37.2 mg/kg in the 1944 sample (date uncertain but sample is of pre-reservoir soil at the soil-sediment boundary) to 126 mg/kg in 1982, then remained stable in the range of 106 to 114 mg/kg to 2001, the most recent date captured in the available core (Figure 2.2h). The most rapid increase in Zn concentration occurred during the 1960s, which correlates with an increase in population and urban land use (Spruill et al., 1998;

Sakowski et al., 2010). In 2006, the watershed was classified as 46% urban (Table 2.1). Based on this evidence, we assigned the pre-1960 samples to the pre-urban category and the post-1960 samples to the transitional category. Pre-urban time periods record a mean Zn isotopic signature of +0.37 ± 0.07‰; n=2. The transitional period is characterized by relatively narrow range of +0.22% to +0.30% with a mean δ^{66}Zn of +0.26 ± 0.06‰; n=6 (Figure 2.2h).

2.4.2 ZN CONCENTRATIONS AND ISOTOPES OF PRE-URBAN, TRANSITIONAL, AND URBAN SEDIMENTS

The aggregated mean Zn concentrations and δ^{66}Zn for the pre-urban, transitional, and urban periods were calculated using the mean value within the appropriate category for each lake (Table 2.2). This approach gives equal weight to each lake and was used to avoid potential bias related to different sample density in the lakes. The aggregated mean uncertainties were similarly computed. It is clear that there is a strong positive relation between Zn concentration and the degree of urbanization (Table 2.2). It also is clear that as the Zn concentration and degree of urbanization increase, δ^{66}Zn declines (Table 2.2).

2.4.2.1 Zn Concentrations and Isotopes in the Pre-Urban Period

The mean concentration of Zn within bulk continental crust is about 72 mg/kg (Rudnick and Gao, 2003), which happens to equal the median background concentration estimated from 35 lake sediment cores, including some of the cores used in this study, by (Mahler et al., 2006). This value is somewhat smaller than the aggregate mean concentration of Zn that we compiled for pre-urban sediments in this investigation of 122 mg/kg. Furthermore, a national-scale watershed investigation (Horowitz and Stephens, 2008) showed that the average concentrations for Zn in river sediments from over 300 rivers that drained un-urbanized forest and rangelands were 130 mg/kg and 85 mg/kg, respectively. We therefore conclude that our aggregate pre-urban Zn

concentration for the lake sediment cores in this study reasonably represents background conditions and that the dominant source of Zn in the pre-urban sediments was natural bedrock and soil material.

The pre-urban Zn isotope signatures for all of the lakes were quite similar, leading to an aggregated mean of +0.32 ± 0.07 ‰ (n=29) (Table 2.2). The pre-urban Zn isotopic composition of the studied lake sediments is thought to represent, at least to a first approximation, the δ^{66}Zn of natural sediment and bedrock. This conclusion is supported by evidence from previous investigations of natural sediments and rocks. For example, the reported δ^{66}Zn of "geochemical background" for soil in the Upper Lot River in France was +0.31 ± 0.04‰ (Sivry et al., 2008). Similarly, stream sediments from the Riou Mort and Riou Viou Rivers that were upstream of potential Zn contamination had δ^{66}Zn values of +0.36‰ and +0.32‰, respectively (Sivry et al., 2008). Another study reported an average δ^{66}Zn of +0.32‰ for the deepest portion of investigated soil profiles that were thought to represent natural geogenic Zn (Juillot et al., 2011). Bigalke and others (2012) reported a range of δ^{66}Zn of +0.22‰ to +0.30‰ for river flood plain sediments from the River Elbe, Germany, that were thought to be unaffected by anthropogenic contamination. Ranges of +0.25‰ to +0.36‰ also were reported for pre-industrial Zn at the site of a Belgian Pb/Zn smelter (Sonke et al., 2008).

The δ^{66}Zn for natural soils and sediments also is consistent with the range of δ^{66}Zn reported for the types of rocks and minerals from which they were derived (e.g., basalts (Marèchal et al., 1999; Chapman et al., 2006; Cloquet et al., 2006), loess (Luck et al., 1999), carbonates (Luck et al., 1999), and clays/shales (Marèchal et al., 2000)). This observation suggests that transport and biogeochemical cycling of Zn does not appreciably affect the Zn isotopic signature of lake sediments.

2.4.2.2 Zn Concentrations and Isotopes in the Transitional Period

The aggregate mean Zn concentration of 239 mg/kg for the transitional period is intermediate between the Zn concentrations for the pre-urban and urban periods (Table 2.2). The aggregate mean δ^{66}Zn for the transitional period of the studied lake sediments is +0.21 ± 0.06 (n = 35) (Table 2.2). This value is thought to represent an intermediate stage of development where there is a mixture of Zn from natural and anthropogenic urban end-member sources. The fact that the aggregate transitional δ^{66}Zn is roughly the halfway point between the mean pre-urban and urban isotopic signatures supports this interpretation.

2.4.2.3 Zn Concentrations and Isotopes in the Urban Period

The aggregate mean concentration for Zn in sediments affected by urban sources of 389 mg/kg is about three times greater than the mean Zn concentration for pre-urban sediments (Table 2.2). Zn concentrations in samples from two of the eight lakes exceed the probable effect concentration of 459 mg/kg (MacDonald et al., 2000), the level above which adverse effects on aquatic life are expected to occur. Horowitz and Stephens (2008) reported a strong correlation between the percentage of urban land use in a given watershed and the Zn concentrations of sediments from the rivers that drain that watershed. The average Zn concentration of sediments in 95 rivers draining watersheds with greater than 50% urbanization was 330 mg/kg (Horowitz and Stephens, 2008). This value is slightly less than our aggregated mean concentration for urban sediments, although here we used a higher land-use threshold of 70% urbanization.

The aggregate mean δ^{66}Zn for the sediment samples deposited in settings and time periods of more than 70% urban land use was +0.13 ± 0.06 ‰; n=15 (Table 2.2). This aggregate urban Zn isotopic composition is thought to represent the δ^{66}Zn for anthropogenic urban Zn contamination. Common sources of urban Zn contamination include tire-wear (Councell et al.,

2004, Thapalia et al., 2010), combustion processes associated with automobiles, waste burning, smelting/refining, power production (e.g., Cloquet et al., 2006; Gioia et al. 2008; Mattielli et al., 2009; Borrok et al., 2010), and the corrosion of galvanized steel (John et al., 2007).

Because ZnO is used as an accelerator in the vulcanization process, it is often present in tire rubber at concentrations greater than one weight percent (Callender and Rice, 2000). Hence, the wearing of tires in urban watersheds is likely to represent a consistent source of anthropogenic Zn that is transported by runoff into nearby water bodies (Callender and Rice, 2000; Davis et al., 2001). The previously reported δ^{66}Zn for tire samples (range of +0.14‰ to -0.10‰; average of +0.04‰; n=5), overlaps with the aggregate δ^{66}Zn of urban contamination for the measured sediment samples (Thapalia et al., 2010).

Because Zn volatilizes at a relatively low temperature (~900°C), most combustion processes also are effective in mobilizing Zn through vaporization (Borrok et al., 2010). This process results in the preferential incorporation of the lighter Zn isotopes into the vapor phase, while the heavier Zn isotopes are sequestered in spent fuels like slag or ash (e.g., Cloquet et al., 2006; Sonke et al., 2002; 2008; Sivry et al., 2008; Mattielli et al., 2009; Borrok et al., 2010). The isotopic composition of anthropogenic Zn related to combustion depends largely on the efficiency of the process and other factors like the amounts of condensation and adsorption of Zn onto atmospheric particles of various sizes (e.g., Mattielli et al., 2009; Borrok et al., 2010). The δ^{66}Zn measured for urban aerosols from PM-10 ambient air collectors and bus air filters and from flue gases from waste incineration was +0.12 ± 0.21‰ and +0.13 ± 0.12‰, respectively (Cloquet et al., 2006). These urban sources of Zn that were derived from combustion processes are also similar to the aggregate urban δ^{66}Zn measured in our study. Additional studies have reported Zn isotopic signatures as low as -1.0‰ for small aerosol particles derived from urban

traffic in Brazil (Gioia et al., 2008), and as low as -0.52‰ for atmospheric particles associated with a Pb-Zn refinery (Matielli et al., 2009).

Because of its ubiquity in urban infrastructure, runoff associated with the corrosion of galvanized steel is another likely source of urban Zn contamination. The δ^{66}Zn for this source, however, is likely a little heavier on average than the aggregate urban Zn signal in our study. Because the smelting and refining process is typically very efficient (>97% of Zn is retained), the average δ^{66}Zn for naturally occurring Zn ore minerals like sphalerite is likely very similar to that for galvanized steel. A study by John et al (2007) reports δ^{66}Zn values for galvanized steel ranging from +0.12‰ to +0.31‰ (n=3), and supports this interpretation. Although likely present in much lower concentrations, the reduction of aqueous divalent Zn to elemental Zn during electroplating has been shown to result in very light Zn isotopes in the metallic phase (e.g., Kavner et al., 2008).

Like the pre-urban Zn signatures, it seems unlikely that urban Zn isotopes in the lake sediments were substantially altered by transport or secondary processing. Like natural Zn, most of the potential sources of urban Zn enter the sediment in the solid phase. Atmospheric deposition would include small dust/ash particles of adsorbed Zn and/or discrete Zn-sulfate, chloride, or other minerals (e.g., Gierè et al., 2006; Wong, et al., 2006). Tire wear would also be carried into the sediment primarily as particulate matter (Wik and Dave, 2009). Although some Zn may leach from the solid particles, it is likely that the larger Zn sediment pool will only be modestly influenced by secondary isotopic fractionation processes.

2.5 A Mixing Model for Pre-urban and Urban Zn

The relationship between Zn isotopes and Zn concentrations for all the lakes is illustrated in Figure 2.3. Excluding the four lowest concentration data points, 1/Zn and δ^{66}Zn are linearly

related with an r^2 coefficient of 0.62. These data form a continuum that represents the mixing of pre-urban (i.e., natural) and urban sources of Zn. This result suggests that we can utilize a binary mixing model to estimate the percentages of natural and urban Zn for any lake sediment sample as follows:

Eq. 2 $$\delta^{66}Zn_{measured} = (\delta^{66}Zn_{pre\text{-}urban} \times X) + (\delta^{66}Zn_{urban} \times [1\text{-}X]),$$

where $\delta^{66}Zn_{measured}$ is the measured isotopic signature for any sample. The $\delta^{66}Zn_{pre\text{-}urban}$ and $\delta^{66}Zn_{urban}$ are the binary end members, and 'X' is the estimated fraction of the pre-urban (natural) Zn source that makes up the isotopic signature of the sample. By re-arranging the equation (Eq. 3), we can estimate the percentages of natural and urban Zn for any sample using the measured $\delta^{66}Zn$ as long as we know the end member pre-urban and urban isotope values.

Eq. 3 $$\text{Natural Zn \%} = [(\delta^{66}Zn_{measured} - \delta^{66}Zn_{urban})/(\delta^{66}Zn_{pre\text{-}urban} - \delta^{66}Zn_{urban})] \times 100$$

The aggregate mean isotopic values for pre-urban and urban Zn (Table 2.2) are not the best choices for binary end members for the mixing model (Eq. 3), as some samples would inevitably fall outside the means, resulting in contributions of natural Zn of less than 0 or greater than 100%. Considering that most or all of these samples contain some contribution from both natural and anthropogenic sources, we instead use "bounding" isotope end members as indicated on Figure 2.3. We selected $\delta^{66}Zn$ values of +0.43 and +0.05, for the bounding end members for natural and urban Zn sources, respectively (Figure 2.3).

Using these end members, we calculated the contributions to each core sample (Table S-1). Applying this approach to the sediment samples collected in this study, we found that the mean contributions of Zn to these lakes from urban sources ranged from 15% (Table Rock Reservoir) to 87% (Newbridge Pond) and those urban sources contributed on average over 50% of the Zn in samples from five of the eight lakes (Table S-1). As there is an established

relationship between Zn isotopes and Zn concentration in the investigated lake sediments (Figure 2.3), a similar mass balance model could be made using Zn concentration. However, the spread of these data, particularly at low concentrations of Zn, could lead to greater uncertainty.

The large anthropogenic contribution of Zn to these urban lakes and the high concentrations, above the PEC sediment quality guideline in some cases, indicate that Zn contamination poses risks to the health of our nation's urban waterways. The aggregated average δ^{66}Zn for urban watersheds is most consistent with an automobile pollution source; tire wear and (or) vehicle emissions.

2.6 Acknowledgements

Funding for this research was provided by a USGS student service contract and a grant from the International Association of Geochemistry (for Thapalia). We thank Rich Wanty for his input, which improved this manuscript.

References

Albarede, F.; Beard, B. L. Analytical methods for Non-Traditional Isotopes. *In Geochemistry of Non-traditional Stable Isotopes*; Johnson, C. M., Beard, B. L., Albarede, F. Reviews in Mineralogy and Geochemistry, v. 55, eds. Mineralogical Society of America: Washington, DC, **2004**, 113-152.

Appleby, P. G.; Oldfield, F. Application of lead-210 to sedimentation studies, in Ivanovich, M., Harmon, S., ed., Uranium-Series Disequilibrium: Applications to Earth, Marine, and Environmental Sciences, 2nd ed.; Clarendon Press: Oxford, 1992, p 910.

Austin, K.; Krueger, E. Natural resource management plan for the Greenville Watersheds, Table Rock/North Saluda; *The Nature Conservancy*, **Jan 2014**. http://www.greenvillewater.com/wp-content/uploads/2014/02/GW_Watershed_Management_Plan.pdf

Baskaran, J.; Naidu, A. S. ^{210}Pb-derived chronology and the fluxes of ^{210}Pb and ^{137}Cs isotopes into continental shelf sediments, East Chukchi Sea, Alaskan Arctic. *Geochim. Cosmochim. Acta* **1994**, 59, 4435-4448.

Bigalke, M.; Kersten, M.; Weyer, S.; Wilcke, W. Isotopes Trace Biogeochemistry and sources of Cu and Zn in an intertidal soil. *Soil Science Society of America Journal* **2012**, 77, 680-691.

Birch, L.; Hanselmann K. W.; Bachofen R. Heavy metal conservation in Lake Cadagno sediments: Historical records of anthropogenic emissions in a meromictic alpine lake. *Water resources, Elsevier Science Ltd.* **1996**, 30 (3), 679-687.

Borrok, D. M.; Giere, R.; Ren, M.; Landa, E. R. Zinc isotopic composition of particulate matter generated during the combustion of coal and coal + tire-derived fuels. *Environ. Sci. Technol.* **2010**, 44, 9219-9224.

Borrok, D. M.; Wanty, R. B.; Ridley, W. I.; Wolf, R.; Lamothe, P. J.; Adams, M. Separation of cooper, iron, zinc from complex aqueous solutions for isotopic measurement. *Chem. Geol*. **2007**, 242, 400-414.

Callender, E.; Rice, K. C. The urban environmental gradient: anthropogenic influences on the spatial and temporal distributions of lead and zinc in sediments. *Environ. Sci. Technol.* **2000**, 34 (2), 232-238.

Candelone, J. P.; Hong, S.; Pellone, C.; Boutron, C. Post-industrial revolution changes in large scale atmospheric pollution of the Northern Hemisphere by heavy metals as documented in Central Greenland snow and ice. *J. Geophys. Res*. **1995**, 100, 16, 605-16.

Carignan, R.; Nriagu, J. O. Trace metal deposition and mobility in the sediments of two lakes near Sudbury, Ontario. *Geochim. Cosmochim. Acta* **1985**, 49, 1753-1764.

Chapman, J. B.; Mason, T. F. D.; Weiss, D. J.; Coles, B. J.; Wilkinson, J. J. Chemical separation and isotopic variations of Cu and Zn from five geological reference materials. *Geostand. Geoanal. Res*. **2006**, 30, 5-16.

Chen, J.; Gaillardet, J.; Louvat, P. Zn isotopes in the Seine River waters, France: A probe of anthropogenic contamination. *Environ. Sci. Technol*. **2008**, 42 (17), 6494-6501.

Cloquet, C.; Carignan, J.; Libourel, G. Isotopic composition of Zn and Pb atmospheric depositions in an urban/periurban area of northeastern France. *Environ. Sci. Technol.* **2006**, 40, 6594-6600.

Councell, T. B.; Duckenfield, K.U.; Landa, E. R.; Callender, E. Tire wear particles of Zinc to the Environment. *Environ. Sci. Technol*. **2004**, 38, 4206-4214.

Davis, A. P.; Shokouhian, M.; Ni, S. Loading estimates of lead, copper, cadmium, and zinc in urban runoff from specific sources. *Chemosphere* **2001**, *44*, 997–1009.

Dolgopolova, A.; Weiss, D. J.; Seltmann, R.; Kober, B.; Mason, T. F. D.; Coles, B.; Stanley, C. J. Use of isotope ratios to assess sources of Pb and Zn dispersed in the environment during mining and ore processing within the Orlovka-Spokoinoe mining site (Russia). *App. Geochem.* **2006**, 21, 563-579.

Frick, E. A.; Hippe, D. J.; Buell, G. R.; Couch, C. A.; Hopkins, E. H.; Wangsness, D. J.; Garrett, J. W. Water Quality in the Apalachicola-Chattahoochee-Flint River basin, Georgia, Alabama, and Florida, 1992-95. *USGS Circular 1164,* **1998**.

Fuller, C. C.; van Geen, A.; Baskaran, M.; Anima, R. Sediment chronology in San Francisco Bay, California, defined by 210-Pb, 234-Th, 137-Cs, and Pu-239, Pu-240. *Marine Chem.* **1999**, *64*, 7-27.

Gierè, R.; Blackford, M.; Smith, K. TEM study of $PM_{2.5}$ emitted from coal and tire combustion in a thermal power station. *Environ. Sci. Technol.* **2006**, 40, 6235-6240.

Giere, R.; Smith, K.; Blackford, M. Chemical composition of fuels and emissions froma coal + tire combustion experiment in a power station. *Fuel* **2006**, 85, 2278-2285.

Gioia, S.; Weiss, D.; Coles, B.; Arnold, T.; Babinski, M. Accurate and precise zinc isotope ratio measurements in urban aerosols. *Anal. Chem*. **2008**, 80 (24), 9776-9780.

Gordon, R. B.; Graedel, T. E.; Bertram, M.; Fuse, K.; Lifset, R.; Rechberger, H.; Spatari, S. The characterization of technological zinc cycles. *Resources Conservation and Recycling.* **2003**, 39 (2), 107-135.

Graedal., T. E.; van Beers, D.; Bertram, M.; Fuse, K.; Gordon, R. B.; Gritsinin, A.; Harper, E. M.; Kapur, A., Klee; R. J., Lifset, R.; Momon, L.; Spatari, S. The multilevel cycle of anthropogenic zinc. *J. of Industrial Ecology*. **2005**, 9(3), 67-90.

Groschen, G. E.; Arnold, T. L.; Harris, M. A.; Dupre, D. H.; Fitzpatrick, F. A.; Scudder, B. C.; Morrow Jr., W. S.; Terrio, P. J.; Warner, K. L.; Murphy, E. A. Water Quality in the Upper Illinois River Basin, Illinois, Indiana, and Wisconsin, 1999–2001. *USGS Circular 1230,* **2004**.

Hornberger, M. I.; Luoma, S. N.; van Green, A.; Fuller, C. C.; Anima, R. Historical trends of metals in the sediments of San Francisco bay, California. *Mar Chemistry.* **1999**, 64, 39-55.

Horowitz, A. J.; Stephens V. C. The effects of land use on fluvial sediment chemistry for the conterminous U.S. Results from the first cycle of the NAWQA Program: Trace and major elements, phosphorus, carbon, and sulfur. *Environ. Sci. Technol*. **2008**, 400, 290-314.

John, S. G.; Park, J. G.; Zhang, Z.; Boyle, E. D. The isotopic composition of some common forms of anthropogenic zinc. *Chemi. Geol*. **2007**, 245, 61-69.

Juillot, F.; Marechal, C.; Morin, G.; Jouvin, D.; Cacaly, S.; Telouk, P. Contrasting isotopic signatures between anthropogenic and geogenic Zn and evidence for post-depositional fractionation processes in smelter-impacted soils from northern France. *Geochem. Cosmochim. Acta* **2011**, 75, 2295-308.

Kavner, A.; John, S. G.; Sass, S.; Boyle, E. A. Redox-driven stable isotope fractionation in transition metals: Application to Zn electroplating. *Geochim. Cosmochim. Acta* **2008**, 72, 1731-1741.

Lamothe, P. J.; Meier A.; Wilson S. The determination of forty four elements in aqueous samples by inductively coupled plasma-mass spectrometry, *US Geol. Surv. Open File Report 02-0223-4,* **2002.** (http://minerals.cr.usgs.gov/icpms/solution.html)

Long, G. R.; Ayers, M. A.; Callender, E.; Van Metre, P. C. Trends in chemical concentration in sediment cores from three lakes in New Jersey and one lake on Long Island, New York: *U.S. Geol. Surv. Water Resources Investigations Report 02-4272*, **2003**, p 32.

Luck, J. M.; Ben Othman, D.; Albarede, F.; Telouk, P. Pb, Zn and Cu isotopic variations and trace elements in rain. *In Geochemistry of the earth's surface*, Armannsson, J., Eds., Balkema, Rofferdam, **1999**, 199-203.

MacDonald, D. D.; Ingersoll, C. G., et al. Development and evaluation of consensus-based quality guidelines for freshwater ecosystems. Archives of Environmental Contamination and Toxicology **2000**, 39, 20-31.

Mahler, B. J.; Van Metre, P. C.; Callender, E. Trends in metals in urban and reference lake sediments across the United States, 1970 to 2001. *Environ. Toxicology and Chem.* **2006**, 25 (7), 1698-1709.

Marèchal, C.; Douchet, C.; Nicolas, E.; Albarède F. The abundance of Zn isotopes as a marine biogeochemical tracer. *Geochem. Geophy. Geosyst*. **2000**, 1, 1999 GC-000029.

Marèchal, C.; Tèlouk, P.; Albarède, F. Precise analysis of copper and zinc isotopic compositions by plasma-source mass spectrometry. *Chem. Geol.* **1999**, 156, 251-273.

Mattielli, N.; Petit, J. C. J.; Deboudt, K.; Flament, P.; Perdix, E.; Taillez, A.; Rimetz-Planchon, J.; Weiss, D. Zn isotope study of atmospheric emissions and dry depositions within a 5 km radius of Pb-Zn refinery. *Atmospheric Environ.* **2009**, 43, 1265-1272.

Planchon, F. A. M.; Boutron, C. F.; Barbante, C.; Cozzi, G.; Gaspari, V.; Wolff, E. W.; Ferrari C.P.; Cescon, P. Changes in heavy metals in Antarctic snow from Coats land since the mid-19th to the late-20th century. *Earth and Planetary Sci. Letters*. **2002**, 200 (1-2), 207-222.

Rohe, W. M. *The Research Triangle: from Tobacco road to global prominence*. 1st ed. University of Pennsylvania Press, ISBN 978-0-8122-4343-7, 2011.

Rudnick, R. L.; Gao, S. Composition of the continental crust. *Treatise on Geochem.* **2003**, Chapter 3, v. 3, ISBN: 0-08-044338-9, 1-64. (http://www.geol.umd.edu/~rudnick/Webpage/Rudnick_Gao_Treatise.pdf).

Sakowski, C., Clark, S., Harwood, A., Kirk, S., Sparrow, A., Waters, A. H. *Travel North Carolina: going native in the Old North State*, 4 ed., John F. Blair Publisher, ISBN 978-0-89587-379-8, 2010.

Shiel, A. E.; Weis, D.; Orians, J. K. Evaluation of zinc, cadmium, and lead isotope fractionation during smelting and refining. *Sci. Total Environ.* **2010**, 408, 2357-2368.

Sivry, Y.; Riotte, J.; Sonke, J.E.; Audry, S.; Schafer, J.; Viers, J.; Blanc, G.; Fredier, R.; Dupre, B. Zn isotopes as tracers of anthropogenic pollution from Zn –ore smelters The Riou Mort-Lot River system. *Chem. Geology* **2008**, 255, 295-304.

Sonke, E. J.; Hoogewerft, J. A.; van der Laan, S. R.; Vangronsveld, J. A. A chemical and mineralogical reconstruction of Zn-smelter emissions in the Kempen region (Belgium), based on organic pool sediment cores. *Sci. Total Environ.* **2002**, 292, 101-119.

Sonke, E. J.; Sivry, Y.; Viers, J.; Freydier, R.; Dejonghe, L.; Andre, L.; Aggarwal, J. K.; Fontan, F.; Dupre, B. Historical variations in the isotopic composition of atmospheric zinc deposition from a zinc smelter. *Chem. Geology* **2008**, 252, 145-157.

Spliethoff, H. M.; Hemond, H. F. History of toxic metal discharge to surface waters of the Aberjona watershed. *Environ. Sci. Technol*. **1996**, 30, 121-128.

Spruill, T. B.; Harned, D. A.; Ruhl, P. M.; Eimers, J. L.; McMahon, G.; Smith, K. E.; Galeone, D. R.; Woodside, M.D. Water Quality in Albemarle-Pamlico Drainage Basin North Carolina and Virginia, 1992-95, *USGS circular 1157*, **1998**.

Stark, J. R.; Hanson, P. E.; Goldstein, R. M.; Fallon, J. D.; Fong, A. L.; Lee, K. E.; Kroening, S. E.; Andrews, W. J. Water quality in the Upper Mississippi river basin, Minnesota, Wisconsin, South Dakota, Iowa, and North Dakota, 1995-98. *USGS Circular 1211,* **2000**.

Thapalia, A.; Borrok, D. M.; Van Metre, P.; Musgrove, M.; Landa, E. R. Zn and Cu isotopes as tracers of anthropogenic contamination in a sediment core from an urban lake. *Environ. Sci. Technol*. **2010**, 44, 1544-1550.

U.S. Geological Survey, Land use and land cover digital data from 1:250,000 and 1:100,000 scale maps, Data user guide 4; *U.S. Geol. Surv.* Reston, VA, **1990**, p 25.

Van Metre, P. C.; Mahler, B. J.; Furlong, E. T. Urban sprawls leaves its PAH signature. *Environ. Sci. Technol*. **2000**, 34, 4064-4070.

Van Metre, P. C.; Wilson, J. T.; Fuller, C. C.; Callender, E.; Mahler, B.J. Collection, analysis, and age-dating of sediment cores for 56 U.S. lakes and reservoirs sampled by the U.S., Geological Survey, 1992-2001. *U.S. Geological Survey Scientific Investigations Report* **2004**, 2004-5184, 180.

Van Metre, P.; Price, K. C.; Wilson, J.; Mahler, B.; Musgrove, M. Contaminant trends reconstructed from a sediment core from Table Rock Reservoir, northwestern South Carolina. *Proceedings of the 2009 South Carolina Environmental Conference*. **2009.**

Vogelmann, J. E.; Howard, S. M.; Yang, L.; Larson, C. R.; Wylie, B. K.; VanDriel, N. Completion of the 1990s National Land Cover Data Set for the Conterminous United States from Landsat Thematic Mapper Data and Ancillary Data Sources. *Photogrammetric Engineering and Remote Sensing* **2001**, 67, 650-662.

Weiss, D.; Rausch, N.; Mason, T.; Coles, B.; Wilkinson, J.; Ukonmaanaho, L.; Arnold, T.; Nieminen, T. Atmospheric deposition and isotope biogeochemistry of zinc in ombrotrophic peat. *Geochim. Cosmochim. Acta* **2007**, 71, 3498-3517.

Wentz, D. A.; Bonn, A. B.; Carpenter, K.D.; Hinkle, S.R.; Janet, M. L.; Rinella, F. A.; Uhrich, M. A.; Waite, I. R.; Laenen, A.; Bencala, K. E. Water quality in the Willamette Basin, Oregon, 1991-95. *USGS Circular 1161*, **1998**.

Wik, A.; Dave, G. Occurrence and effects of tire wear particles in the environment- A critical review and an initial risk assessment. *Environ. Pollution* **2009**, 157, 1-11.

Wong, S.C. C.; Li, X.; Thornton, I. Urban environmental geochemistry of trace metals. *Environ. Pollution* **2006,** 142, 1-16.

Tables

Table 2.1. Lake information and land use percentages (http://www.mrlc.gov/).

Name	Nearest Major City, State	Watershed Area (km^2)	Urban % NLCD 2001	Urban % NLCD 2006
Berkeley Lake	Atlanta, GA	3.01	66	66
Lake in the Hills	Chicago, IL	24.02	66	80
Newbridge Pond	Nassau, Long Island, NY	12.96	99.6	99.6
Palmer Lake	Minneapolis, MN	58.22	75	77
Lake Panola	Atlanta, GA	0.54	5.5	5.5
Table Rock Reservoir	Greenville, SC	39.24	0	0
Tanasbrook Pond	Portland, OR	10.49	63	65
Lake Wheeler	Raleigh, NC	72.31	45	46

Table 2.2. Mean Zn concentration and δ66Zn for pre-urban, transitional, and urban periods of land use for the eight studied lakes.

Lake or Reservoir	Pre-urban (0 to ~5% urban land use)			Transitional (~5% to 70% urban land use)			Urban (>70% urban land use)		
	Ave [Zn] (mg/kg)	Ave δ^{66}Zn (‰)	n	Ave [Zn] (mg/kg)	Ave δ^{66}Zn (‰)	n	Ave [Zn] (mg/kg)	Ave δ^{66}Zn (‰)	n
Berkeley Lake	ND	ND		427±81.3	0.17±0.07	10	ND	ND	
Lake in the Hills	98.8±36.4	0.30±0.05	4	122±8.6	0.26±0.08	5	111±11.1	0.22±0.06	3
Newbridge Pond	ND	ND		ND	ND		777±244.6	0.09±0.07	9
Palmer Lake	179±4.4	0.35±0.07	2	225±33.1	0.24±0.06	5	280±16.8	0.09±0.06	3
Lake Panola	159±20.4	0.23±0.06	6	159	0.13±0.06	1	ND	ND	
Table Rock Reservoir	110±19.6	0.36±0.08	13	ND	ND		ND	ND	
Tanasbrook Pond	142.6	0.30±0.09	1	280±30.1	0.17±0.05	8	ND	ND	
Lake Wheeler	46.6±8.3	0.36±0.07	3	107±12.9	0.26±0.06	6	ND	ND	
Aggregated mean	**123±21.0**	**0.32±0.07**	**29**	**239±55.4**	**0.21±0.06**	**35**	**389±141.7**	**0.13±0.06**	**15**

All reported errors are 2σ standard deviation.
n = number of samples used in calculation of the means for each lake within each category.
ND = No data available for this land use category.

Figures

Figure 2.1: Location of lakes investigated in this study.

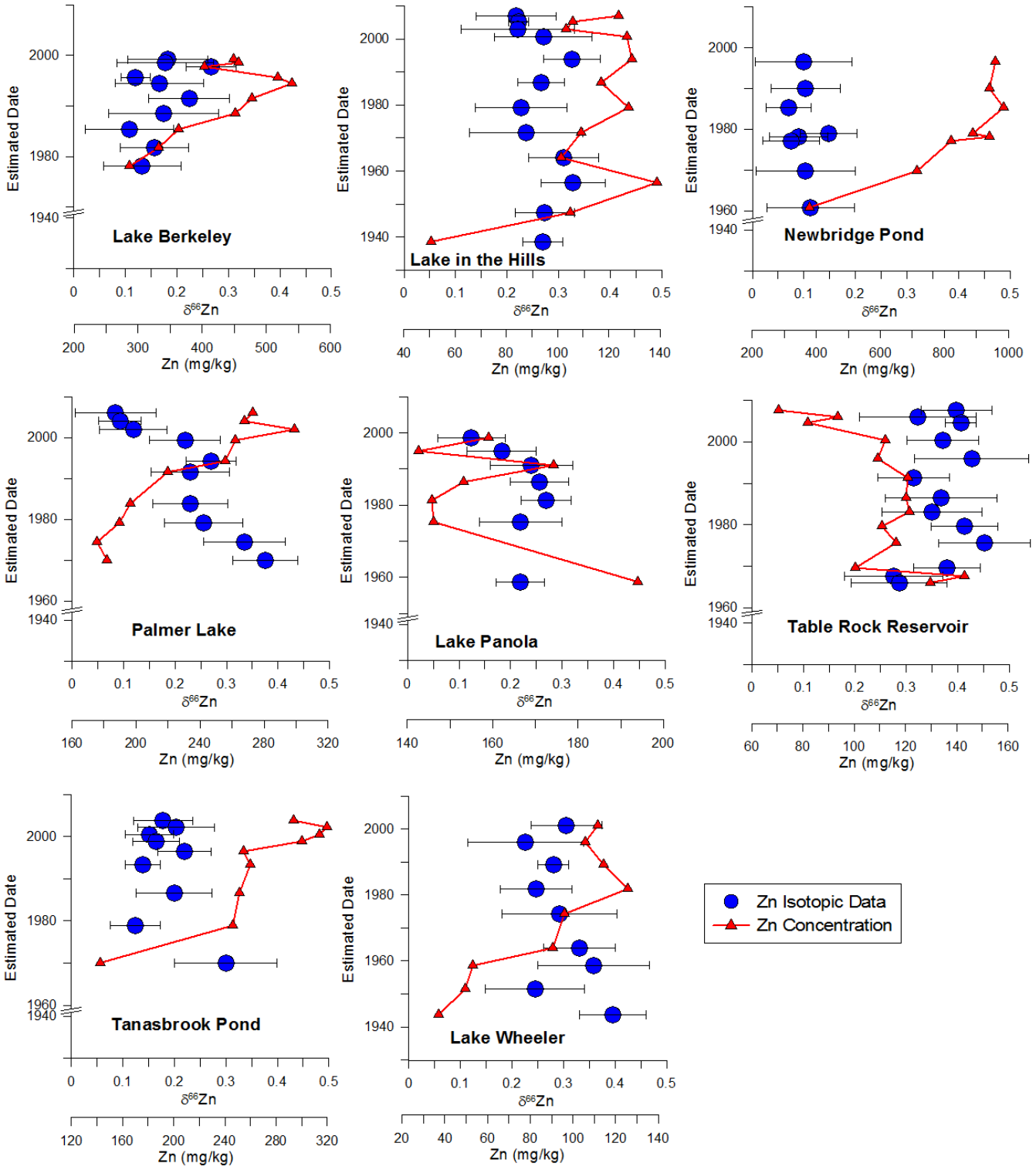

Figure 2.2: Zn concentration and isotope data for all the studied lakes, including (a) Berkeley Lake, (b) Lake in the Hills, (c) Newbridge Pond, (d) Palmer Lake, (e) Lake Panola, (f) Table Rock Reservoir, (g) Tanasbrook Pond, and (h) Lake Wheeler.

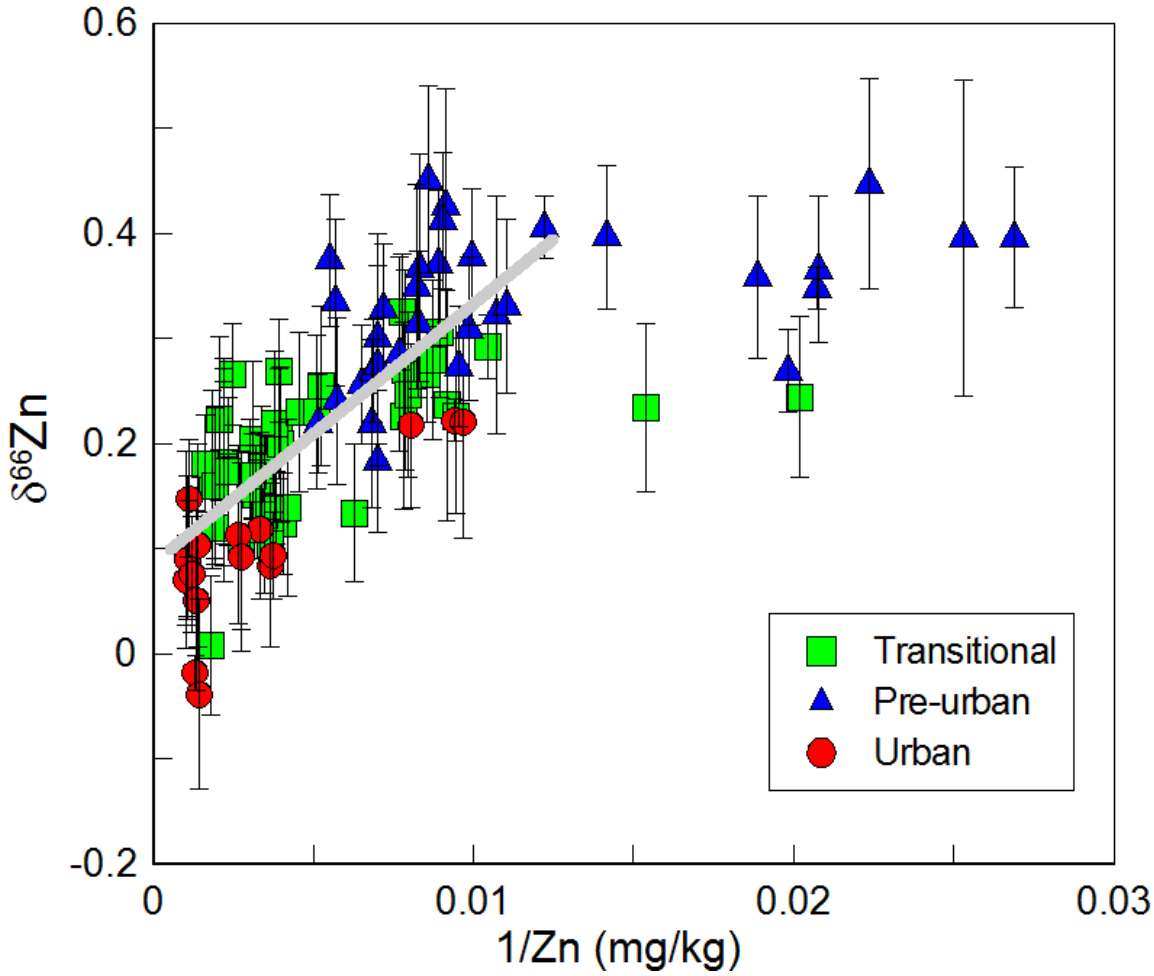

Figure 2.3: δ^{66}Zn versus 1/Zn in mg/kg for all the lake sediment data (Blue circles = pre-urban; Green triangles = transitional; Red squares = urban). The solid gray line represents a best-fit of the data, excluding the four lowest Zn concentration points. The r^2 for the line is 0.62.

Supplementary Info

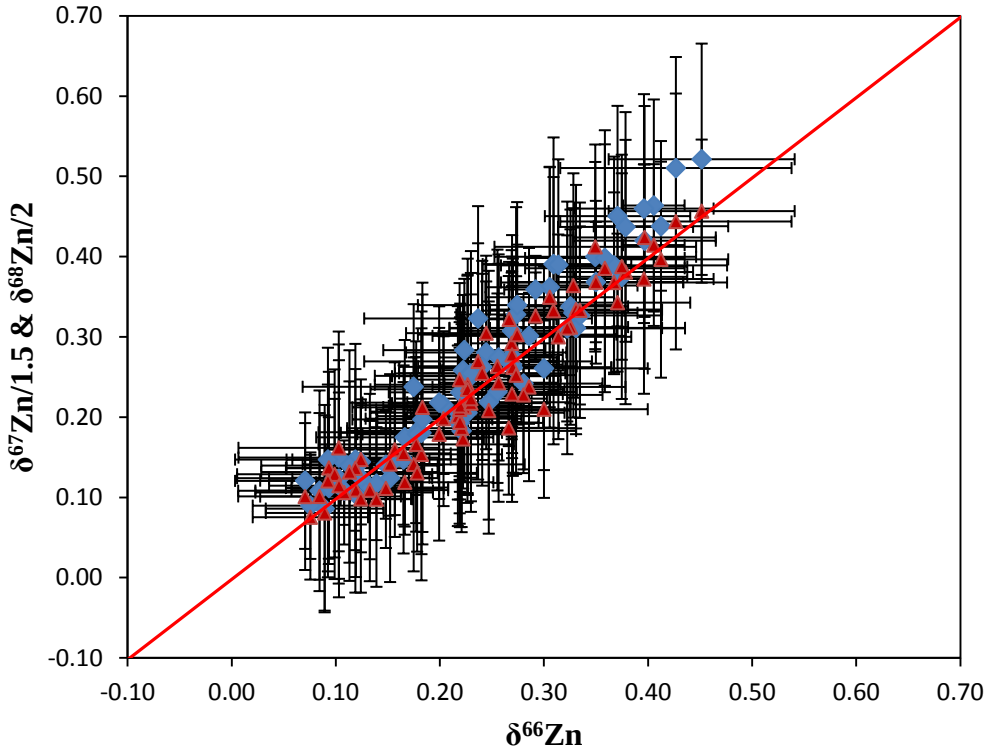

Figure S-1: $\delta^{68}Zn/2$ (red points) and $\delta^{67}Zn/1.5$ (blue points) versus $\delta^{66}Zn$. The isotopic data fit the expected mass dependency relationship, demonstrating the absence of spectral interferences.

Table S1: Isotopic and Concentration data of eight lakes in U.S.

Sample ID	Depth (cm)	Estimated Dates	Average $\delta^{66}Zn$	2s	Average $d^{67}Zn$	2s	Average $d^{68}Zn$	2s	n	Zn (mg/kg)	Digestion replicates
Lake in the Hills											
LKH-0-4	2	2006.9	0.22	0.08	0.29	0.10	0.40	0.14	4	124	2
LKH-4-8	6	2005.2	0.22	0.02	0.39	0.09	0.35	0.06	6	106	4
LKH-8-12	10	2003	0.22	0.11	0.27	0.12	0.37	0.13	5	103	2
LKH-12-16	14	2000.6	0.27	0.09	0.39	0.13	0.52	0.14	6	127	2
LKH-20-24	22	1994	0.33	0.06	0.51	0.12	0.62	0.12	4	129	2
LKH-28-32	30	1986.9	0.27	0.05	0.40	0.04	0.64	0.07	4	117	2
LKH-36-40	38	1979.3	0.23	0.09	0.38	0.15	0.48	0.14	5	128	2
LKH-44-48	46	1971.6	0.24	0.11	0.48	0.14	0.54	0.15	4	109	2
LKH-52-56	54	1964.1	0.31	0.07	0.59	0.16	0.67	0.17	4	101	2
LKH-60-64	62	1956.4	0.33	0.06	0.49	0.13	0.73	0.14	5	139	2
LKH-68-72	70	1947.4	0.27	0.06	0.49	0.13	0.50	0.12	5	105	2
LKH-76-80	78	1938.6	0.27	0.04	0.41	0.10	0.58	0.12	9	50.5	4
Berkley Lake											
BRK 0-1	0.5	1999.1	0.18	0.08	0.27	0.15	0.31	0.16	7	449	3
BRK 1-2	1.5	1998.5	0.18	0.09	0.27	0.11	0.33	0.11	5	457	2
BRK2-3	2.5	1997.7	0.27	0.05	0.40	0.11	0.37	0.08	4	404	2
BRK 4-5	4.5	1995.7	0.12	0.03	0.15	0.04	0.22	0.11	4	518	2
BRK 5-6	5.5	1994.5	0.17	0.09	0.26	0.12	0.24	0.06	5	541	3
BRK7 to 8	7.5	1991.5	0.22	0.08	0.43	0.09	0.43	0.09	4	478	3
BRK 9-10	9.5	1988.5	0.17	0.11	0.36	0.10	0.28	0.13	5	451	2
BRK 11-12	11.5	1985.4	0.11	0.09	0.16	0.04	0.21	0.06	3	363	3
BRK 13-14	13.5	1981.8	0.16	0.07	0.22	0.07	0.32	0.11	6	332	3
BRK 15-16	15.5	1978.2	0.13	0.08	0.17	0.12	0.22	0.09	5	286	3
Table Rock Res.											
TBL 0-0.5	0.25	2007.6	0.40	0.07	0.63	0.09	0.85	0.16	3	71	2
TBL 0.5-1	0.75	2006.1	0.32	0.11	0.47	0.12	0.62	0.16	3	93	2
TBL-1-1.5	1.25	2004.7	0.41	0.03	0.70	0.13	0.83	0.10	5	82	3
TBL 2.5-3	2.75	2000.4	0.37	0.07	0.68	0.14	0.69	0.09	4	112	2
TBL 4-4.5	4.25	1996.0	0.43	0.11	0.77	0.14	0.89	0.16	4	109	2
TBL 5.5-6	5.75	1991.4	0.31	0.07	0.58	0.13	0.60	0.13	4	121	2
TBL 7-7.5	7.25	1986.4	0.37	0.11	0.58	0.14	0.74	0.11	4	120	2
TBL-8-8.5	8.25	1983.1	0.35	0.10	0.60	0.12	0.82	0.13	5	121	2
TBL-9-9.5	9.25	1979.6	0.41	0.06	0.66	0.08	0.79	0.15	4	111	2
TBL10-10.5	10.25	1975.6	0.45	0.09	0.78	0.14	0.91	0.09	5	116	3
TBL-11.5-12	11.75	1969.6	0.38	0.06	0.66	0.14	0.76	0.16	3	100	2
TBl 12-12.5	12.25	1967.7	0.27	0.10	0.51	0.13	0.61	0.11	5	143	2

TBL 12.5-13	12.75	1966.0	0.29	0.09	0.45	0.11	0.48	0.12	4	130	2
Lake Wheeler											
WEE 1.1-0-3	1.5	2001	0.31	0.06	0.54	0.15	0.70	0.16	7	112	2
WEE 1.1-3-6	4.5	1996	0.23	0.09	0.31	0.10	0.47	0.14	6	106	3
WEE 1.1-6-9	7.5	1989	0.28	0.08	0.36	0.11	0.46	0.09	5	114	2
WEE 1.1-9-12	10.5	1982	0.25	0.08	0.33	0.16	0.42	0.14	9	126	3
WEE 1.1-12-15	13.5	1974	0.29	0.03	0.54	0.04	0.65	0.05	5	96	2
WEE 1.1-15-18	16.5	1964	0.33	0.08	0.47	0.13	0.67	0.16	5	90	3
WEE 1.1-18-21	19.5	1959	0.36	0.08	0.60	0.16	0.77	0.15	10	53	3
WEE 1.1-21-24	22.5	1952	0.24	0.08	0.42	0.12	0.61	0.06	7	49	2
WEE 1.1-24-27	25.5	1944	0.40	0.07	0.69	0.14	0.74	0.14	9	37	3
Tanasbrook Pond											
TNB.1. 0-3	1.5	2003.7	0.18	0.06	0.27	0.08	0.26	0.10	7	294	3
TNB.1-3-6	4.5	2002.1	0.20	0.07	0.32	0.09	0.40	0.11	7	320	3
TNB.1-6-9	7.5	2000.5	0.15	0.05	0.19	0.13	0.28	0.06	5	314	2
TNB ZN 9-12	10.5	1998.8	0.17	0.05	0.22	0.12	0.31	0.09	7	300	3
TNB.1-12-15	13.5	1996.4	0.22	0.05	0.30	0.09	0.39	0.13	7	254	3
TNB.1-15-18	16.5	1993.3	0.14	0.03	0.18	0.07	0.20	0.11	5	260	2
TNB.1-21-24	22.5	1986.6	0.20	0.07	0.33	0.12	0.36	0.13	5	252	2
TNB.1-27-30	28.5	1979.0	0.12	0.05	0.22	0.08	0.20	0.12	9	246	3
TNB.1-33-36	34.5	1970.0	0.30	0.10	0.39	0.13	0.42	0.11	7	143	3
Lake Panola											
PAN.B 0.5	1.5	1998.5	0.12	0.07	0.19	0.09	0.29	0.10	8	159	2
PAN.B 2-3	2.5	1994.9	0.18	0.07	0.30	0.16	0.42	0.16	6	143	2
PAN.B 4-5	4.5	1990.9	0.24	0.08	0.39	0.12	0.51	0.14	10	174	2
PAN.B 6-7	6.5	1986.5	0.26	0.06	0.41	0.13	0.49	0.15	13	153	2
PAN.B 8-9	8.5	1981.3	0.27	0.05	0.46	0.12	0.56	0.12	7	146	2
PAN.B 10-11	10.5	1975.3	0.22	0.08	0.29	0.13	0.42	0.13	7	146	2
PAN.B 14-15	14.5	1958.6	0.22	0.05	0.31	0.08	0.49	0.12	8	194	2
Newbridge Pond											
NEW.3 2-3	2.5	1996.5	0.10	0.09	0.19	0.10	0.26	0.13	9	958	3
NEW.3 12-13	12.5	1990.0	0.10	0.07	0.18	0.15	0.23	0.12	7	942	2
NEW.3 18-19	18.5	1985.3	0.07	0.04	0.18	0.09	0.20	0.09	7	984	2
NEW.3 26-27	26.5	1979.0	0.15	0.06	0.21	0.07	0.22	0.07	5	889	2
NEW.3 27-28	27.5	1978.1	0.09	0.06	0.13	0.13	0.16	0.12	6	942	2
NEW.3 28-29	28.5	1977.2	0.08	0.06	0.13	0.07	0.15	0.08	8	822	3
NEW.3 36-37	36.5	1969.7	0.10	0.10	0.22	0.16	0.32	0.13	7	714	2
NEW.3 46-47	46.5	1960.8	0.11	0.08	0.21	0.14	0.26	0.11	6	378	2

NEW.3 48-49	48.5	1958.7	0.09	0.09	0.22	0.14	0.24	0.12	9	363	3
Lake Palmer											
PLM.WB 0-1	1.5	2006.1	0.08	0.08	0.16	0.13	0.20	0.10	11	273	3
PLM.WB 2-3	2.5	2004.2	0.09	0.04	0.17	0.09	0.27	0.12	9	268	2
PLM.WB 4-5	4.5	2002.0	0.12	0.07	0.22	0.11	0.27	0.15	10	299	3
PLM.WB 6-7	6.5	1999.5	0.22	0.07	0.35	0.11	0.43	0.12	8	262	2
PLM.WB 10-11	9.5	1994.3	0.27	0.05	0.40	0.12	0.46	0.13	7	256	2
PLM.WB 12-13	12.5	1991.6	0.23	0.08	0.38	0.16	0.43	0.14	5	220	2
PLM.WB 18-20	19	1983.9	0.23	0.07	0.38	0.13	0.45	0.10	7	197	3
PLM.WB 22-24	23	1979.2	0.26	0.08	0.35	0.12	0.53	0.15	8	190	3
PLM.WB 26-28	27	1974.6	0.33	0.08	0.49	0.11	0.67	0.13	6	175	2
PLM.WB 30-32	31	1970.0	0.37	0.06	0.56	0.15	0.78	0.12	7	182	2

SECTION 3

An Integrated Geochemical, Geophysical And Sedimentological Approach To Delineate Freshwater-Brackish Water Intrusion From Well Logs Of The Hueco Bolson, El Paso Area

3.1 Abstract

Determining the quantity and quality of aquifers is critical for planning future growth in the arid regions of West Texas, southern New Mexico and northern Mexico. It is vital to accurately delineate the boundary between the fresh and brackish water of an aquifer, especially in regions where aquifers are the primary sources of water supply. The objective of this study is to determine how both structure and sedimentology play a vital role in controlling the location of freshwater in the northern part of Hueco Bolson Aquifer. Our study indicates that subsurface faults act as barriers to flow and serve to compartmentalize fresh/saline water in the east of Northern part of the Hueco Bolson Aquifer. Well logs suggest the depositional framework and sedimentological facies of this region represents playa sediments. It appears that saline water is concentrating in regions where the playa sediments are thicker. Integrating both digital well logs and geochemical analysis of these wells clearly delineate the boundary of saline and fresh water and its relation to structural and sedimentological features. Increased understanding of controls on the location of saline/fresh water will aid in future groundwater flow modeling and resource management. This study also will help to predict where we might be more likely to encounter fresh water in basins that have not yet been drilled and explored in the desert southwest region.

3.2 Introduction

The El Paso, Texas-Juarez, Mexico region is located in the tectonically active Rio Grande Rift where the stress changes strike from north-south to northwest-southeast. This region includes basins that contain alluvial aquifers that are the sources of water for the municipal needs of El Paso and Ciudad Juarez, Mexico. The Hueco Bolson, an asymmetrical basin that covers approximately 1.6 million acres (0.65 million hectares), is located east of the Franklin Mountains

and west of the Hueco Mountains (Figure 3.1). The basin forms the Hueco Bolson aquifer (HBA) that is cut by faults that appear to serve as either barriers or conduits to regional groundwater flow. It is difficult to trace many of these faults at the surface due to the highly urbanized nature of the region.

The HBA consists of unconsolidated to slightly consolidated deposits of fluvial, evaporitic, alluvial fan and aeolian origin having a maximum thickness of 9,000 ft (Mattick, 1967). The HBA contains both fresh water and brackish where the top part at about 250 to 400 ft produces good quality water and the bottom part consists of primarily brackish to saline water. It is vital to understand how the boundary between fresh and brackish water of the HBA changes over time in order to avoid contamination of the fresher water. One important step is to identify the major subsurface structures and stratigraphy of the aquifer that act as conduits or barriers to fluid flow to minimize the incursion of the brackish water into fresh water supplies. Here we attempt to use a combination of geophysical well-logs, geochemical water analysis and microgravity data to locate subsurface structures, such as faults, and lithological changes that control water flow and salinity.

The El Paso Water Utilities (EPWU) has noted salinity increases throughout production wells in the HBA due to the increase in concentrated salts (evapotranspiration on the surface) and shallow subsurface salt precipitation from a series of droughts (increased aridity) in the 1940s and 1950s (Fisher and Mullican, 1990). Precipitation after droughts dissolves significant amounts of sodium, calcium, magnesium, chloride and sulfate ions from shallow/surface salt crusts that recharge the aquifer and changes salinity, especially the fresh water in the shallow parts of the HBA (Young, 1981). Some of the production wells have been retired and plugged due to the excessive TDS concentrations. Understanding the groundwater chemistry of the

producing wells is useful for identifying the path of recharge and the lateral extent of groundwater flow. This study provides in depth knowledge of subsurface structures and how they interact with the groundwater flow and recharge in the northern Hueco Bolson. In addition, this study helps provide information to augment existing groundwater flow models and aids in the development of new freshwater wells for sustainable resource management.

3.2.1 OBJECTIVES OF THE STUDY

This present study focuses on:

- Identifying lateral and vertical distribution of groundwater quality within the subsurface
- Tracking the variations of water quality in terms of salinity, especially Cl and SO_4 during the ~50 year period of water production from the bolson
- Observing the relationship between cation and anion distribution to understand the variation of groundwater composition and its sources.
- Analyzing the role subsurface structures e.g., faults and depositional sedimentological facies play in groundwater quality.

3.2.2 LOCATION OF THE STUDY AREA

The Franklin Mountains and the Hueco Mountains define the eastern and western boundaries of the Hueco Basin (Figure 3.1a). Our study area lies to the north of the downtown El Paso region from Loop 375 to the Texas-New Mexico border (Figure 3.1a).The northern boundary of the Hueco basin is a groundwater divide separating it from the Tularosa basin. The Hueco basin extends southward to the Sierra del Presidio in Mexico (Figure 3.1b).

The cross-section shown in Figure 3.2 (Heywood and Yager, 2003), illustrates the Hueco Bolson is a deep basin bounded by normal faults along both the Franklin and Hueco Mountains. About 200 ft (60 m) of Rio Grande alluvium overlies the Hueco Bolson deposits in the valley portions

of the study area (Figure 3.2). Note that fresh groundwater is limited to a relatively thin lens on the western side of the asymmetric Hueco basin with highly saline water found below it. Previous studies have not related the major and minor faults to groundwater flow. This study addresses the role of subsurface faults and the depositional framework on the groundwater flow and water chemistry within the Northern HBA.

3.2.3 GEOLOGICAL SETTING

Figure 3.3 shows the geological map of the study area. The geological history of the El Paso region spans complex geologic processes that range from Precambrian to Cenozoic in age. The details of these geologic processes are outlined in the previous studies of Lovejoy (1976), LeMone and Simpson (1983), Seager and Mack (1986), Baldridge (2004), and McMillan et al. (2000). Compressional forces associated with the subduction of the Farallon Plate about 50 Ma (Seager and Mack, 1986; Baldridge, 2004; Seager 2004) initiated crustal deformation and shortening, uplift and tilting of the Franklin Mountains (Lovejoy, 1976). In middle Eocene to Oligocene time, magmatic activity produced intrusions into Cretaceous age rocks to form the Cerro de Cristo Rey, the Campus Andesite and other smaller intrusive bodies in the El Paso and Sierra de Juarez area (Hoffer, 1971; Lovejoy, 1976; Henry and Price, 1985; Keller, 1990). These intrusions predate Cenozoic extensional events but postdate the compressional Laramide orogeny (McMillan et al., 2000). During Laramide deformation, maximum principal horizontal stress, S1, was compressive and directed to the east-northeast and this compression ended in the early Eocene (Henry and Price, 1985). Basaltic magma intruded Basin and Range normal faults from about 24 Ma and this igneous activity ceased at about 17 Ma (Henry and Price, 1985). The igneous activity indicates a shift of S1 from compression to north to north-northwest Basin and Range extension at about 24 Ma (Henry and Price, 1985). This region underwent another change

in S1 direction from east-northeast to west-northwest extension (current orientation) about 10 Ma as the Rio Grande rift opened (Henry and Price, 1985).

The Rio Grande Rift extends from central Colorado to west Texas and northern Chihuahua, Mexico and consists of a series of asymmetrical grabens, including the Hueco bolson (Chapin, 1971; Seager et al., 1984; Collins and Raney, 1991; 2000; Keller and Baldridge, 1999). Two different styles of basins were produced due to the two phases of extension in the Rio Grande rift (Seager et al., 1984; Morgan, et al., 1984). During mid-Oligocene to early Miocene, extension resulted in the formation of broad and relatively shallow basins with low angle normal faults. In the mid-Miocene to Quaternary periods, extension produced high angle faults bounding relatively deep and narrow basins (Morgan, et al., 1984; Keller and Baldridge, 1999). Recent studies using geophysical and petrophysical mapping techniques have found that extension of the Rio Grande rift is still continuing today along faults reactivated in the Quaternary (Avila, 2011; Marrufo, 2011; Budhathoki, 2013).

Hueco Bolson basin fill is composed of fluvial, lacustrine and aeolian sediments of Tertiary to Quaternary in age (Figure S1 in Appendix; Hadi, 1991; Anderholm and Heywood, 2003; Haywood and Yager, 2003). Stratigraphically, the Fort Hancock Formation mostly consists of lacustrine and alluvial fan deposits along with some fluvial deposits of the ancestral Rio Grande River (Gustavson, 1990; Hawley, et al., 2002). The Camp Rice Formation, overlying Fort Hancock Formation, is mostly composed of sand and gravels of a braided fluvial system and alluvial fans (Collins and Raney, 1991). Wells tap water from aquifers in both the Fort Hancock and Camp Rice Formation and they are the primary sources of groundwater in El Paso region. Sediments in the Hueco Basin are broadly divided into five major categories based on depositional environments: 1) fluvial, 2) alluvial fan, 3) lacustrine-playa, 4) playa margin, and 5)

recent alluvial facies (Haywood and Yager, 2003; Marrufo, 2011). Most fluvial deposits of the HBA are related to the ancestral Rio Grande which was braided system depositing pebbly medium to coarse sand sediments (Gustavson, 1990; Haywood and Yager, 2003; Mack et al., 2006). Playa lake sediments were carried out to the basin by the northern ancestral Rio Grande in the central, eastern and southeastern parts of HBA (Gustavson, 1990). Playa lake deposits found in the central basin consist of predominantly fine grained silt and clay from settling of suspension with thick shale beds (Doser and Langford, 2006). Playa margin deposits found closer to the edges of the basin are mainly composed of clayey silts and silty clays along with carbonate nodules and white silty sands (Doser and Langford, 2006; Marrufo, 2011).

3.3 Data Collection (Methodology)

We use a combination of water well logs, microgravity surveys and geochemical analyses of water wells to identify faults and facies changes and their relations to the observed water chemistry (both freshwater and brackish water) of the northern HBA. The location of water wells from the northern HBA where both geochemical and log data were collected are shown in the Figure 3.4. Since the geochemical data of the well samples are close to each other, this data set allows us to adequately distinguish the connectedness of the aquifer units and the differences between them. The data collection for this project involved two steps:

1. Compilation and documentation of well data and water quality information
2. Comparison of these data with previous geophysical and geological investigations

1. We used water geochemical data and well logs of 44 wells obtained from the EPWU, U.S. Geological Survey (USGS), Texas Water Development board and other published studies (e.g., Druhan et al., 2008) in the northern HBA. We utilized geochemical data from the EPWU for 35 production wells that have been collected over 50+ years. In this

study, we have done well log analysis on 18 digital log data to understand the depositional environments in northern HBA. Four major depositional facies and erosional surfaces are established by grain size analysis from well cuttings at well 601 (Marrufo, 2011) located to the south of the study area (Figure 3.4) are extrapolated to classify facies in the study area. Budhathoki (2013) utilized digital well log suites to enhance the understanding of the subsurface stratigraphic facies based on the sedimentological and stratigraphic framework of the HBA presented by Marrufo (2011). This included examining log characteristics, stacking patterns, and erosional surfaces to characterize depositional environments (see Budhathoki, 2013). In order to use existing well data from all sources, we evaluated the nomenclature, accuracy and location of the wells. We converted all data to the same format (i.e. units) and incorporated it into a common database. The data were assembled and incorporated in GIS maps showing type of data obtained for each well (see Figure 3.4). Isotopic data from selected wells in the northern HBA were found from a literature search and these interpretations are utilized to understand the recharge and groundwater flow patterns.

2. After a detailed literature review, we compiled various results of studies conducted in the El Paso region that focused on geology and geophysics of the Hueco Bolson basin and tectonics of the Rio Grande rift. In particular, we use results from microgravity studies conducted in the south-central HBA (Marrufo, 2011; Avila, 2011) and from microgravity data collected and modeled in the northern HBA by Budhathoki (2013).

3.4 Results/Discussions

We analyzed chemical concentrations for major solutes and Total Dissolved Solids (TDS) with respect to time and space both vertically and laterally across our study area. Then we

collectively compared TDS and chloride concentrations to similar studies that have been conducted for waters of the Rio Grande system and other arid regions (e.g. Wen et al., 2005; Druhan et al., 2008). We also used ion trend plots and Piper diagrams to examine changes in reactive solutes (sodium, calcium, magnesium, potassium, sulfate and bicarbonate) within the study area. These ions interact with mineral phases in different flow paths such as mixing with ground water and evaporation within the HBA.

3.4.1 TDS AND CL LIMITS FOR DRINKING WATER

Aqueous salinity refers to the dissolved mineral content of the water which is reported as total dissolved solids (TDS) in mg/L or parts per million (ppm) (USGS, 1999). Several categories of salinity are classified based on TDS concentration ranging from freshwater to brines (Table 3.1, Hanor, 1994).

The United States Environmental Protection Agency (USEPA) national drinking water standards for chloride (250 mg/L), sulfate (250 mg/L), and TDS (500 mg/L) are also known as recommended maximum concentration levels. These are the maximum desirable concentrations for potable waters, although most humans can tolerate higher concentrations of these inorganic constituents. Concentration of Total Dissolved Solids (TDS) is used to characterize the water quality and chloride is one of the components of TDS. In Texas, the standard for TDS is 1000mg/L and for chloride is 250 mg/L, as used to define potable fresh groundwater (Hutchison, 2006). The chloride limit often exceeds drinking water standard before TDS in the wells of the Hueco Bolson (Bredehoeft, et. al., 2004). Alternatively, chloride concentration data can be used to map distributions in salinity where a chloride concentration between 250-500 mg/L is considered as transitional between fresh and brackish water (Bredehoeft, et. al., 2004).

3.4.2 DISTRIBUTION OF GROUNDWATER QUALITY IN NORTHERN HBA

Groundwater quality varies with depth in the HBA and distance from the mountain front along different recharge pathways. We analyzed the vertical and lateral variation in groundwater quality using TDS depth maps and integrated cross sectional profiles of microgravity, depositional facies and geochemical variation. In order to differentiate the geochemical trends of the wells, we have separated the wells into two distinct groups and compared with isotopic data from previous studies for wells in the area. Based on the location of a well and TDS values, we classified wells either as mountain front (MF) wells near the Franklin Mountains or central basin wells (CB) wells within the basin, as they have significant changes of salinity (TDS) in the HBA. The individual TDS, Cl and SO_4 measurements were averaged over different depth and time from which the water is tapped by El Paso Water Utilities as represented in the appendix table A1.

Cl and SO_4 are primarily used to analyze the trends of the MF and CB wells. Trend analysis of Cl and SO_4 shows the following four distinct Cl and SO_4 trends**:** 1:2 trend; 1.5:1 trend; 4:1 trend; 12:1 trend (Figure 3.5). The low concentration of Cl ions occurs in the potable fresh water zones of about 15% MF wells forming one distinct trend with a Cl: SO_4 ratio of 1:2. The majority of MF wells (85%) indicate a Cl: SO_4 ratio of 1.5:1 trend but MNST05 is categorized as a CB well (Figure 3.5). About 53% of the CB wells show high Cl (greater than 200 mg/L) and low HCO_3 (less than 100 mg/L) concentrations in the brackish-saline water quality zones. 53% of CB wells have a Cl: SO_4 ratio of 4:1, except for one MF well, TH43A (Figure 3.5) that also shows this ratio. In some wells, such as in CB well 62, the deeper samples show a 4:1 trend whereas a few shallow well samples show a 1.5:1 trend (Table 3.2). This 4:1 trend agrees well with the majority of earlier studies for CB well MNST02 and MF well TH43A (Druhan et al., 2008). The high salinity end member of CB well 521 from this study fits a Cl:

SO_4 ratio of 12:1; consistent with the CB well FBT10 and NH series wells that we categorize as MF wells (Druhan et al., 2008). The average values of time for all the trends of wells are given in the Table 3.2 and compared with datasets from Druhan et al, 2008.

The overall chemical character of the groundwater of wells in the study area is best displayed through use of Piper diagrams. Piper diagrams are used to classify the water by hydrochemical facies, and overall geochemical mixing/evolutionary trends of the groundwater. Hydrochemical facies show distinct zones of cation and anion concentrations as a function of lithology, water-rock interaction and flow patterns of the aquifer (Figure S2; Back, 1966). The trilinear Piper diagram shows all well data plotted between the HCO_3 and Cl end members of the anion triangle and between the Na+K and Ca end members of the cation triangle (Figure 3.6). Both cation and anion points from the samples are then projected on to a central diamond shaped plot that is parallel to the upper edges of the trilinear diagrams. The Piper diagram (Figure 3.6) shows three classes of hydrochemical facies: theCa-Na-HCO_3 type, Na-Cl type and mixed Ca-Na-HCO_3-Cl type. The general trend of freshly recharged groundwater, a Ca-Na-HCO_3 type, is observed in MF wells while the CB wells have more saline water of the Na-Cl type. The HCO_3 type groundwater has low TDS concentrations and occurs near the areas with freshwater infiltration. The relative concentrations occur in the order of Ca >Na+K>Mg for cations and HCO_3>Cl>SO_4 for anions in the recharge zones (MF). Most of the saline wells with TDS of 1000 mg/L to 10,000 mg/L have cation concentrations in the order of Na+K > Ca >Mg and anions in the order Cl>SO_4>HCO_3 moving towards the CB. Mixed Ca-Na-HCO_3-Cl facies are recorded by both MF and CB wells.

3.4.2.1 Ion Relations and Sources of Major Components in HBA

We analyzed the relationship of cations and anions for all wells in Table 3.2 except those studied by Druhan et al. (2008) where all the cations and anions data are unavailable. The TDS values below 1000mg/L (low salinity) indicate the groundwater samples have a low content of soluble salts (Figure 3.7). For most MF wells with TDS below 500 mg/L, the Na/Ca ratio is also low (<3). For instance, wells 52 and 33 (MF wells with cyan circles) have freshwater with TDS below 500 mg/L and Na/Ca ratios less than 3. The highest TDS values are observed in the CB wells. The data are more scattered above 1500 mg/L with Na/Ca ratio greater than 3, as seen in wells 521, 53, 54 with red triangles (Figure 3.7).

We used scatter diagrams (Figure 3.8 a-f) to characterize the ion ratios of potential sources of salinity and to differentiate between them. Bicarbonates (HCO_3), sulfates (SO_4), chloride (Cl), sodium (Na), calcium (Ca), and magnesium (Mg) ions have been enriched in HBA wells through time. The similar trend was observed by Wen, et al., 2005 in the Ejina basin of northwest China and Adi (2013) in western Saudi Arabia.

Figure 3.8a, a plot of Ca+Mg vs. SO_4+ HCO_3, shows two distinct groups of data within the northern HBA. The group of data that lies above the 1:1 line shows the abundance of Ca+Mg relative to SO_4+ HCO_3 in the 12:1 trend (CB) wells. The data group that lies below the 1:1 line indicates more sulfate and bicarbonate ions might be leaching from calcareous sediments and gypsum in the 1:2 trend (MF) wells.

Figure 3.8b shows the Ca+Mg vs. HCO_3 clearly indicate two trends in the data. The MF wells (1:2 and 1.5:1 trends) seem to have excess amounts of HCO_3 compared to the CB wells (4:1 and 12:1 trends). Except for 8% of the data that fit the 1.5:1 trend, all the data that fit the 1:2, 1.5:1, 4:1 trends fall below the 1:1 line showing less Ca+Mg and more HCO_3 ions. Excess of HCO_3 ions in these wells have been balanced by cations such as Na +K (Adi, 2013). Data from

high salinity wells (12:1 trend) plot above the 1:1 line indicating a deficiency of HCO_3 relative to Ca+Mg (Figure 3.8b).

Figure 3.8c shows a plot of Na+K vs. Cl + SO_4: Note that all the data fall on or below the 1:1 line. Most (95%) of the low salinity MF wells (1:2 trend) do not contain Cl + SO_4 ions. On the other hand, the high salinity CB wells (12:1 trend) have more Cl + SO_4 as compared to Na+K and they fall below 1:1 line. As expected, the other MF (1.5:1 trend) and CB (4:1 trend) wells have low Cl+ SO_4 and Na+K values that lie between the two end-members (the 12:1 and 1:2 trends).

The general trend for Na vs. Cl in Figure 3.8d is the same as in Figure 3.8c. We can clearly distinguish between the two end-members: Cl ions are elevated in high salinity wells (12:1 trend) and are low in low salinity wells (2:1 trend). When the Na/Cl molal ratio is equal to 1, it typically indicates the salt sources are from halite dissolution in the HBA (Meybeck, 1987). Approximately 20% of data show Na is greater than 1 and fall below the 1:1 line, suggesting the excess Na ions are released from silicate weathering (Meybeck, 1987).

Figure 3.8e shows Na+K vs. total cations where low salinity (MF) wells do not fall on the 1:1 line. This plot shows the distribution of total cations increases in the 12:1 trend (CB) wells as compared to 4:1 and 1.5:1 trends. Most of the data fall below the 1:1 line suggesting that the cations come from silicate weathering (Wen et al., 2005; Adi, 2013).

Figure 3.8f shows a plot of HCO_3 vs. Cl ions in which we can differentiate between two end-members, 1:2 trend and 12:1 trend. Low salinity (MF) wells have HCO_3 dominant and high salinity (CB) wells have more Cl ions.

A Gibbs plot can be used to deduce the process, such as precipitation, evaporation, and rock-water interaction that governs the water composition and aquifer lithological characteristics

(Gibbs, 1970; Wen et al., 2005). Figure 3.9 shows the variation in the ratios of Na/Na+Ca and $Cl/(Cl+HCO_3)$ with respect to TDS. The TDS versus cations plot (Figure 3.9, left) suggests the cations are coming from evaporative processes that are common in arid regions such as the HBA. The TDS versus anions (Figure 3.9, right) shows the low salinity water of MF wells, both the 1.5:1 and 4:1 trends; have anions coming from rock weathering. The high salinity CB wells have anions predominantly obtained from the evaporation processes. Thus the Gibbs plots suggest the composition of water is affected both during chemical weathering of rock forming minerals and evaporation of recharge along the Franklin Mountains and periphery. A field leach test from the calcareous sediments shows anions can dissolve easily (be leached out) into the water as compared to cations from the dissolution of soil salts (Thapalia et al., 2011). We can clearly observe a similar anion chemistry of groundwater in the HBA as shown in the Gibbs plots (Figure 3.9). Previous studies have highlighted different processes governing the chemical evolution of water in HBA including evapotranspiration of precipitation, infiltration and dissolution of gases and minerals, ion exchange, and mixing of fresh water and brine (Anderholm and Heywood, 2003).

3.4.2.2 Vertical Variation

We used Surfer 8.0 software to generate TDS distribution maps in wells at depths ranging from less than 500ft, 500 to 800ft, and greater than 800 ft (Figures 3.10 to 3.12). The individual TDS measurements for each well were averaged over different depth and time as provided the data in El Paso Water Utilities as shown in the appendix Table A1. Each well has different producing intervals and the samples from that corresponding depth are utilized to generate the salinity distribution maps. The cooler colors (blue) indicate fresh groundwater and warmer color

(red and pink) indicate brackish and saline water, respectively. Also, each map is labeled with contour lines to show TDS variations.

A) TDS Distribution at 500ft (Figure 3.10):

The shallow part of the HBA parallel to the Franklin Mountains along the boundary near well 52 (Figure 3.10) contains TDS below 1000mg/L. Some of the samples near the eastern boundary of the study area show higher salinities (> 3500 mg/L). Freshwater with TDS of less than 500 mg/L is observed in small pockets that are limited to the mountain front near wells 52 and 33; the southern basin at wells 40, 51, 522, 62; and the northwestern basin at wells 42, E5, LF4, and E6. The freshwater pockets are positioned between the mountain front infiltration zone and the deeper saline aquifer and are a primary source for freshwater in the El Paso region (Wilkins, 1986; Hibbs, et al., 1997).

B) TDS Distribution at 500-800ft (Figure 3.11):

This depth section shows separate pockets of freshwater and brackish water but the fresh water (TDS < 500 mg/L) zone is narrower than in Figure 3.10. A freshwater pocket is found at southwest corner of map near well 52 that extends to southeast corner near well 601, 522 and 40A; however brackish groundwater (with TDS up to 4000mg/L) is encountered near wells NH1, NH2 and TH43A which are close to the mountain front north of freshwater well 52. Interestingly, the freshwater seems to be bounded by the East Franklin Boundary fault that extends diagonally to the west near well 52 (Figure 3.3). This might suggest the fault acts as a structural control between the freshwater and brackish water zones. The southeastern edge of the fresh water zone is clearly bounded by NW-SE striking faults mapped by Marrufo (2011) and Collins and Raney (2000). In addition, faults mapped by Collins and Raney (2000) can be

extended to the northwest to connect to recently identified faults (Budhathoki, 2013) that appear to form the freshwater-brackish water boundary in the northern portion of the study area.

C) TDS at 800-1100ft (Figure 3.12):

Some wells do not penetrate to this depth, but the remaining wells show freshwater is limited to the mountain front near wells 52 and 33 and to wells 29, 51, 62, 521, and 601 in the basin and the southeastern boundary of the study area. The salinity increases with depth and studies have reported TDS values exceeding 35,000 mg/L in the deepest sections of the basin (Hibbs et al., 1997).

3.4.2.3 Lateral Distribution of TDS and Cl

The sample location map shows all wells along with the types of data available for each well in the study area (Figure 3.4). We selected three east-west oriented profiles and one north-south oriented profile to examine the variation in TDS, Cl and SO_4 over the past 50 years (Figure 3.13). These profiles are chosen because the geologic contacts, densities, and fault constraints along these profile lines are reasonably well understood from previous studies (e.g., Collins and Raney, 1991; 2000; Hawley et al., 2009; Avila, 2011; Marrufo, 2011; Budhathoki, 2013).

I. Profile A-A' (Figure 3.14A, B and C)

This west-east profile crosses the northern edge of study area along the Texas-New Mexico border (Figure 3.13). Groundwater from north of the New Mexico/Texas state line is reported to have TDS > 1000 mg/L (A Binational Publication, 1998); however well E6, closest to the mountain front, has a TDS in the range of 500 mg/L. The TDS value increases to 800 mg/L in well E7 and then decreases dramatically to 300mg/L in well LF4 (Figure 3.14A and C). Fresh groundwater occurs in the range of 300-885 ft in wells E6, E7 and LF4, but brackish water

is abundant at depths greater than 1000ft in well E3A (Figure 3.14B, C) (see appendix table A1). This abrupt change in water chemistry between the three wells suggests the freshwater pockets might not connect to each other. Seager (1980) suggested a fault is located between wells E7 and LF4 as shown by the dashed line in Fig 14A. In addition, the geochemical profile shows a change in TDS and Cl concentration in the water samples over time (Figure 3.14C). Water chemistry in wells E6 and LF4 remains the same over a time period of about 50 years. In contrast, well E7 has experienced an increase in salinity since 1976 to the present time as indicated by changes in TDS and Cl.

Water samples of all wells along profile A-A' section are mostly dominated by Na and Ca (cations) and Cl and HCO_3 (anions) (Figure 3.15). The Piper diagram for this cross-section shows the dominance of Na-Ca-HCO_3 in well E6 (circles) and Na-Cl in well E7 (squares). Well LF4 (triangles) shows a mixing trend between Na-Cl and Ca-HCO_3. Wells close to Franklin Mountains seems to have predominantly more Na-Ca- HCO_3, and Cl ions become dominant towards the basin.

The gravity profile (Figure 3.14A) shows a major anomaly where it crosses the prominent East Boundary Fault of the Franklin Mountains (Richardson, 1909; Lovejoy, 1976) on the west side of the profile. Other gravity anomalies are associated with previously mapped faults I and II (Figure 3.14A; Collins and Raney, 2000) and newly interpreted normal faults (fault 3, 4 and 5) in the eastern part of the profile (Budhathoki, 2013, Figure 3.14A). Budhathoki's results are in close agreement with the geology based on well log data and the position of mapped faults (Collins and Raney, 2000). Based on detailed well log analysis of the depositional environment (Budhathoki, 2013) we suggests fresh water is produced mostly from playa margin facies at depth ranges of 600-850 ft in well E3A (Figure 3.14B).

II. Profile B-B'(Figure 3.16A, B and C)

The profile B-B' extends from the foothills of the Franklin Mountains (Figure 3.10) similarly as in profile A-A' but there is a distinct change in the TDS from west to east (Figure 3.16A and C). Figure 3.16 (A) shows gravity profile B-B' as described in Budhathoki (2013), where seven anomalies were interpreted as faults. Two of these faults, faults IV, VII have been previously mapped by Collins and Raney (2000) and five new faults (8, 9, 16, 22, 24, and 25) were recognized from the microgravity survey (Budhathoki, 2013). Well 35 and MNST2 are located in a graben between fault 24 and fault 25 but well 35 and MNST2 lies approximately 960 ft and 400 ft away, respectively from the hanging wall of fault 25. This indicates the permeability increases in the hanging wall of the fault and salinity increases. The THNH wells also reside in the hanging wall block of the East Franklin Fault where the permeability increases due to the minor faults (faults 15 and 16). Both THNH wells are located close to mountain front on a hanging wall block of the East Franklin fault but high TDS indicates the presence of a brackish water pocket bounded by faults 16 and 15. Change in orientation having N-S strike direction of East Franklin Fault to more NE-E trend of faults 15 and 16 at the same latitude cut across the grain of most basin structures and complicate the groundwater flow paths.

Freshwater is present in alluvial fan and playa margin facies at 350-690 ft with correspondingly low TDS, Cl and SO_4 in well 36A (Figure 3.16B). In well 35, the TDS concentration varies from 400 to 1500 mg/L and the Cl concentration is between 100 to 500 mg/L. Even sulfate concentration increases more than 200 mg/L in well 35 indicating the influence of water rock interaction such as the dissolution of gypsum deposits in the HBA. Facies analysis (Figure 3.16B) of well 36A shows freshwater is associated with the playa margin facies at 600 ft and brackish was is associated with the playa lake facies observed at 800. Facies

analysis of MF wells THNH1 and THNH2, indicate brackish water is associated with the lower part of alluvial fan and playa margin deposits around 700 ft. At depths >1100ft brackish to saline water is found in the playa lake deposits in the THNH series wells. Towards the east, CB well MNST2 found brackish water at a much shallower depth (<600ft) in playa margin deposits (Figure 3.16B). The brackish water and saline water are vertically stacked as seen in Figure 3.16B indicating there are isolated saline pockets stratigraphically. The geochemistry study does suggests the salinity increases in the MF wells (THNH wells) due to vertical flow of deeper saline waters along the complex faults and reached the shallow sections in response of groundwater pumping. Well 59 is located around 250 ft on the hanging wall side of fault 8 bounded by fault VII. The geochemical profile also suggests the faults 8 and VII may serve as a boundary between fresh and brackish water and that the boundary can be extended to the north.

With the exception of high TDS in THNH series wells, well 36, located close to the mountain front, records fresh groundwater with a low TDS of 600 mg/L. A drastic increase in TDS (up to 1500 mg/L) occurs in well 35, located 1km west of well 36 and confirms that the fresh water pocket observed in well 36 is small in extent. The TDS again decreases to 800mg/L towards the basin in well 59, indicating the lack of connectivity of the two freshwater pockets. The geochemical profile of wells 36 and 59 remains the same in time period of about 50 years (Figure 3.16C). Well 35 records an increase in salinity by change in concentrations of both TDS and Cl from 1965 to 1998 and then a decrease to the present.

Water samples in profile B-B' are dominated by Na and Ca (cations) and Cl, HCO_3, SO_4 (anions) (Figure 3.17). The Piper diagram shows the dominant signature of Na-Cl in well 59 (inverted triangles). Well 35 (squares) shows the water evolves between Na-SO_4 to Ca-HCO_3.

Well 36A (circles) also shows mixing between Na-Cl and Na-HCO_3 but the water has a greater signature of HCO_3.

III. Profile C-C' (Figure 3.18A, B and C)

This west-east profile starts adjacent to the foothills of the Franklin Mountains (well 52) to the basin (well 521) (Figure 3.13). Our profile C-C' is close to the gravity profile BB' of Avila (2011) and part of this profile is represented in Figure 3.18A. Budhathoki (2013) identified new normal faults13, 12, and 11 located east of the East Franklin Boundary Fault (EFBF) and near the wells 52, 40A and 521, respectively, in addition to fault 9. Well 52 reside in the hanging wall of fault 13. Fault 12 can be extrapolated between wells 29B and 40A which are marked by changes in TDS and Cl concentration. Also the noticeable increase in the TDS and Cl concentration between well 521 and well 40A suggests the discontinuity in a freshwater pocket might be due to the presence of fault 11 between the wells. Fault 9 can be extrapolated to fault IX (Budhathoki, 2013; Figure 3.18A). Fault 9 shows the continuity of freshwater-brackish water boundary that was identified previously (Bredehoeft, 2004) based on distinct salinity changes between wells 521 and FBT04.

Well log analysis shows the shallow (<300 ft) alluvial fan and the playa margin (<650 ft) deposits of wells 29B and 40A have freshwater pockets. The deeper playa lake deposits (>900 ft) have brackish water in CB wells 521 and FBT04. Also, the MF well (TH43A) that has high TDS is located in playa margin and playa lake deposits (Figure 3.18B).

This profile is in agreement with the general interpretation of groundwater quality where fresh groundwater with low TDS is observed near the mountain front and salinity progressively increases towards the basin (Figure 3.18A and C) as the groundwater flow direction is eastward

and southward from the mountains (Knowles and Kennedy, 1958).The geochemical signatures of water samples in profile C-C' represent distinct three groups; a) Na-Ca-HCO_3, b) Na-Cl and c) mixing of these two end members (a and b) in the Piper diagram (Figure 3.19). As predicted, well 52 near the mountain front is dominated by Na-Ca-HCO_3 as in well E6, a freshwater recharge signature from the Franklin Mountains. Well 521, located in the basin, has a predominant Na-Cl signature. The Cl concentration is higher in well 29B (>200 mg/L) and less in well 31 and 40A (<100 mg/L) indicating freshwater in these wells have slightly different compositions with Na-Ca-HCO_3 signatures (Figure 3.19). The wells in geochemical profile CC' do record a significant change in time period of about 50 years (Figure 3.18C). Well 521 however show a distinct increase in salinity (both TDS and Cl) from 1995 to the present.

IV. Profile Y-Y' (Figure 3.20A, B and C)

This northeast-southwest trending profile extends from the exterior to the interior of the basin (Figure 3.13).Well 601 located near the southwest edge of the study area (i.e., exterior of the basin) is a newer well drilled in 2005 with low TDS of 400mg/L. Moving towards the interior of the basin the TDS increases to the northeast from 900 mg/L in well 59 to 1700 mg/L in well 57 (Figure 3.13; data in appendix). This salinity increase of over 1500 mg/L towards the CB wells is consistent with the previous studies (A Binational Publication, 1998).

The gravity profile for Y-Y' passes across NW-SE striking structures with several anomalies associated with normal faults (Collins and Raney, 2000; Budhathoki, 2013; Figure 3.20A). Three faults (I, II, VII) coincide with earlier interpreted faults (Collins and Raney, 2000) and three new faults (8, 9, 10) identified by Budhathoki (2013) may extend to the south to merge with faults identified by Marrufo (2011). Fault 11 separates freshwater in wells 522 and 62 from more saline well 521. Fault 10 can be extended to fault 24 (near well 35 on profile B-B', Figure 3.16A)

which is a boundary between distinct water chemistries observed in wells 44 and MNST5. Freshwater pockets are smaller in extent and bounded by N-S trending subsurface faults as shown in Figure 3.22. As we observe in Figure 3.20B, playa margin and playa lake facies increases towards the basin that corresponds to the increase in salinity.

The geochemical profile shows the geochemistry of well 62 remains the same over the past 50 years. Wells 521, 44, and 59 record the significant increase in both the TDS and Cl concentration since 1987 (Figure 3.20C). The geochemical signatures of water samples in profile Y-Y' represent samples from the mixing zone and the end members of Na-Cl composition (Figure 3.21). Wells 601, 522, 62, and 44 are in the zone of fresh water with abundance of Na-Ca-HCO_3 and low TDS; whereas, well 59 and MNST5 are in the saline water zone with Na-Cl-SO_4 and high TDS.

3.5 Discussions/Interpretations:

Generally, wells drilled near the mountain front have the thickest freshwater layers (up to approximately 1320 ft (400 m) thick) but the freshwater layer becomes thinner with increasing distance from the Franklin Mountains (Druhan et al., 2008). Well log studies of the HBA shows both the MF and CB wells have increasing Cl concentration as the water move from the Camp Rice to Fort Hancock formations. The Fort Hancock formation consists of lacustrine sediments with evaporites and carbonate nodules deposited during an interconnected playa lake depositional environment (Gustavson, 1990; Marrufo, 2011).Well log and grain size analysis indicate coarser grain sizes are associated with alluvial fan and fluvial facies near the mountain front having poorly sorted sediments. Sediments derived from adjacent uplifted areas are generally finer grained and better sorted with distance from source and are found in playa lake facies. Wells in the freshwater part of the aquifer that have lower TDS than 800 ppm are mostly

found in alluvial fan facies and wells in playa lake facies are brackish having higher concentration of TDS (>800 ppm). Grain size decreases towards the east, from alluvial fan to playa sediments. This controls the lateral movement of brackish water (from east) into the freshwater zone (to the west). The volume of clay increases gradually to the east as seen between wells 601 and 610 in the south (Marrufo, 2011). A similar trend was observed between MNST5 and FBT04, and between MNST3 and MNST2 suggesting the same distribution of sedimentary facies in the northern HBA.

Previous studies indicate the subsurface flow path in the study area appears to be from the west (MF) towards the southeast (CB) (Knowles and Kennedy, 1958). Detailed $\delta^{18}O$ isotopic studies have shown that precipitation is the primary recharge source in both the MF and CB wells of HBA, but recharged water is found at a much shallower depth, 750 ft (225 m) below the surface in CB wells, as compared to 990-1485 ft (300-450 m) below the surface in MF wells (Druhan et al., 2008). Water isotopes showed the similarity between the MF wells near the Franklin Mountains as well as modern groundwater samples from the southern Tularosa Basin, suggesting modern day precipitation recharge in the MF wells (Witcher, et al., 2004; Druhan, et al., 2008). The low salinity (1:2 ratio of $Cl:SO_4$) MF wells are enriched in HCO_3 and Ca+Mg, and have low Na+K indicating young freshwater might be derived from weathering of limestone and calcium-magnesium silicates of the Franklin Mountains. The potable freshwater zones of 1:2 ratio ($Cl:SO_4$ ratio) are consistent with the ratio found in Tularosa Basin groundwater, even though the Tularosa aquifer is more gypsiferous as compared to the more halitic HBA (Druhan et al., 2008). Both $Cl+SO_4$ and Na+K increases in the 1.5:1, 4:1 and 12:1 $Cl: SO_4$ trends, suggesting a common source of ions for all the waters but that the salinity of wells progressively increases to east. As groundwater moves towards the CB wells along its flowpath from west to

east, Cl becomes the dominant ion, indicating the hydrochemical evolution towards saline water in the central basin. Mature groundwater, having a long residence time, evolved from halite dissolution and carbonate nodules of the Fort Hancock Formation has enriched Cl ions (Fisher and Mullican, 1990; Anderholm and Heywood, 2003; Marrufo, 2011). Deep monitoring wells record the highest Cl concentration (>15,000 mg/L) saline water in playa deposits (Groschen, 1993; Hibbs and Merino, 2007).

Chloride (Cl) is considered a conservative solute as it rarely interacts with other solutes or mineral phases, so freshwater pockets show variation in Cl concentration. For instance, Cl concentration is higher in well 29B (>200 mg/L) and lesser in well 31 and 40A (<100 mg/L) in profile CC'. This may be associated with different rock-water interactions along flow paths from west to east (Figure 3.23). The geochemical trends show Na concentration generally increases linearly with high Cl concentration away from recharge areas, indicating the dilute recharge water mixes with NaCl when the water moves along the flow path. The dissolution of evaporites in the playa lake deposits during water rock interaction with HBA sediments cause increases in salinity, Na+K, Cl and total cations, as observed both in MF well E3A and CB wells 521 and MNST02 (Fig 3.9). Piper diagram (Figure S3) of the wells in the center of the study area suggests the similarity in water chemistry of wells due to identical water-rock reactions along the flow paths.

Water samples analysis from MF wells THNH1 and THNH2 collected at 500 ft to 1510 ft (150 m to 460 m) below the surface indicate brackish to saline water whereas the surrounding wells yield freshwater at the same depth (see TDS maps in Figures 3.10, 3.11, 3.12). We observe similar sedimentological facies in MF wells but TDS data indicate evidence for isolated saline water pockets located stratigraphically at different depths in these THNH wells suggests a

major change in water chemistry (Figure 3.18B). Faults of two orientations (the N-S strike direction of the East Franklin Fault and E-W trend of faults 15 and 16) might be more favorable for vertical groundwater flow. Previous studies of isotopic data also suggest these THNH wells have an evaporated water source (to CB wells) indicating a common origin but that has undergone a different degree of evaporation (Witcher et al., 2004; Druhan et al., 2008).

Seager (1980) reported that Hueco Basin has developed tension fractures/fissures in the basin fill deposits located near CB wells (<100 ft or 30 m). These fractures are associated with topographic depressions that provide the rapid moisture and solute movement within the HBA (Scanlon, et al., 1999). The low isotopic $\delta^{18}O$ values (~11‰) found in the shallow parts of CB wells confirm that localized modern infiltration from storm events is occurring (Hibbs and Merino, 2007; Druhan et al., 2008). In addition, high amounts of bromide ions at shallower depths in the CB wells and Cl isotopic data ($^{36}Cl/Cl$) suggest the salinity increases are related both to water upwelling vertically along faults as well as evaporative saline recharge from the infiltration pathways located at the surface (White et al., 1997; Groschen, 1993; Scanlon, et al., 1999; Hibbs and Merino, 2007; Druhan, et al., 2008).

The temporal evolution of fresh to saline groundwater over 50 years is recorded by the increase in TDS and Cl concentration corresponding to the effect of pumping in the HBA. During droughts, excessive pumping coupled with minimum freshwater recharge allows saline water to encroach from the central basin increasing the salinity of groundwater, as in well 44 (Figure 3.20C). Studies have reported the saline groundwater is moving upward from deeper parts of the aquifer (White et al., 1997) and from the east (Hutchinson, 2006). In some wells, such as well 35, there was an increase in salinity from 1965 to 1993 and then a decrease to the present time. This indicates recharge of freshwater might directly be occurring from fault 24

adjacent to well 35 (Fig 3.10). Both municipal and military pumping of the HBA increased by a factor of 6 between 1950 and 1990 and then decreased by 24% during the time period of 1990 to 1994. This is reflected by the TDS and Cl that mirrors the pumping increasing and then decreasing trends in geochemical profile of 50+ years (A Binational Publication, 1998). In addition, for some wells, such as well 42 (Fig 3.11, 3.13) the recharge pathways are associated with faults (19, 21, 22) because at 500-800 ft depth there is fresh groundwater with abundance of Na-Ca-HCO_3 which is similar to the fresher groundwater recharge from the Franklin Mountains.

Generally, fault systems in the tectonic active basin (e.g., Hueco Basin) may act as horizontal flow barriers as a consequence of sediment deformation and displacement of sedimentary layers that lead to lower connectivity (Seager, 1980; Knott, 1993Heywood and Griffith, 2013;). Simulation of hydrologic conductivities at the Baton Rouge Fault of south Louisiana show that higher pressure saltwater from downdip fault block seeps towards the updip fault block across the fault after groundwater development in the updip side of fault (Nasreen, 2003; Heywood and Griffith, 2013**)**. A number of studies have shown vertical or lateral fluid flow along the more intensely fractured and permeable damaged fault zone in response of pumping (Forster and Evans, 1991; Hooper, 1991; Evans et al., 1997; Stoessell, 2002; Heywood and Griffith, 2013). Abrupt water chemistry change is common in both MF and CB wells that might be due to fault zones. Moreover, fault zones accumulate finer materials (i.e., fault gouge) that can isolate fresh water in footwall block from surrounding saline water pockets (Forster and Evans, 1991; Evans et al., 1997; Stoessell, 2002; Nasreen, 2003; Stoessel, and Prochaska, 2005). For instance, the presence of an inferred fault (dashed line in Fig 3.14A) as in geological map by Seager (1980) between wells E7 and LF4 is perhaps a possible cause for the distinct water chemistry change within 700 m (2300 ft) distance. The hanging wall tends to have more saline

water in the CB wells and the boundary of fresh-saltwater seems to be distinct. For instance, the mapped boundary faults IX and X (Collins and Raney, 2000) near wells 521 and MNST5, faults B and C (Marrufo, 2011) near wells 607 and 610, and faults 7, 8 (Budhathoki, 2013) near wells 59 and MNST2 appear to separate the fresh and brackish (Figure 3.22). However, faults may also act as conduits for fluid flow in the northern HBA. For example, minor faults such as fault 24 (Budhathoki, 2013) adjacent to well 35 and fault 27 (Budhathoki, 2013) close to well 40A seem to act as conduits (Figure 3.10, 3.11, 3.13). Also, faults 19, 21 and 22 (Budhathoki, 2013) near well 42 and fault 12 (Budhathoki, 2013) adjacent to well 516 appear to act as conduits for freshwater flow.

The distribution of Cl concentration, presence of Quaternary faults and increase in clay volume and evaporites indicate the controlling role of faults as a barrier between freshwater and brackish water in the CB wells of the northern HBA (Figure 3.22, 3.23). However, we need to further investigate water chemistry using oxygen and sulfur isotopic composition of the well samples to unravel the recharge pathway and the water-rock interaction complexities.

3.6 Conclusions

Water quality is an important parameter in developing fresh groundwater supplies, especially in arid regions. Water quality is dependent on facies changes and subsurface structures (faults). Geochemical trends are helpful for understanding the flow paths in the aquifer.

Hydrochemical facies of MF wells in the HBA are dominated by Ca-Na-HCO_3 that interact with the carbonates of recharge areas in the Franklin Mountains. Alluvial fan deposits near the mountain front have coarser grained sediments that are poorly sorted and have low transitivity to the groundwater flow. Water-rock interaction between halites/evaporites and carbonate nodules present in the deeper Fort Hancock Formation increases salinity in the CB

wells with abundant Na-Cl dominated water chemistries. The saline CB wells are also associated with fine grained playa lake deposits and sediments with well sorting.

Locating subsurface faults is very important to understanding structural framework of aquifers. The faults appear to act as barriers in the eastern part of the study area, whereas in the western part of the study area they act as a conduit for saline water vertical upflow from deeper aquifers.

Geochemical changes over time also show the similar trends in salinity change as pumping history of the wells. The profile also provides information regarding the source of recharge in the wells where water taps from the well.

Our study suggests that the integration of microgravity with detailed well logs is important locating the subsurface faults, understanding basin stratigraphy and the basin's subsurface geometry. Geochemical study of the water helps to aid in interpretation of subsurface flow and the extent of the freshwater in the aquifers. Integrating the geochemistry, geophysics and geology leads to a better understanding of the location and flow of continuing groundwater development for a region.

3.7 Acknowledgements

This research was supported by student research grants from the Geological Society of America (GSA) and American Association of Petroleum Geologists (AAPG). Anita Thapalia was a recipient of 2013 WTGS E. Russell Lloyd Scholarship and a 2013 Southwest section AAPG Scholarship. The authors are grateful to Scott Reinert, Eric Bangs, and Alfredo Ruiz from El Paso water Utilities for providing well logs and the geochemical data of the wells. The authors especially thank John Hawley for his help in data collection. We want to thank Dr. Mark Baker for discussions related to groundwater geochemistry and well log analysis. The authors thank Sandy Marrufo, and Victor Avila for providing the permission to use gravity data in this study

and want to recognize Galen Kaip, Niti Mankhemthong, Felix Ziwu, Victor Avila, Martin Sandoval, Mark Lucero, and Alay Gebregiorgis for assisting in the fieldwork.

References

A Binational Publication, Jan 1998. Transboundary aquifers and Binational groundwater database for the city of El Paso/Ciudad Juarez area. *International Boundary and Water Commission, United States of America and Mexico.* (Data accessed in Feb, 2014). http://www.ibwc.state.gov/Water_Data/binational_waters.htm#BasGeoNRockSedTypes

Al-Ahmadi, M. E., 2013. Hydrochemical characteristics and evalution of groundwater quality in Wadi As Sab, a western Saudi Arabia. *International Journal of Scientific & Engineering Research.* vol 44, 1, issn 2229-5518.

Anderholm, S.K., and C.E. Heywood, 2003. Chemistry and age of ground water in the southwestern Hueco Bolson, New Mexico and Texas: U.S. Geological Survey Water-Resources Investigations Report 02-4237, 22 p. http://nm.water.usgs.gov

Avila, V.M., 2011. An investigation of the seismic hazards of the El paso-Juarez region: The nature and extent of the southern east Franklin Mountains fault zone: Unpublished M.S. Thesis, Univ. of Texas at El Paso, El Paso, TX, 51 p.

Back, W., 1966. Hydrochemical facies and groundwater flow patterns in Northern part of Atlantic Coastal Plain. *Hydrology of aquifer systems*. Geological survey professional paper 498A.

Baldridge, W.S., 2004. Geology of the American Southwest A Journey through Two Billion Years of Plat-Tectonic History. *Cambridge University Press*, 280p.

Bense, V.F., and M.A. Person, 2006. Faults as conduit-barriers to fluid flow in siliclastic Sedimentary aquifers. *Water Resources Research*, Vol. 42, W05421, pp. 1-18.

Bredehoeft, J., Ford, J., Harden, B., Mace, R., Rumbaugh, J., III., 2004. Review and interpretation of the Hueco Bolson groundwater model. *Prepared for El Paso Water Utilities Report 39*: Electronic document, available at www.epwu.org/water/hueco_bolson.html

Budhathoki, P., 2013. Integrated geological and geophysical studies of the Indio Mountains and Hueco Bolson, west Texas. Unpublished Ph.D. Dissertation, Univ. of Texas at El Paso, El Paso, TX, 124 p.

Chapin, C. E., 1971. The Rio Grande rift part 1: modifications and additions: *New Mexico Geological society*, Annual Field Conference Guidebook, No.22, pp.191-201.

Collins, E. W., and Raney, J. A., 1991. Tertiary and Quaternary Structure and Paleotectonics of the Hueco Basin, Trans-Pecos Texas and Chihuahua, Mexico. *The University of Texas at Austin, Bureau of Economic Geology*, Geological Circular 91-2, 44p.

Collins, E. W., and Raney, J. A., 2000. Geologic map of West Hueco Bolson, El Paso Region, Texas: The University of Texas at Austin, Bureau of Economic Geology, Miscellaneous Map No. 40, scale 1:100,000, 24 p.

Doser, D.I. and Langford, R.P., 2006. Characterization of Aquifer Extent and Quality for Desalination and Brine Disposal Projects: *Report W-06-04*.

Druhan, J. L., Hogan, J.F., Esatoe, C.J., Hibbs, B.J., Hutchison, W.R., 2008. Hydrochemcial controls on groundwater recharge and salinization: a geochemical analysis of the northern Hueco Bolson aquifer, Texas, USA. *Hydrogeology*, 16, 281-296.

Eastoe, C.J., Hibbs, B.J., Olivas, A.G., Hogan, J.F., Hawley, J., Hutchinson, W.R., 2008. Isotopes in the Hueco Bolson aquifer, Texas (USA) and Chihuahua (Mexico): local and general implications for recharge sources in alluvial basins. *Hydrogeology Journal*, 16, 737-747.

Evans, J. P., Forster, C. B., and Goddard, J. V., 1997. Permeability of fault-related rocks, and implications for hydraulic structure of fault zones. *Journal of Structural Geology*, v.19, pp. 1393-1404.

Fisher, R.S. and Mullican, W.F., 1990. Integration of ground-water and vadose-zone geochemistry to investigate hydrochemical evolution: a case study in arid lands of the northern Chihuahuan Desert, Trans-Pecos Texas. *University of Texas at Austin, Bureau of Economic Geology*, Geol Circ 90-5.

Forster, C. B., and Evans, J. P., 1991. Hydrogeology of fault zones and crystalline thrust sheets: Results of field and modeling studies. *Geophysical Research Letters*, v. 18, pp. 979-982.

Gibbs, R.J., 1970. Mechanisms controlling world water chemistry. *Science*, 17, 1088-1090.

Groschen, G. E., 1993. Simulation of ground-water flow and the movement of saline water in the Hueco Bolson aquifer, El Paso, Texas and adjacent areas. *U.S. Geological Survey open-file report* 92-171.

Gustavson, T. C., 1990. Arid basin depositional systems and paleosols: Fort Hancock and Camp Rice Formations (Pliocene-Pleistocene) Hueco Bolson, West Texas and adjacent Mexico. *The University of Texas at Austin, Bureau of Economic Geology*, Report of Investigations 198, 49 p.

Hadi, J., 1991. A Study of the structure and subsurface geometry of the Hueco Bolson: Unpublished M.S. Thesis, Univ. of Texas at El Paso, El Paso, TX, 88 p.

Hanor, J.S. 1994. Origin of saline fluids in sedimentary basins. In: Parnell J (ed) Geofluids: origin, migration and Evolution of fluids in sedimentary basins. *Geological Society Special Publication* 78: 151-174.

Hawley, J.W., J.F. Kennedy, B.J. Hibbs, and M. Cleary, 2002. Basin-fill aquifers of the southern New Mexico border region, USA and Mexico: Their hydrogeologic framework, and related aspects of groundwater flow and chemistry. *In Integrated Trans-boundary Water Management*: Proceedings of a special joint conference of Universities Council on Water Resources (UCOWR), Environmental & Water Resources Institute of ASCE (EWRI), U.S. Army Corps of Engineers Institute for Water Resources (CEIWR), and National Ground Water Association (NGWA), pp.164-172.

Hawley, J.W., Kennedy, J.F., Grandos-Olivas, A., and Ortiz, M.A., 2009. Hydrogeologic Framework of the Binational Western Hueco Bolson-Paso del Norte Area, Texas, New Mexico, and Chihuahua: Overview and Progress Report on Digital-Model Development: *New Mexico Water Resources Research Institute*, Technical Completion Report 349, 45 p.

Henry, C.D., and J.G. Price, 1985. Summary of the tectonic development of Trans-Pecos Texas. *The University of Texas at Austin, Bureau of Economic Geology*, Miscellaneous Map No. 36, 8 p.

Heywood, C.E. and Yager, R.M., 2003. Simulated ground-water flow in the Hueco Bolson, an Alluvial-basin aquifer system near El Paso, Texas: *U.S. Geological Survey Water-Resources Investigations Report* 02-4108, 55 p.

Heywood, C.E. and Griffith, J.M, 2013. Simulation of Groundwater Flow in the "1,500-Foot" Sand and "2,000-Foot" Sand and Movement of Saltwater in the "2,000-Foot" Sand of the Baton Rouge Area, Louisiana. *U.S. Geological Survey Open-File Report*, 1153, 79 p. http://pubs.usgs.gov/of/2013/1153/.

Hibbs, B. J. and M. Merino, 2007. A geologic source of salinity in the Rio Grande aquifer near El Paso, Texas: *New Mexico Journal of Science*, Vol. 44, 1, 17, pp. 165-181.

Hibbs, B.J., Boghici, R.N., Hayes, M.E., Ashworth, J.B., Hanson, A.T., Samani, Z.A., Kennedy, J.F., Creel, B.J. 1997. Transboundary aquifers of the El Paso/Ciudad Juraez/Las Cruces region. *Texas Water Development Board and New Mexico Water Resources Research Institute*, technical contract nos X 996343-01-0 and X-996350-0100, USEPA, Washington, DC, 145 pp.

Hoofer, J.M., 1971. Mineralogy and petrology of the Santo Tomas-Black Mountain Basalt field, Portiollo volcanics, south-central New Mexico. *Geological Society of America Bulletin*, v. 82, p. 603-612.

Hooper, E. C. D., 1991. Fluid migration along growth faults in compacting sediments. *Journal of Petroleum Geology*, v. 14, no. 2, pp.161-180.

Hutchison, W.R., 2006. Groundwater Management in El Paso, Texas: Unpublished Ph.D. Dissertation, Univ. of Texas at El Paso, TX, El Paso, 329 p.

Jones, B.U.P, 2007. Occurrence and chemical character of groundwater within Samford Valley, Southeast Queenland. Queensland University of Technology, School of Natural Resource Sciences, Thesis CRICOS No. 00213J, p40

Keller, G.R., Morgan, P. and Seager, W.R., 1990. Crustal structure, gravity anomalies and heat flow in the southern Rio Grande rift and their relationship to extensional tectonics. *Tectonophysics*, Vol. 174, pp. 21-37.

Keller, G.R. and Baldridge, W.S., 1999. The Rio Grande Rift: A geologic and geophysical overview: Rocky Mountain Geology, 34(1), 121-130.

Knott, S. D., 1993. Fault seal analysis in the North Sea. *American Association of Petroleum Geologists*, v. 77, no. 5, pp. 778-792.

Knowles , D.B. and Kennedy, R. A., 1958. Ground-water resources of the Hueco Bolson northeast of El Paso Texas. *U.S. Geological Survey Water-Supply Paper*, 1426, 185p.

LeMone, D. V. and Simpson, R. D., 1983. Cretaceous biostratigraphy of the Franklin Mountains, El Paso County, Texas: In Allen, R. (Editor), Delaware Basin, *West Texas Geological Society*, 82–76, pp. 85–87.

Leggat, E.R. and Davis, M.E., 1966. Anlog model study of the Hueco Bolson near El Paso, Texas. *Texas Water Development Board*, Report 28.

Lovejoy, E.M., 1976. An Interpretation of the Structural Geology of the Franklin Mountains, Texas: *New Mexico Geological Society Guidebook*, 26th Field Conference, Las Cruces, pp. 261-268.

Mack, G.H., W.R. Seager, M.R. Leeder, M. Perea-Arlucea, and S.L. Salyards, 2006, Pliocene and Quaternary history of the Rio Grande, the axial river of the southern Rio Grande rift, New Mexico, USA: *Earth-Science Reviews*, Vol. 77, pp. 141-162.

Marrufo, S.S., 2011. An integrated geological and geophysical study of the fresh and brackish water boundary in the Hueco bolson, West Texas: Unpublished M.S. Thesis, Univ. of Texas at El Paso, El Paso, TX, 108 p.

Mattick, R. E., 1967. A seismic and gravity profile across the Hueco Bolson, Texas, in Geological Survey research, 1967. *US. Geological Survey Professional paper 575-D*, p. D85-D91.

McMillan, N. J., Dickin, A. P., and Haag, D. 2000. Evolution of magma source regions in the Rio Grande Rift, southern New Mexico: *Geological Society of America Bulletin*, Vol. 112, pp. 1582–1593.

Nasreen, M., 2003. The Effect of Faults upon Ground Water Flow in the Baton Rouge Fault System. Theses and Dissertations. University of New Orleans, Paper 54

Richardson, G.B., 1909. Description of the El Paso quadrangle, Texas: *U.S. Geological Survey Folio Series* 166, 11 p.

Seager, W.R., 1980. Quaternary fault system in the Tularosa and Hueco Basins, Southern New Mexico and West Texas. *New Mexico Geological Society Guidebook, 31st Field conference, Trans-Pecos Region,* 131-135.

Seager, W.R., 2004. Laramide (late Cretaceous to Eocene) tectonics of southwestern New Mexico; in Mack, G.H., and Giles, K.J., eds., The Geology of New Mexico: A geologic history: *New Mexico Geological Society*, Special Publication 11, pp. 183-202.

Seager, W.R. and Mack, G.H., 1986. Laramide paleotectonics of southern New Mexico: *American Association of Petroleum Geologists Memoir*, Vol. 41, pp. 669-685.

Seager, W. R., Shafiqullah, M., Hawley, J.W. and Marvin, R.F., 1984. New K-Ar dates from basalts and the evolution of the southern Rio Grande. *Geological Society of America Bulletin*, Vol. 95, No.1, pp. 87-99.

Scanlon, B.R., Langford, R.P. and Goldsmith, R.S., 1999. Relationship between geomorphic settings and unsaturated flow in an arid setting. *Water Resources,* 55, 4, 983-999.

Stoessel, R. K. and Prochaska, L., 2005. Chemical evidence for migration of deep formation fluids into shallow aquifers in South Louisiana, Trans: *Gulf Coast Association Geological Society,* Vol.55, pp. 794-808.

Stoessell**,** R. K., 2002, Chemical evidence for updip migration of brines on Lake Pontchartrain Faults. *2000 National Ground Water Association Exposition***,** December 8-11, 2002, Las Vegas, Nevada.

Thapalia, A., Borrok, D. M., Nazarian, S., and Garibay, J., 2011. Assessment of Corrosion Potential of Coarse Backfill Aggregates for Mechanically Stabilized Earth Walls. *Journal of the Transportation Research Board*, 2253, 63-72.

USGS, 1999. Where do all the salts go?: The potential effects and management of salt accumulation in south-central Arizona: *USGS Fact Sheet* 170-98.

Wen, X., Wu, Y., Su, J., Zhang, Y., Liu, F., 2005. Hydrochemical characteristics and salinity of groundwater in the Ejina Basin, Northwestern China. *Environmental Geology*, 48, 665-675.

Wilkins, D.W., 1986. Geohydrology of the southwest alluvial basins, regional aquifer-sytems analysis of Colorado, New mexico, and Texas. *U.S. Geological Survey Water Resources Investigation Report* 84-4224, 61 pp, plates

Witcher, J.C., King, J.P., Hawley, J.W., Kennedy, J.F., Williams, J., Cleary, M., Bothern, L., 2004. Sources of salinity in the Rio Grande and Mesilla Basin Groundwater, New Mexico water Resources *Research Institute Technical Completion Report No. 330, New Mexico State University, Las Cruces, NM*, 183p.

White, D.E., Baker, E.T., Jr. and Sperka, R., 1997. Hydrology of the shallow aquifer and uppermost semiconfined aquifer near El Paso, Texas: *U.S. Geological Survey Water-Resources Investigations Report* 97-4263, 37p.

Young, P.W., 1981. Evaluation of surface and ground irrigation waters the Lower El Paso Valley emphasizing Hudspeth County, Texas. *West Texas Council of Governments*, 219.

Tables

Table 3.1: Salinity nomenclature and corresponding TDS ranges (Hanor, 1994)

Description	**TDS (mg/L)**
Freshwater	0-1000
Brackish water	1000-10000
Saline water	10000-35000
Average value of seawater	35000
Brine	>35000

Table 3.2: Compiled average Cl: SO_4 values and Cl:SO_4 trends of wells and published data from Drunhan et al (2008). The Cl and SO4 values are averaged over the depth and time from where the water is tapped from the aquifers. More details in both time and depth of some of wells discussed in the profile section. SD indicates the standard deviation of the Cl/SO_4

Well	**Dates**	**Average Cl**	**SD**	**Average SO_4**	**SD**	**# of samples**	**Cl/SO_4**	**Average Cl/SO_4**	**Cl/SO_4 SD**
1: 2 (Cl: SO_4) **trend (MF)**									
EPWU 52	1961-2013	25.68	14.41	49.94	7.36	25	0.57		
EPWU 33	1957-2013	36.35	30.54	44.16	14.96	49	0.78	0.59	0.17
LF-1	1988-2009	157.62	69.12	435.58	219.5	35	0.44		
1.5: 1 (Cl: SO_4) **trend (MF)**									
EPWU 31	1957-2007	96.07	16.06	69.71	8.73	39	1.42		
EPWU 29	1956-2013	140.39	45.18	70.46	16.33	48	2.11		
EPWU 40	1959-2013	59.47	9.68	61.15	32.85	47	1.21	1.51	0.36
EPWU E-5	1965-2010	105.45	71.93	63.15	58.56	29	1.91		
EPWU 42	1958-2007	96	54.1	51	8.62	45	1.70		

LF-4	1989-2013	48.18	7.7	32.08	8.95	13	1.60		
EPWU 35	1958-2009	305	137.1	161	78.4	42	1.97		
EPWU 36	1958-2007	109.12	29.45	94.24	22.22	34	1.16		
EPWU 24	1952-2013	67.71	24.33	62.16	8.57	54	1.08		
EPWU 25	1953-2013	96.07	20.52	73.49	7.11	54	1.32		
EPWU 27	1955-2013	130.85	41.77	89.17	11.03	30	1.46		
EPWU 516	1992-2012	90.7	35.21	74.05	20.09	16	1.23		
EPWU 28	1956-2013	82	7.65	89	6.45	52	0.92		
EPWU 32	1957-2010	97.92	17.35	73.09	7.55	50	1.35		
E3A*		144.57	26.99	91.1	44.08	3	1.84		
MNST05*		312.2	8.06	169.95	44.47	2	1.90		
4: 1 (Cl: SO_4) **trend (CB)**									
EPWU 601	2005-2010	90.43	7.1	36.01	4.29	5	2.93	4.07	0.76
EPWU 522	2005-2012	108.08	15.36	32.16	7.45	7	3.78		
EPWU 62	1966-2007	110.38	52.99	35.36	11.88	28	3.32		
EPWU 44	1960-2013	177.36	122.8	35.73	11.91	41	5.34		
EPWU 59	1965-2010	298.91	62.67	80.38	61.29	10	4.36		
EPWU E-6	1974-2013	157.27	14.7	41.63	8.22	14	3.89		
MNST02*		3585.67	1169	765.23	145.1	3	4.63		
TH 43A*		420.36	142.1	115.44	50.36	4	4.31		
12: 1 (Cl: SO_4) **trend (CB)**									
EPWU 521	1992-2011	293.61	24.4	24.27	3.7	13	11.94	11.90	0.84
EPWU 54	1955-1974	563.11	221.5	66.61	74.42	17	13.32		
EPWU 61	2000-2006	292	150.8	28	14.7	8	12.01		
EPWU 53	1955-2000	480.81	194	58.03	55.18	32	11.24		
FBT 10*		881.3	467.3	119.26	96.6	7	10.77		
NH1*		2333.36	1851	281.48	269.7	5	11.38		
NH2*		7179.5	1507	697.75	140.8	9	11.23		

* Data from Druhan et al., (2008).

Figures

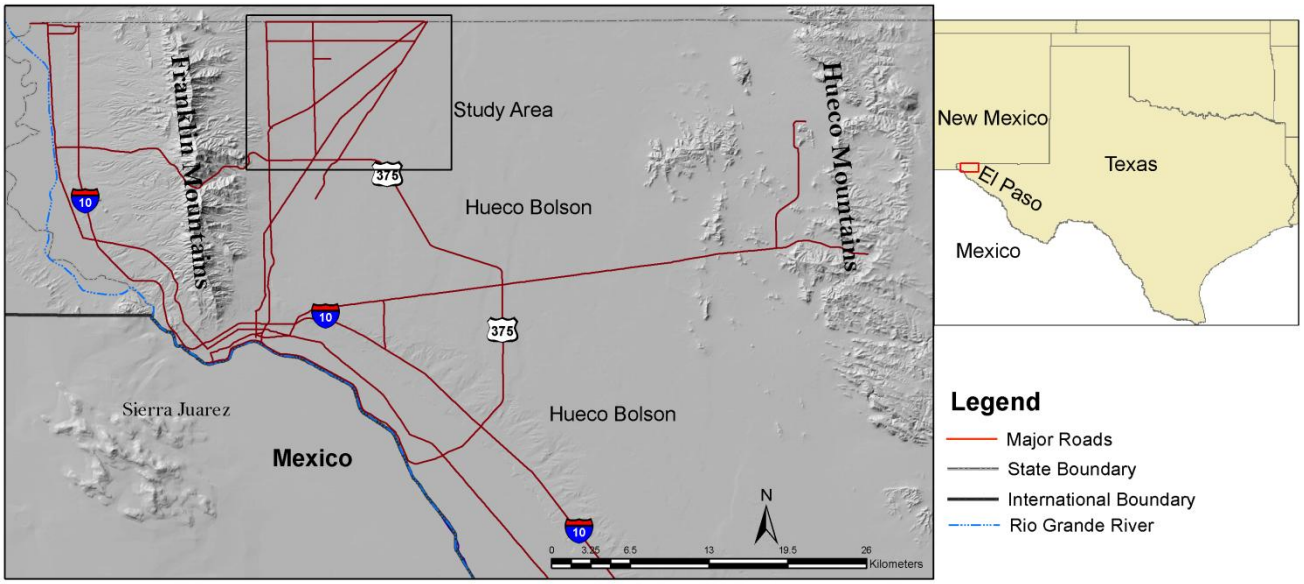

A)

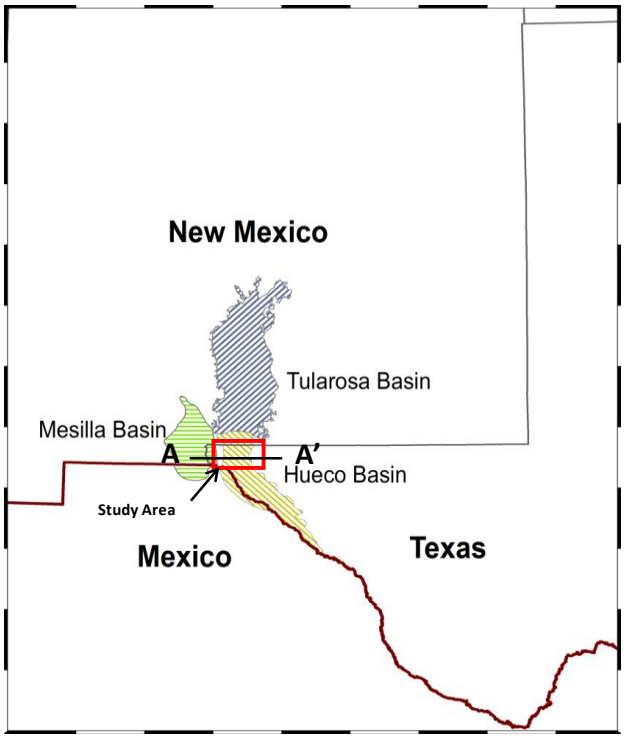

B)

Figure 3.1: (A) Location of the study area outlined by the box. (B) Map showing the Hueco basin bounded by the Tularosa Basin in the north and Mesilla Basin in the west. Details of cross-section AA' are shown in Figure 3.2.

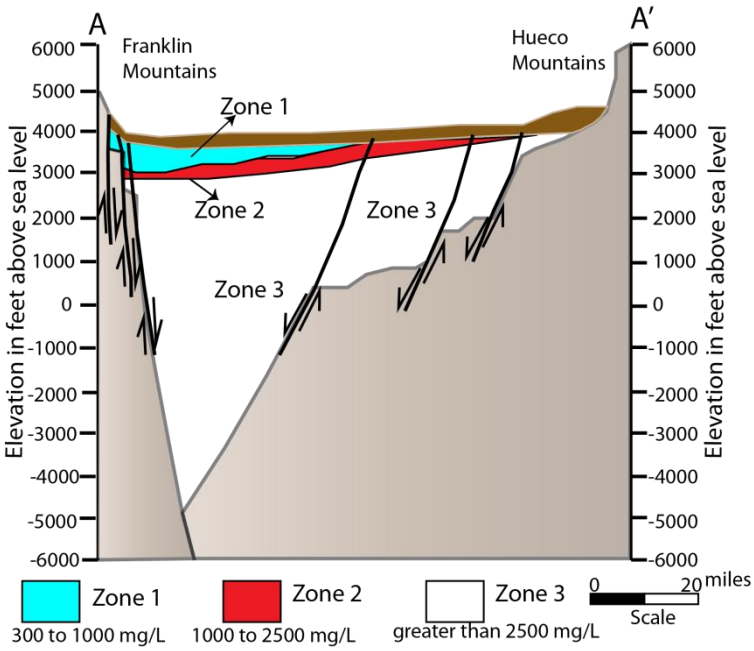

Figure 3.2: Cross-section AA' (location in Figure 1) showing the three different zones of groundwater with their TDS values. Note that the basin fill sediments are represented in this figure as brown colored upper layer above Zone 1. Modified from Heywood and Yager (2003)

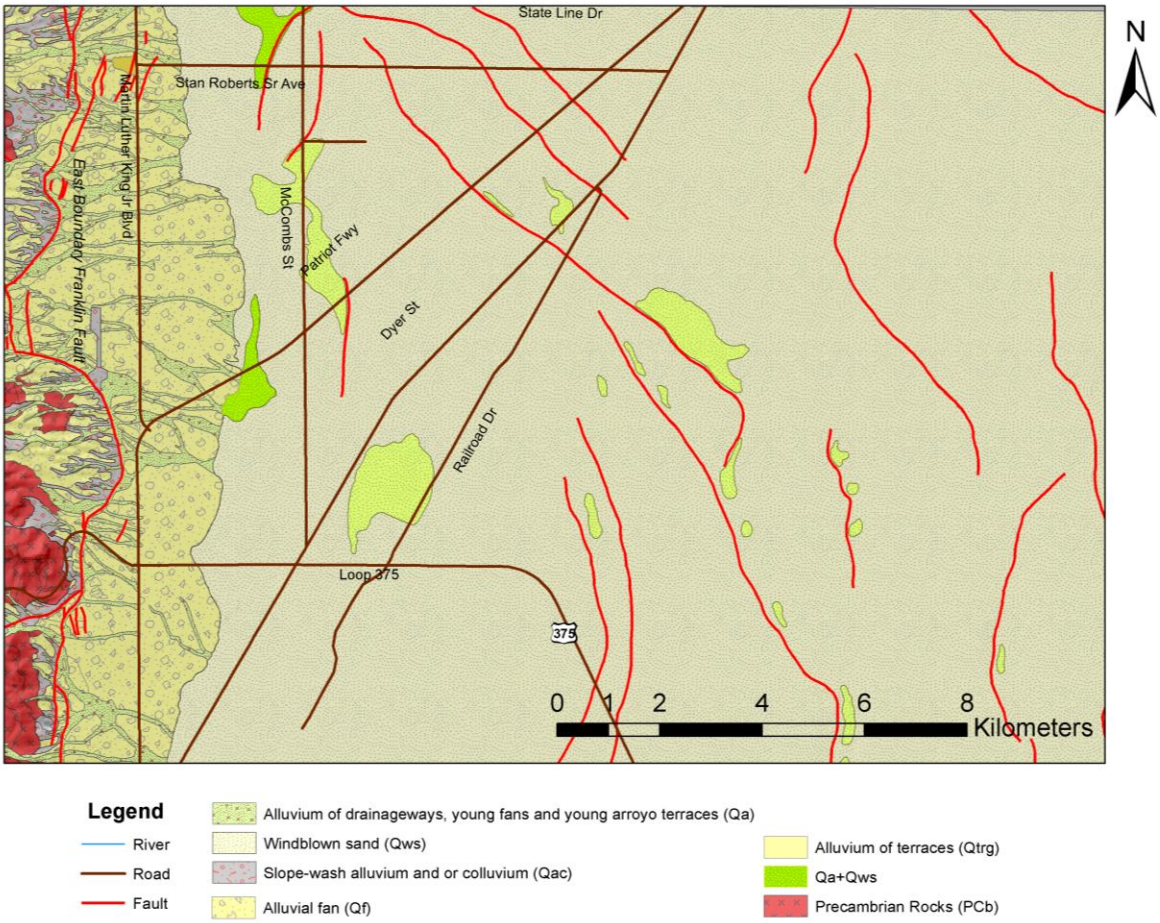

Figure 3.3: Geological map of the northern Hueco basin (modified from Collins and Raney, 2000)

A)

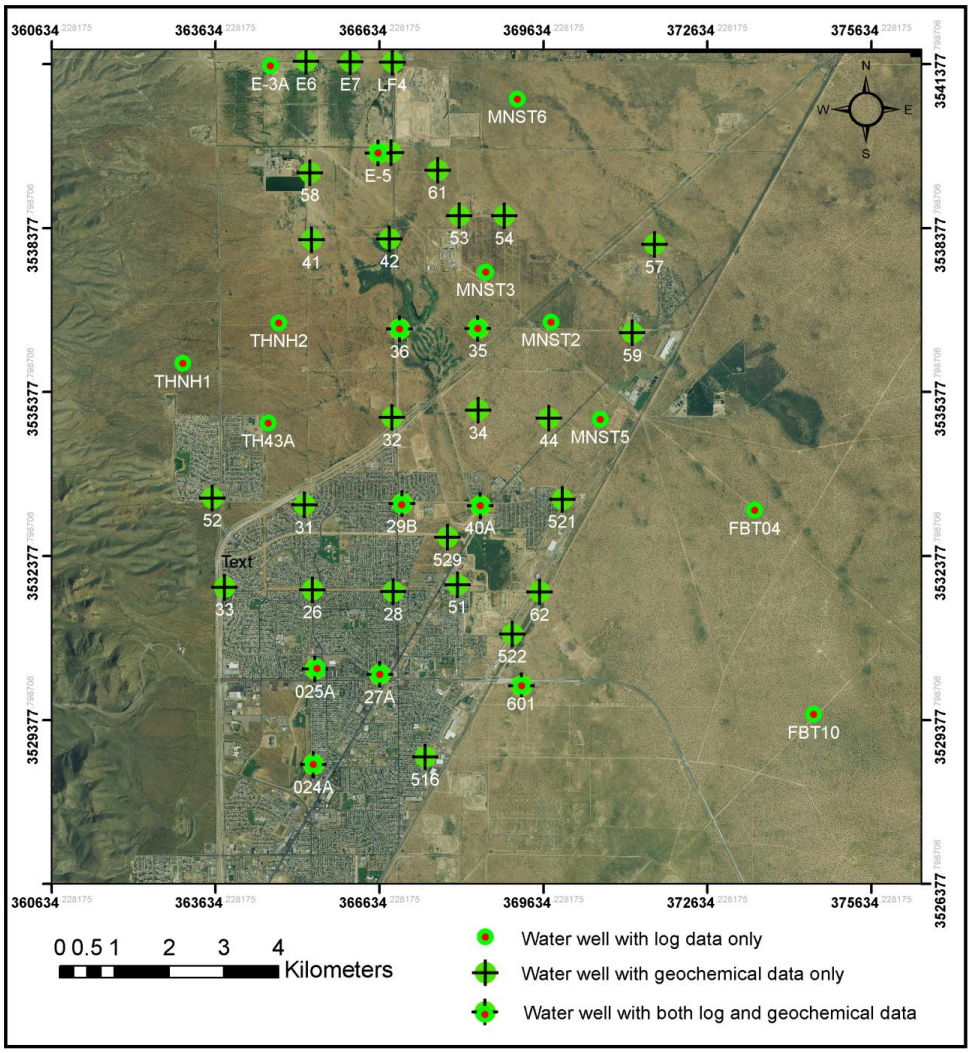
360634
363634
366634
369634
372634
375634
3541377
3538377
3535377
3532377
3529377
3526377
E-3A
E6
E7
LF4
MNST6
E-5
58
61
53
54
41
42
MNST3
57
THNH2
36
35
MNST2
59
THNH1
TH43A
32
34
44
MNST5
52
31
29B
40A
521
FBT04
529
Text
33
26
28
51
62
522
025A
27A
601
FBT10
024A
516
N
W
E
S
0 0.5 1 2 3 4
Kilometers
Water well with log data only
Water well with geochemical data only
Water well with both log and geochemical data

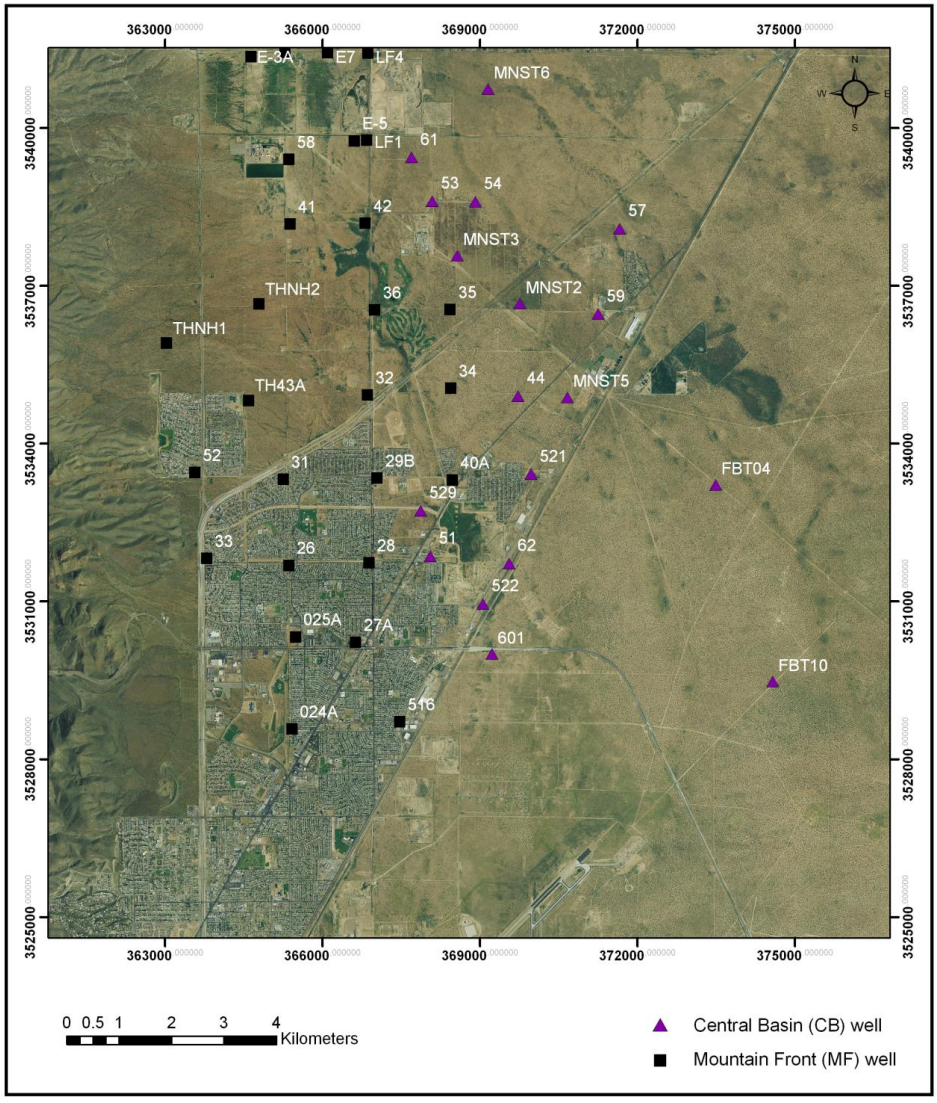

B)

Figure 3.4: (A) Location of the wells within the study area. (B) Classification of MF and CB wells of the study area based in the TDS values. White labels are well names used in subsequent text and figures as provided by the El Paso Water Utilities.

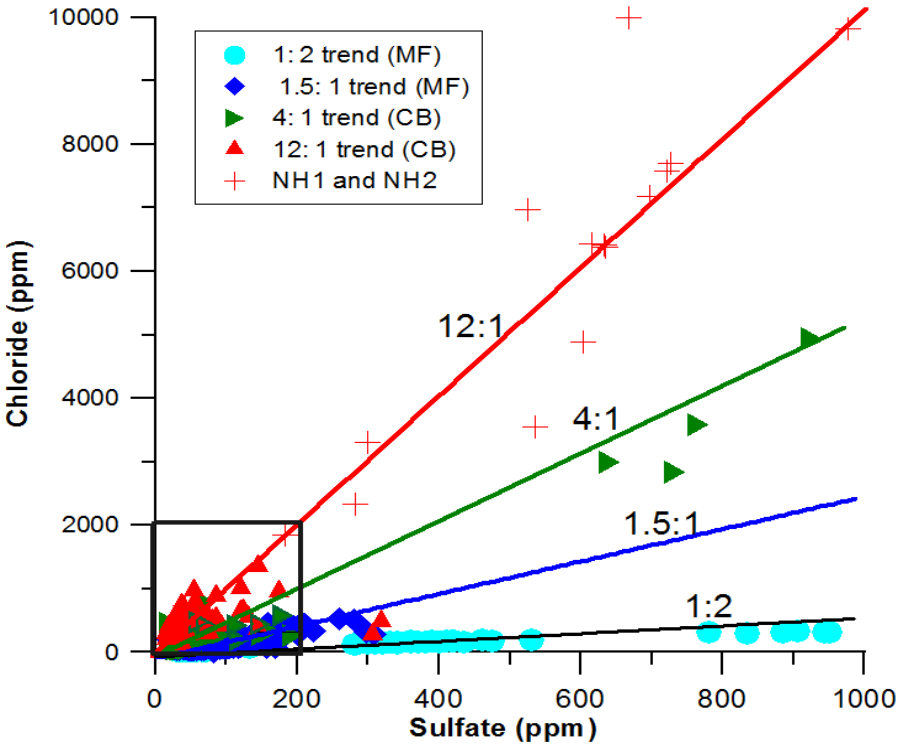
1: 2 trend (MF)
1.5: 1 trend (MF)
4: 1 trend (CB)
12: 1 trend (CB)
NH1 and NH2
12:1
4:1
1.5:1
1:2
Chloride (ppm)
Sulfate (ppm)
0
2000
4000
6000
8000
10000
0
200
400
600
800
1000

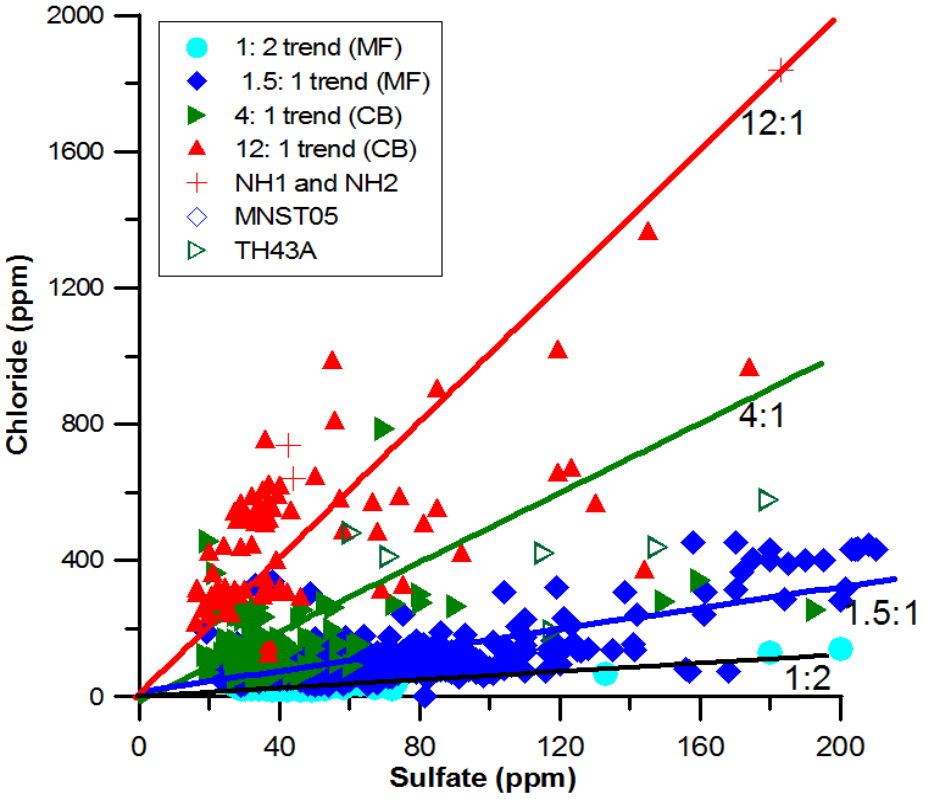
1: 2 trend (MF)
1.5: 1 trend (MF)
4: 1 trend (CB)
12: 1 trend (CB)
NH1 and NH2
MNST05
TH43A
12:1
4:1
1.5:1
1:2
Chloride (ppm)
Sulfate (ppm)
0
400
800
1200
1600
2000
0
40
80
120
160
200

Figure 3.5: (Top) Chloride vs. Sulfate trends for all the well samples. Note the individual measuremts were taken at different time intervals and different depths as presented in the Appendix table A1.(Bottom) Inset of figure A showing region within the black rectangle. Four trends are recognized from all the MF and CB wells (see Figure 4 for well locations). The cyan circles represent the 1:2 trend and blue diamonds represent the 1.5:1 trend of MF wells. The red triangles indicate the12:1 trend and green right pointing triangles are the 4:1 trend of CB wells. Low salinity end members are the MF wells shown as cyan circles and high salinity end member from CB wells as red triangles.

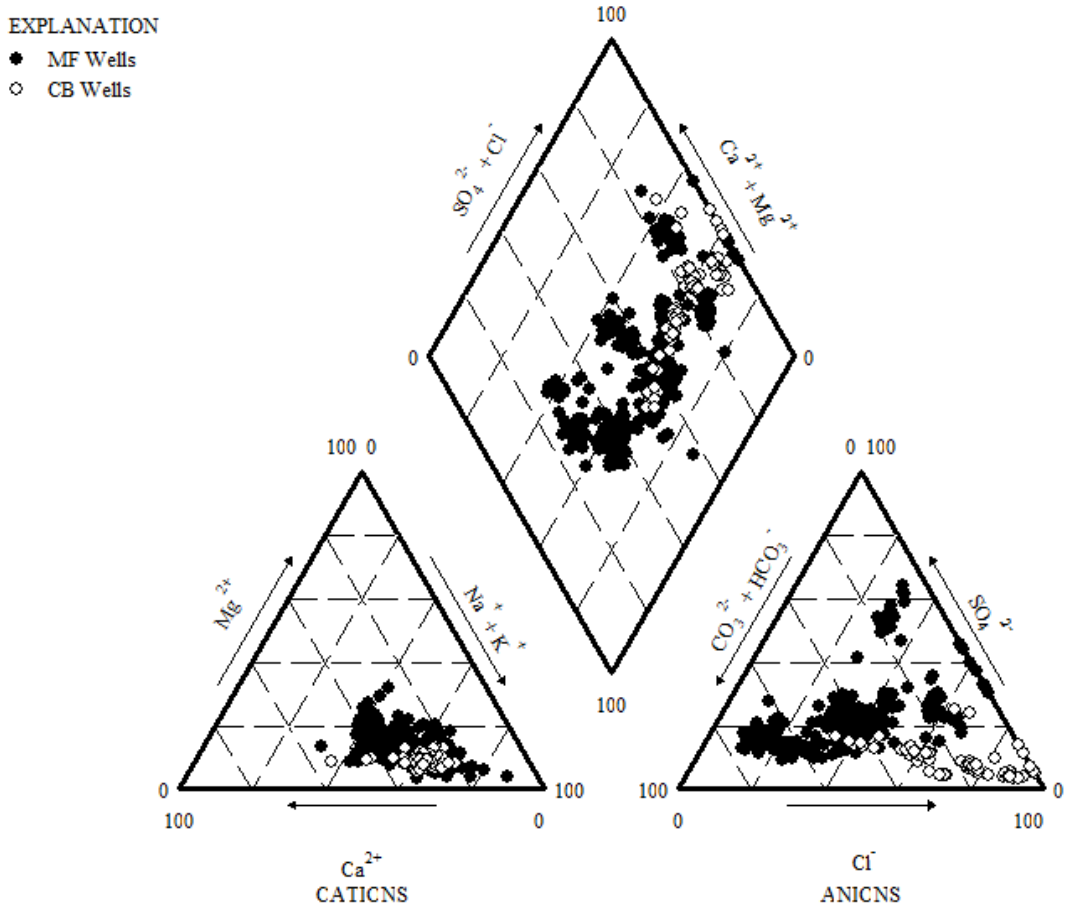

Figure 3.6: Piper diagram of all MF (closed circles) and CB (open circles) wells in the study area. In this diagram, the points are plotted in the Na-Ca and Cl-HCO_3 dominated regions in the cation and anion triangles, respectively

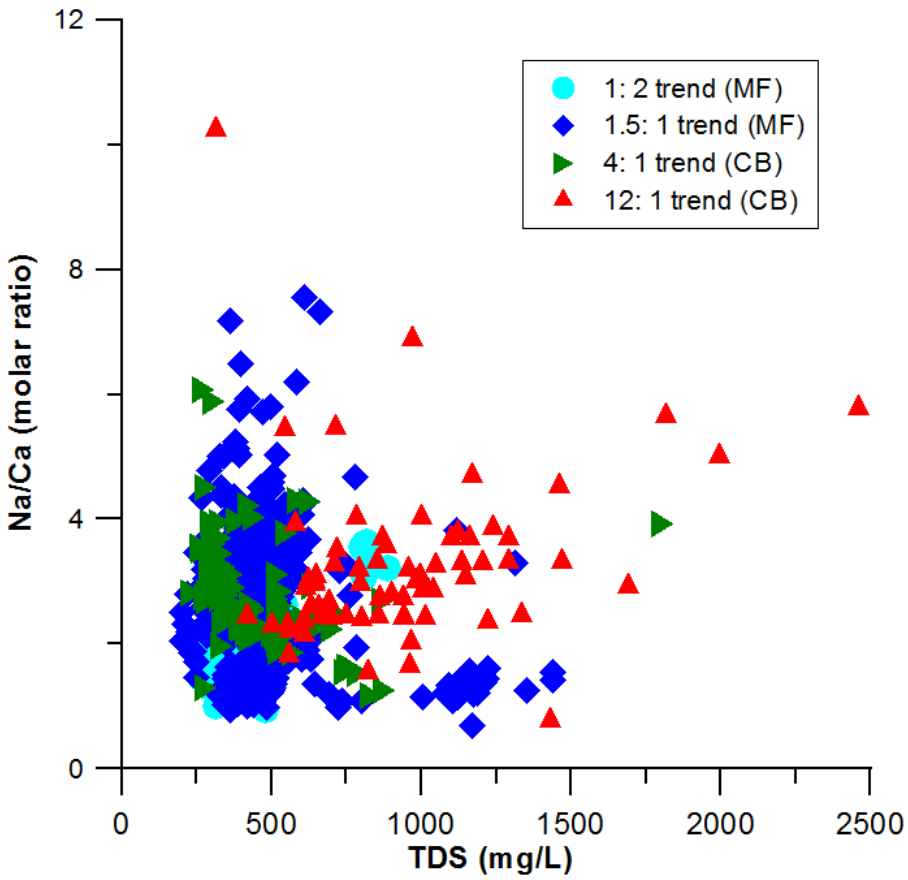

Figure 3.7: Variation of TDS with respect to Na/Ca molar ratio in the study area. MF wells 52 and 33 are represented as cyan circles and CB wells 521, 53, 54 with red triangles as two end members. Most of the MF wells are represented as blue diamonds and CB wells with green right pointing triangles.

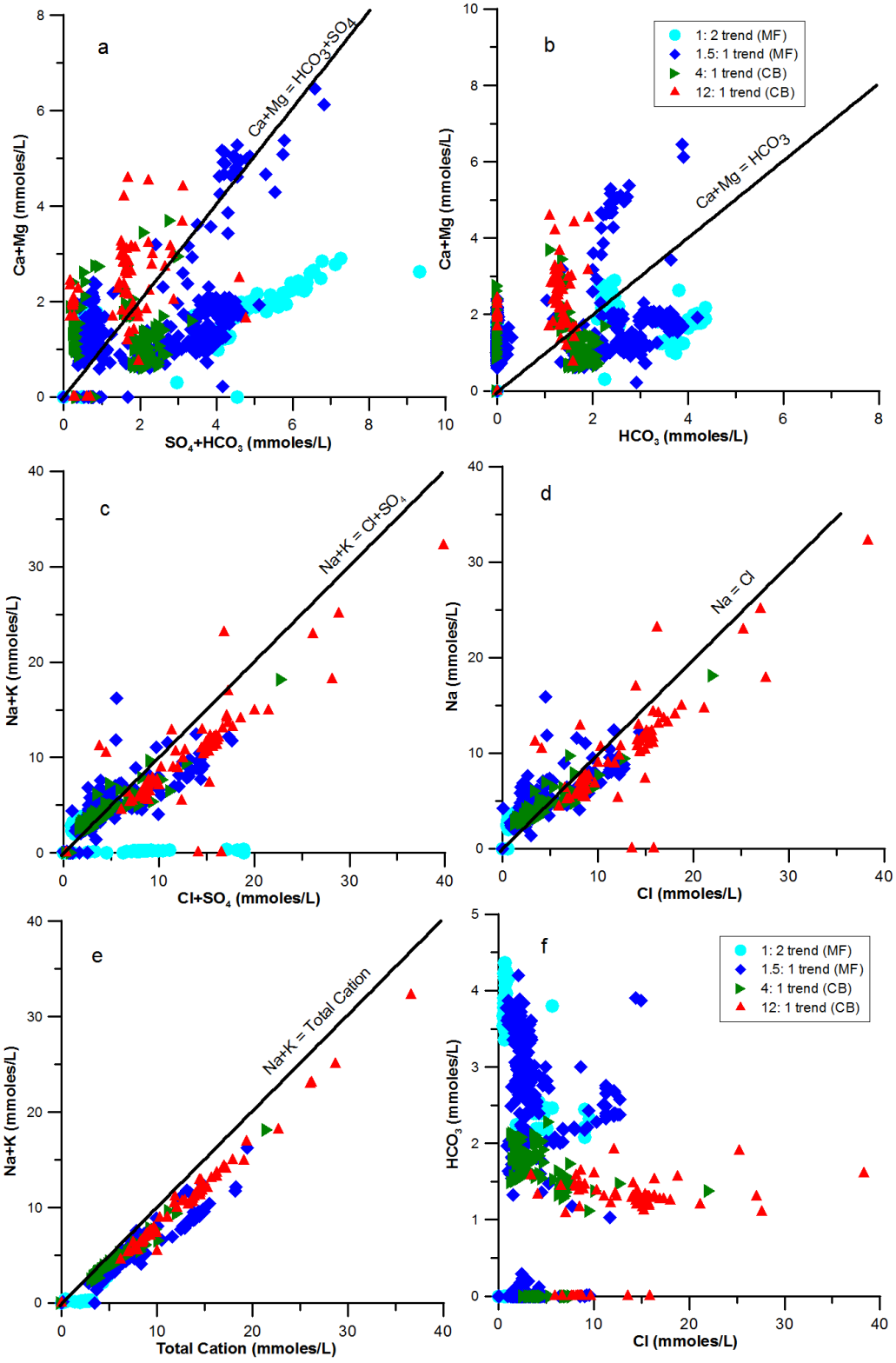

Figure 3.8: Ionic relations and sources of major components in groundwater. The symbols are the same as in Figure 7 for the four Cl: SO_4 trends observed in the MF and CB wells.

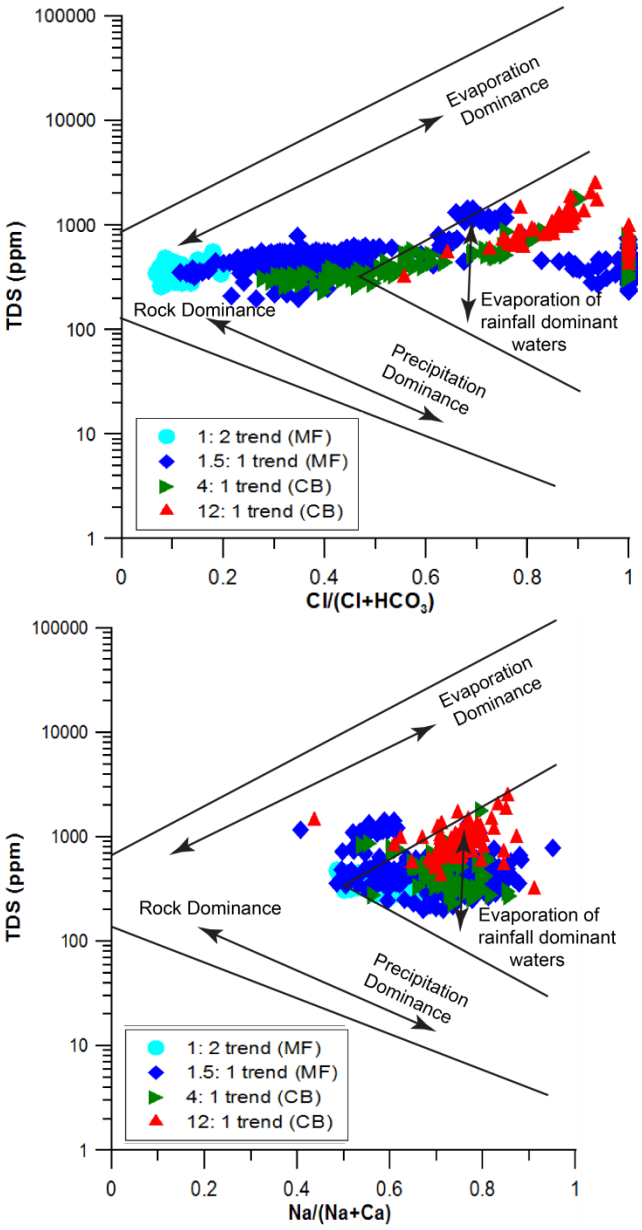

Figure 3.9: Gibbs plot govering groundwater chemistry. The symbols are the same as in Figure 7 for the four Cl: SO_4 trends of the MF and CB wells.

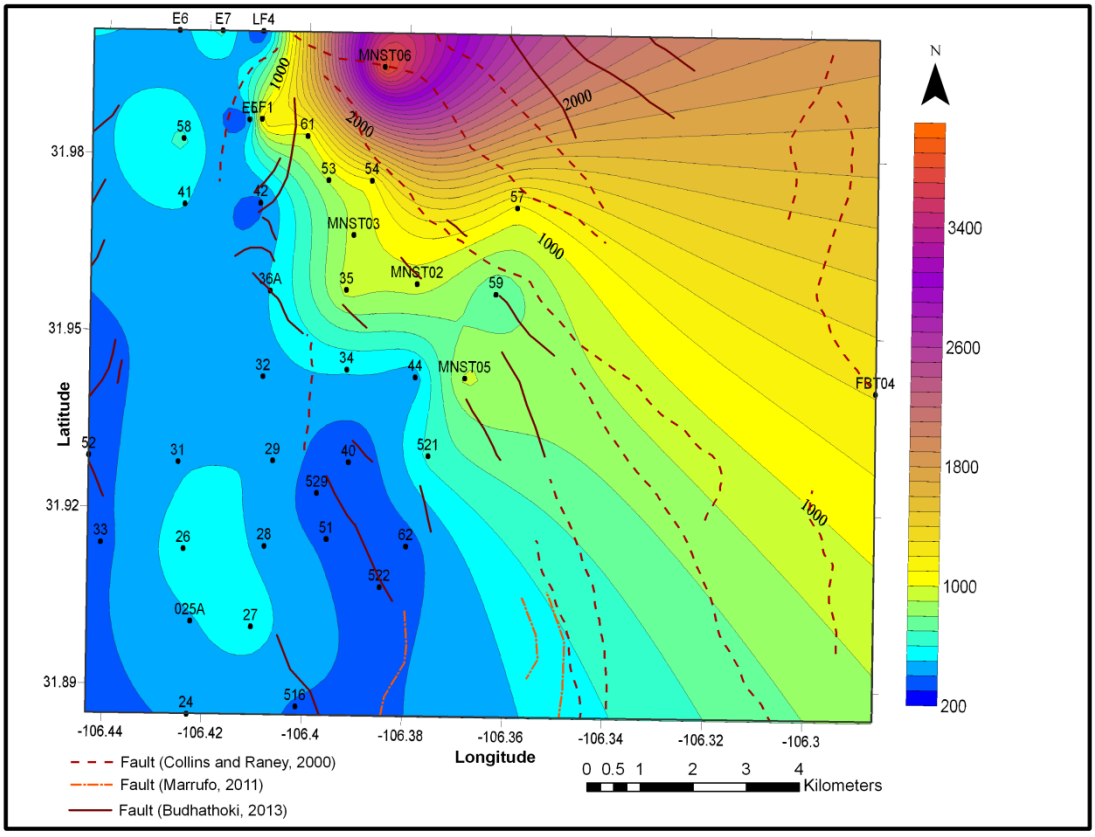

Figure 3.10: TDS concentration map (units of mg/L, 200 mg/L contour interval) for wells at or less than 500ft depth and the relationship with the mapped faults of the area. Faults with dashed lines are from Collins and Raney (2000) and Marrufo (2011) and solid lines from Budhathoki (2013).

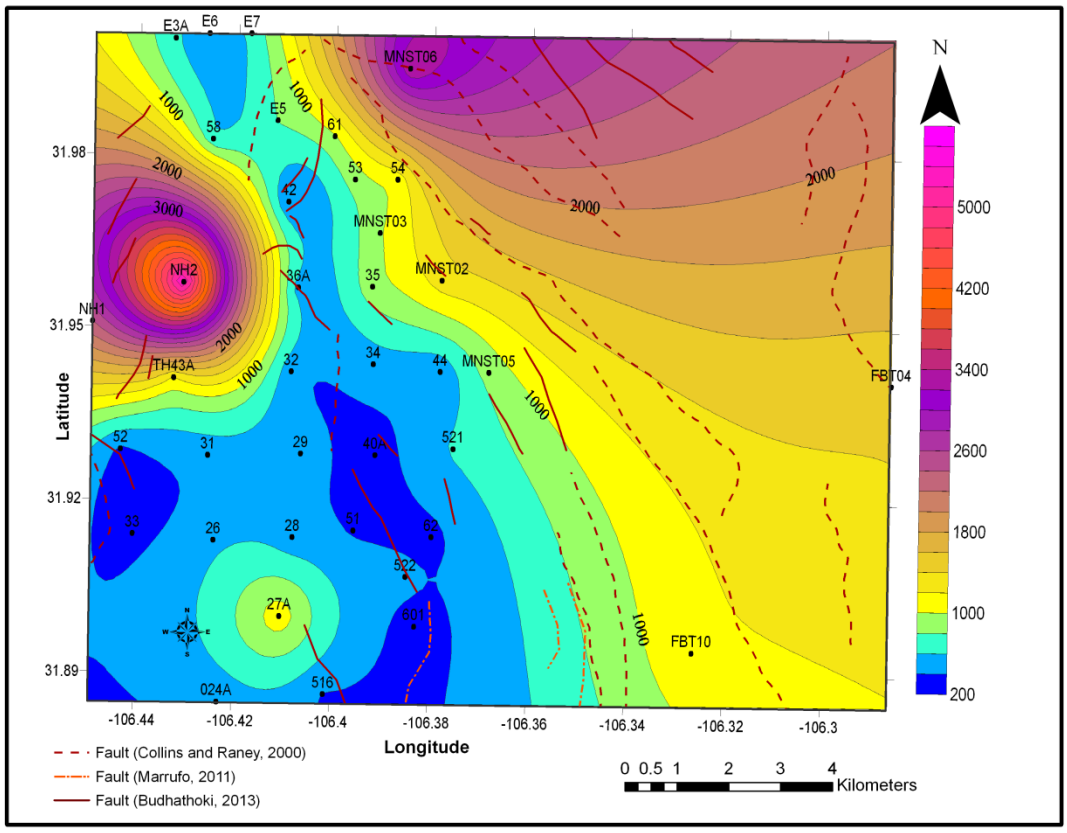

Figure 3.11: TDS concentration map at 500-800ft depth and the relationship with mapped faults in the area. Faults with dashed lines are from Collins and Raney (2000) and Marrufo (2011) and solid lines from Budhathoki (2013). Contour interval is 200 mg/L.

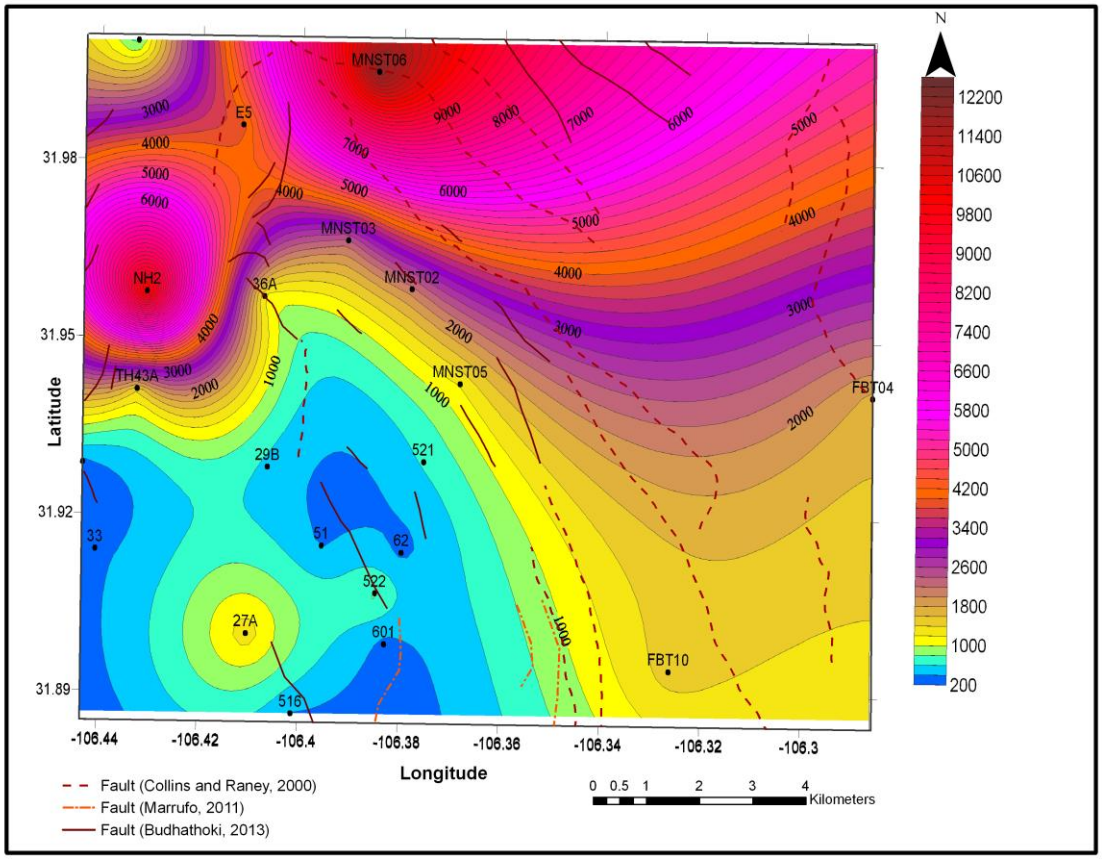

Figure 3.12: TDS concentration map at 800-1100ft depth and its relationship with the mapped faults of the area. Faults with dashed lines are from Collins and Raney (2000) and Marrufo (2011) and solid lines from Budhathoki (2013). Contour interval is 200 mg/L

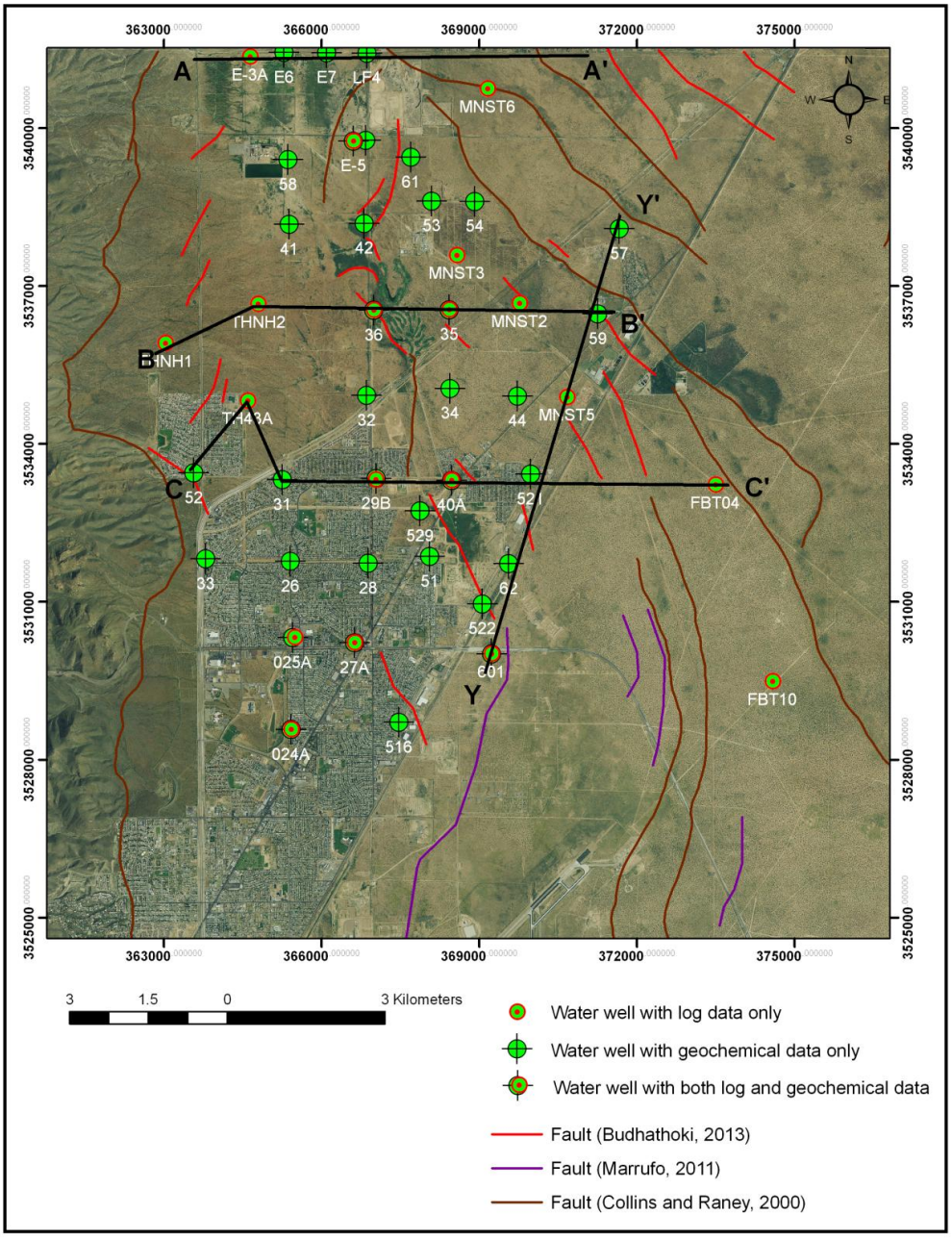

Figure 3.13: Profiles selected to compare chemical changes with geology of the study area. Three east-west oriented profiles (A-A', B-B', C-C') and one north-south oriented profile (Y-Y') were constructed to examine the variations in geochemistry of 50+ years.

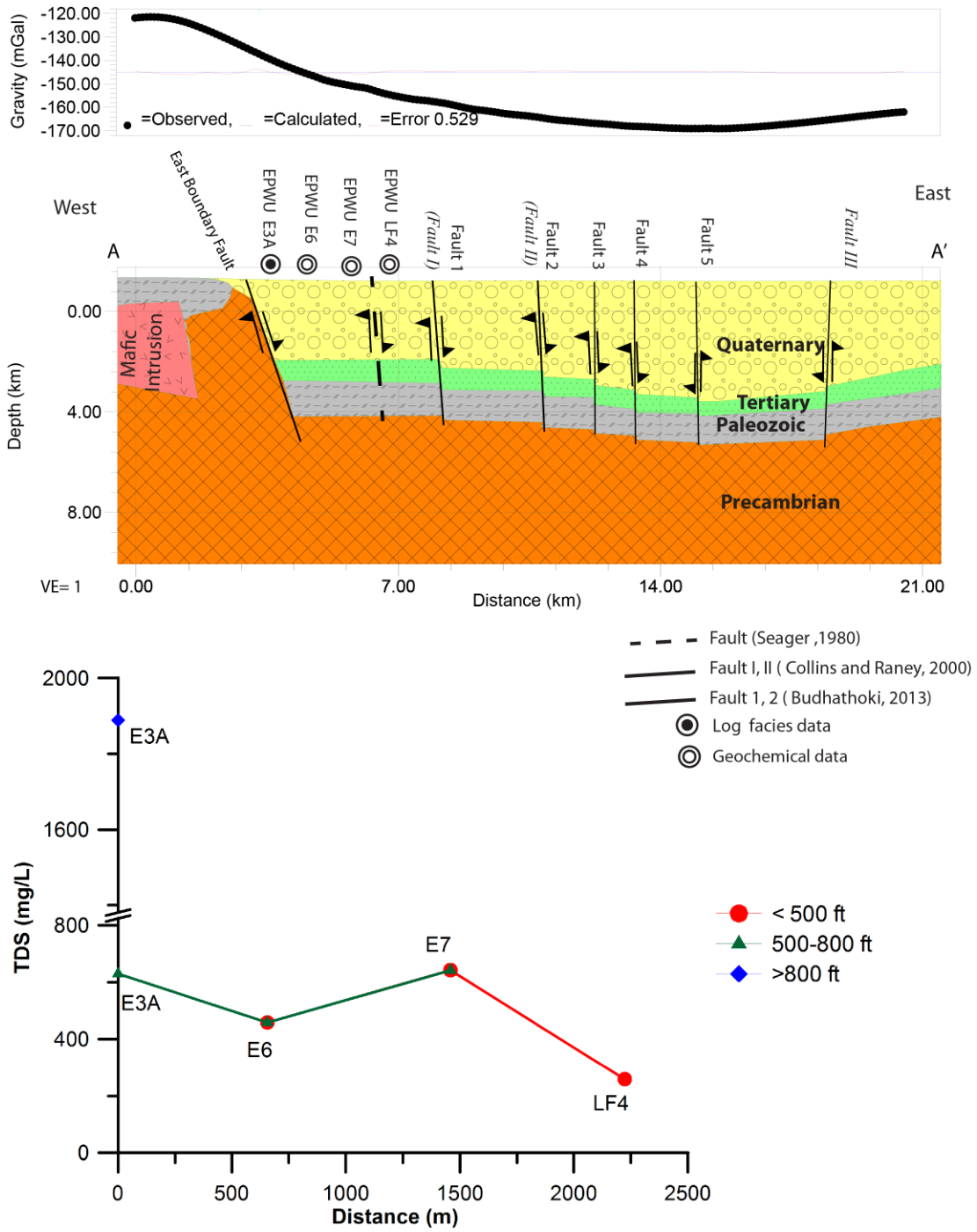

Figure 3.14(A): Geologic profile based on gravity modeling from Budhathoki (2013) (top) and changes in average TDS (bottom). Note that well logs were only available for well E3A.

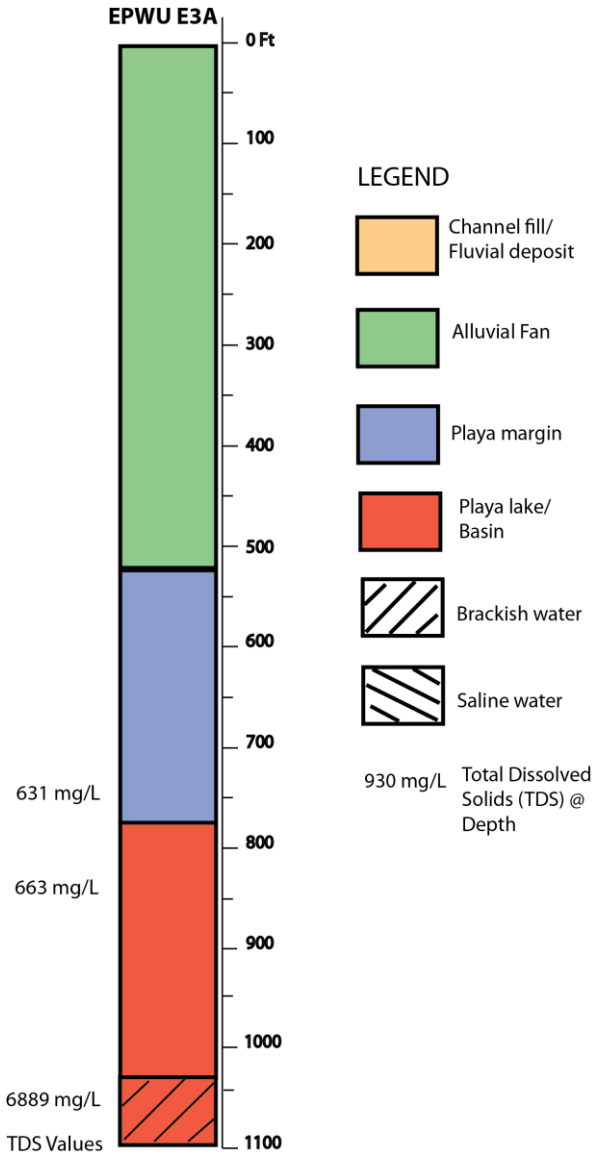

Figure 3.14(B): Facies from well log analysis (Budhathoki, 2013 and this study). Note that TDS values are averaged over depth.

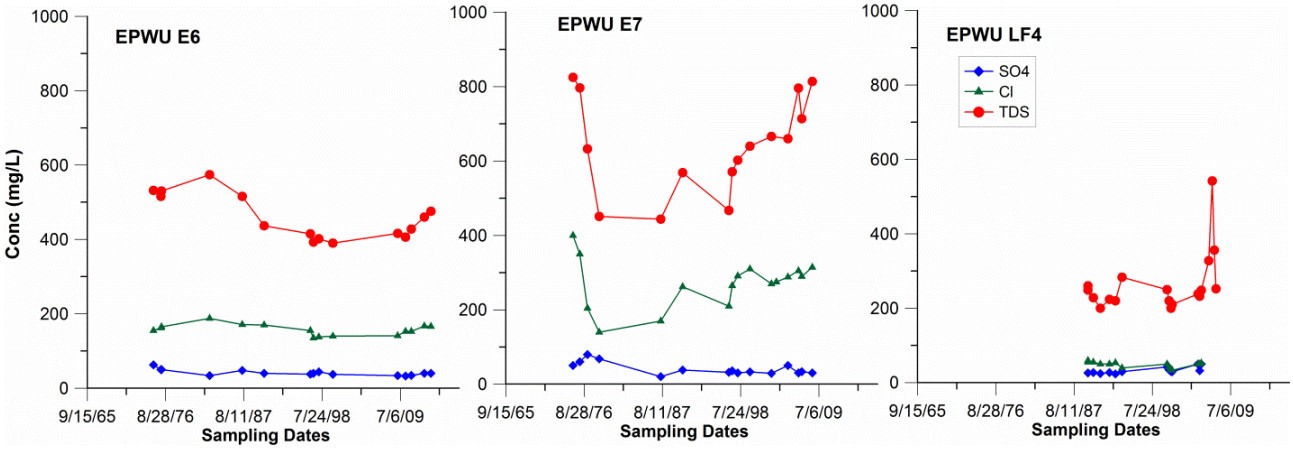

Figure 3.14(C): Geochemical profile (this study) shows the change in TDS and inorganic constituents over the past ~50 years. The values are averaged over the certain depth and time periods as data provided by El Paso Water Utilities in Appendix table A1.

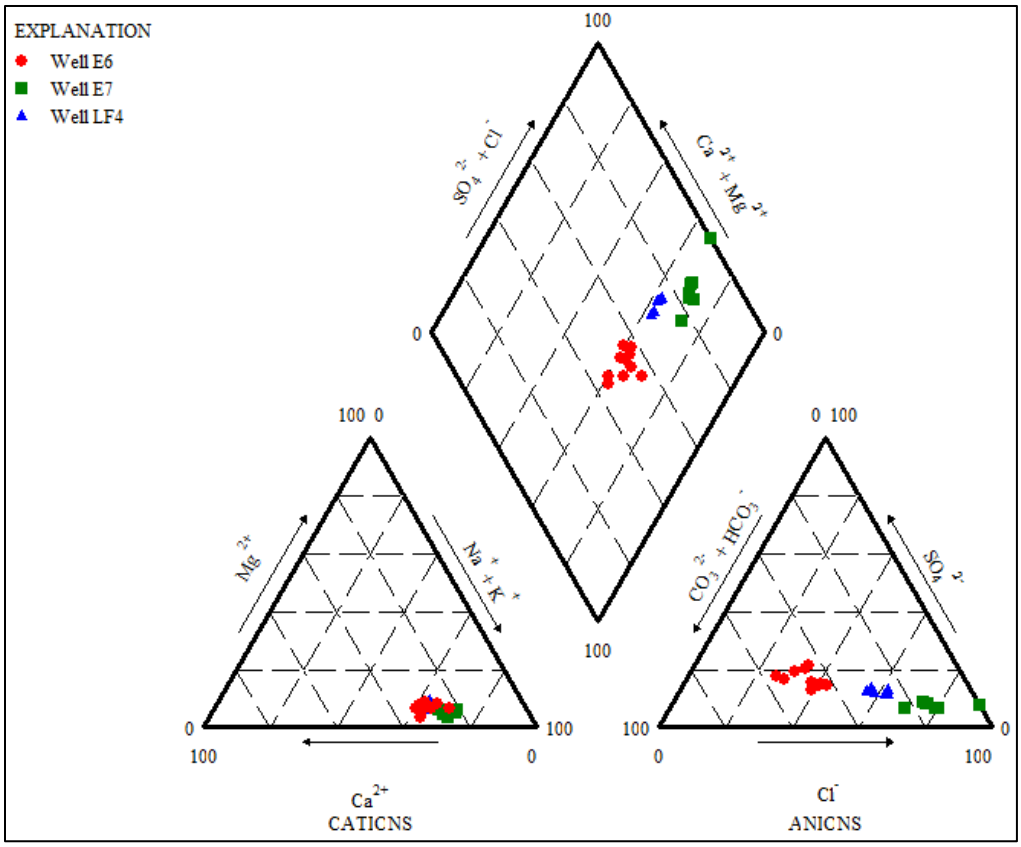

Figure 3.15: Piper diagram representation of hydrochemical data from wells along Profile A-A'. In this diagram, circles represent well E6, squares represent well E7 and triangles represent well LF4. Each well data are averaged over the depth of aquifer from where El Paso Water Utilities withdrawal the water (Appendix Table A1).

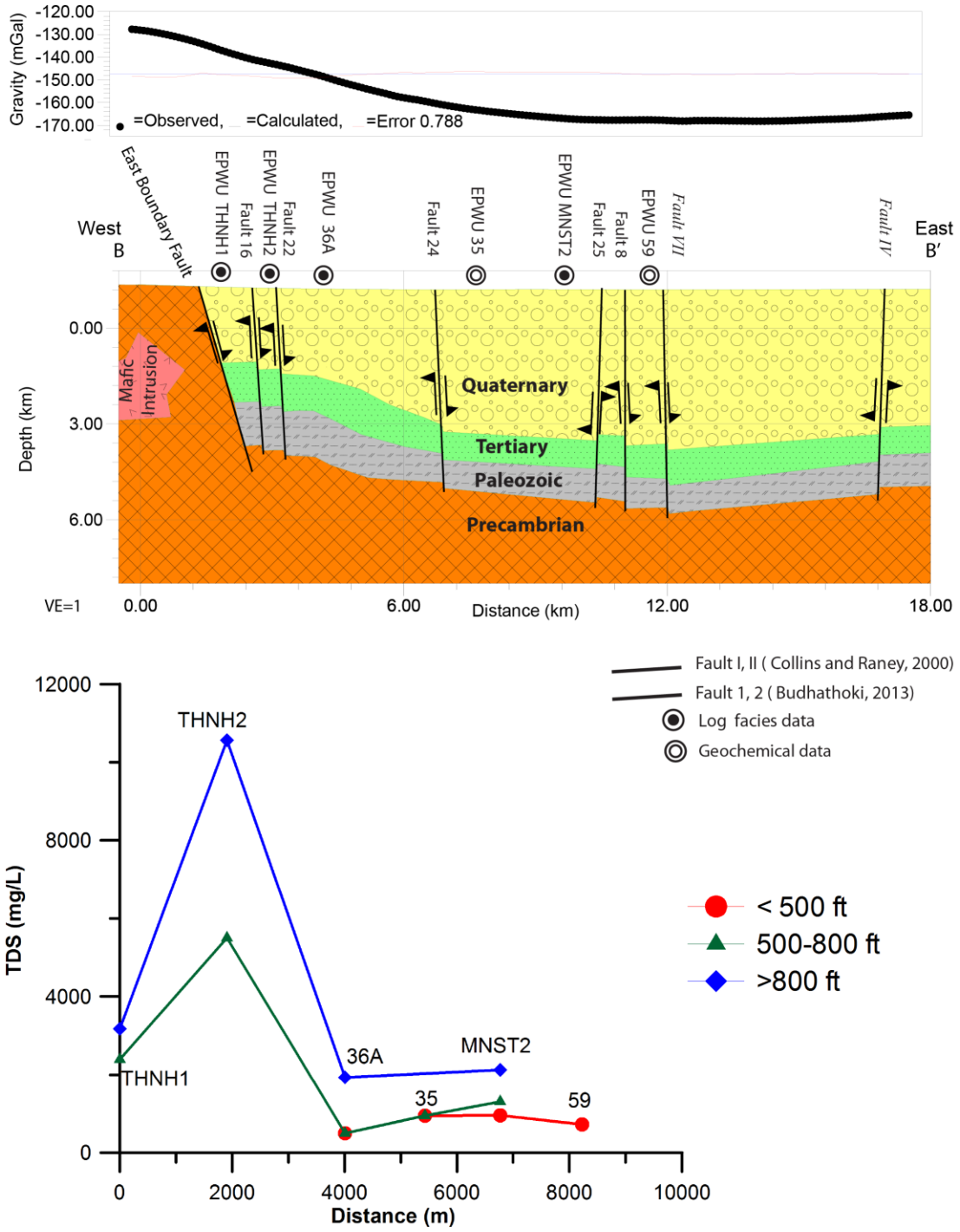

Figure 3.16(A): Gravity profile from Budhathoki (2013).

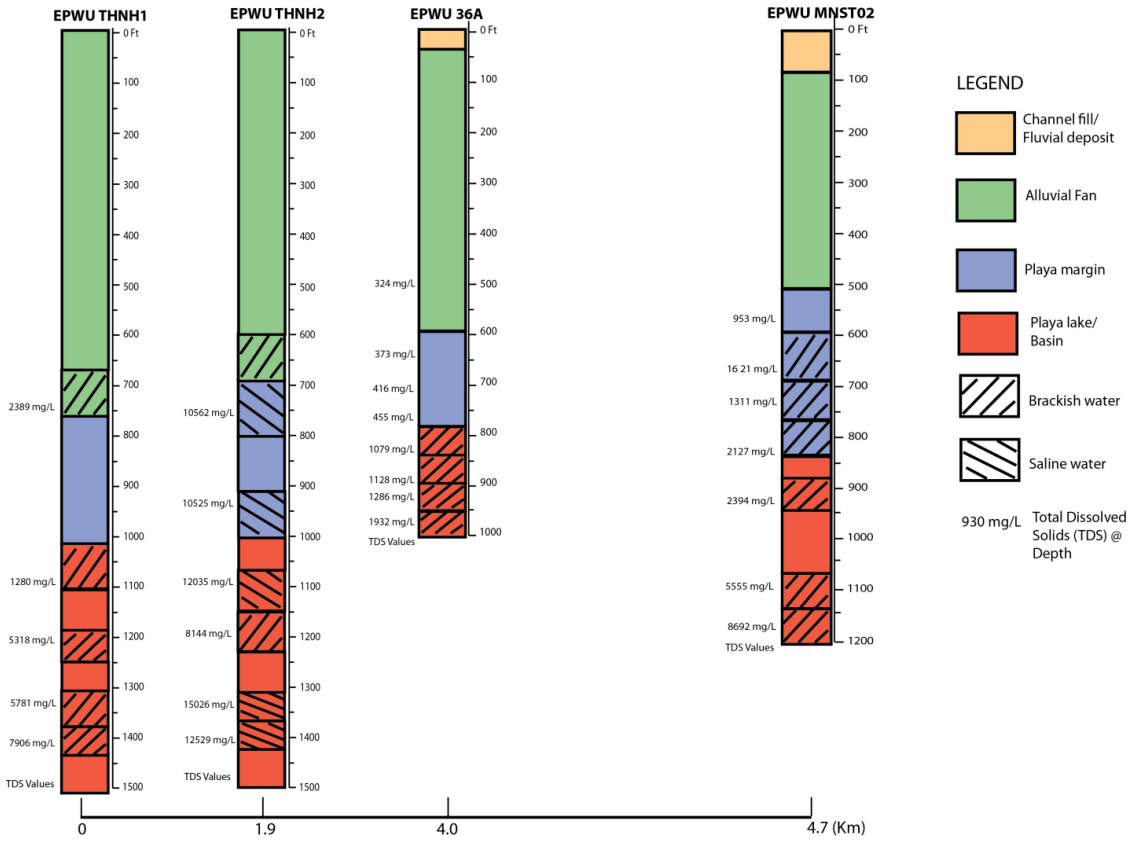

Figure 3.16(B): Facies determined from well log analysis by Budhathoki (2013) and this study. Note that TDS values are averaged over depth.

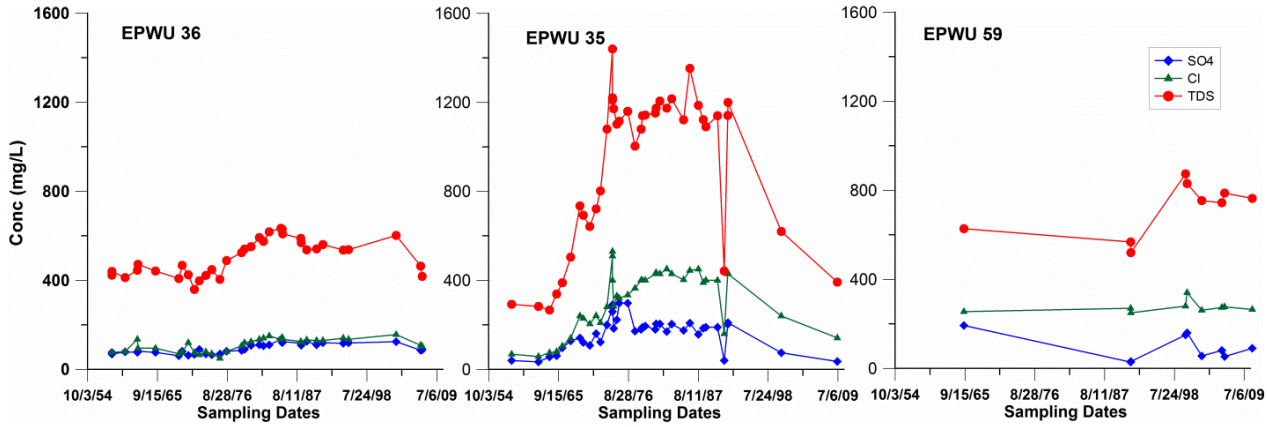

Figure 3.16(C): Geochemical profile (this study) indicating the change in water chemistry over the past ~50 years. The values are averaged over the certain depth and time periods as data provided by El Paso Water Utilities in Appendix table A1.

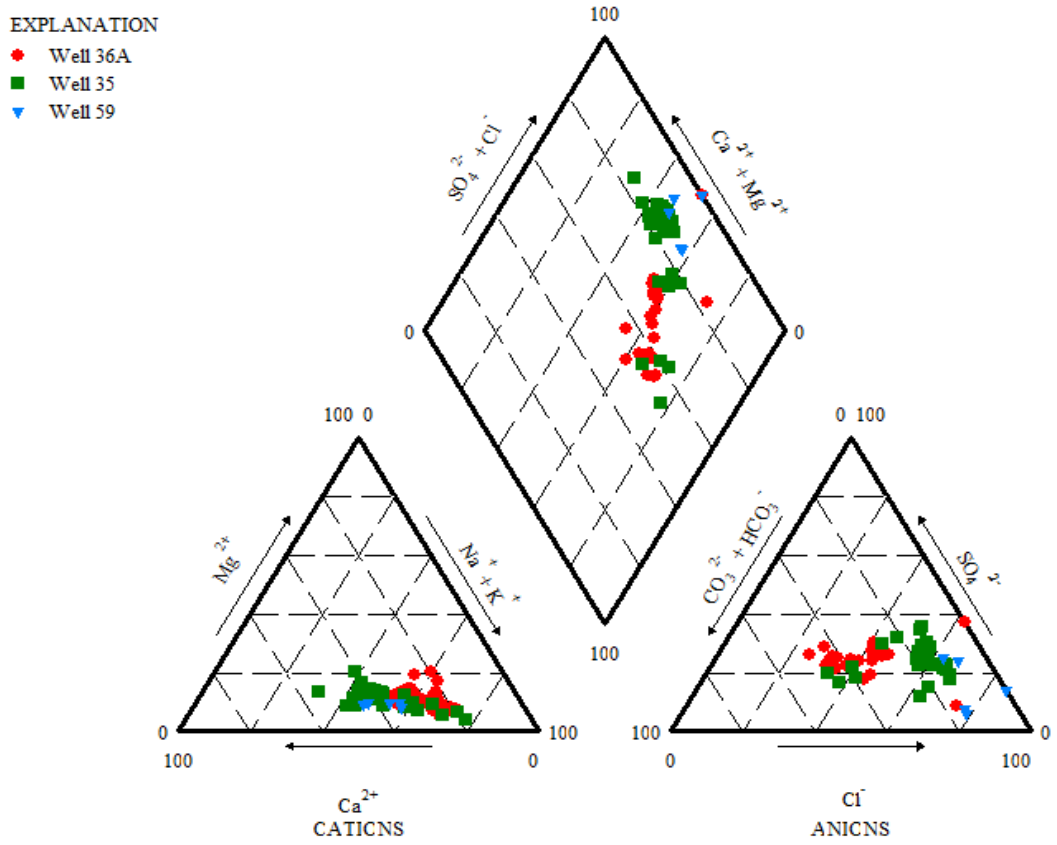

Figure 3.17: Piper diagram representation of hydrochemical data of Profile B-B'. In this diagram, circles represent well 36A, squares represent well 35 and inverted triangles represent well 59. Each well data are averaged over the depth of aquifer from where El Paso Water Utilities tap the water (Appendix Table A1).

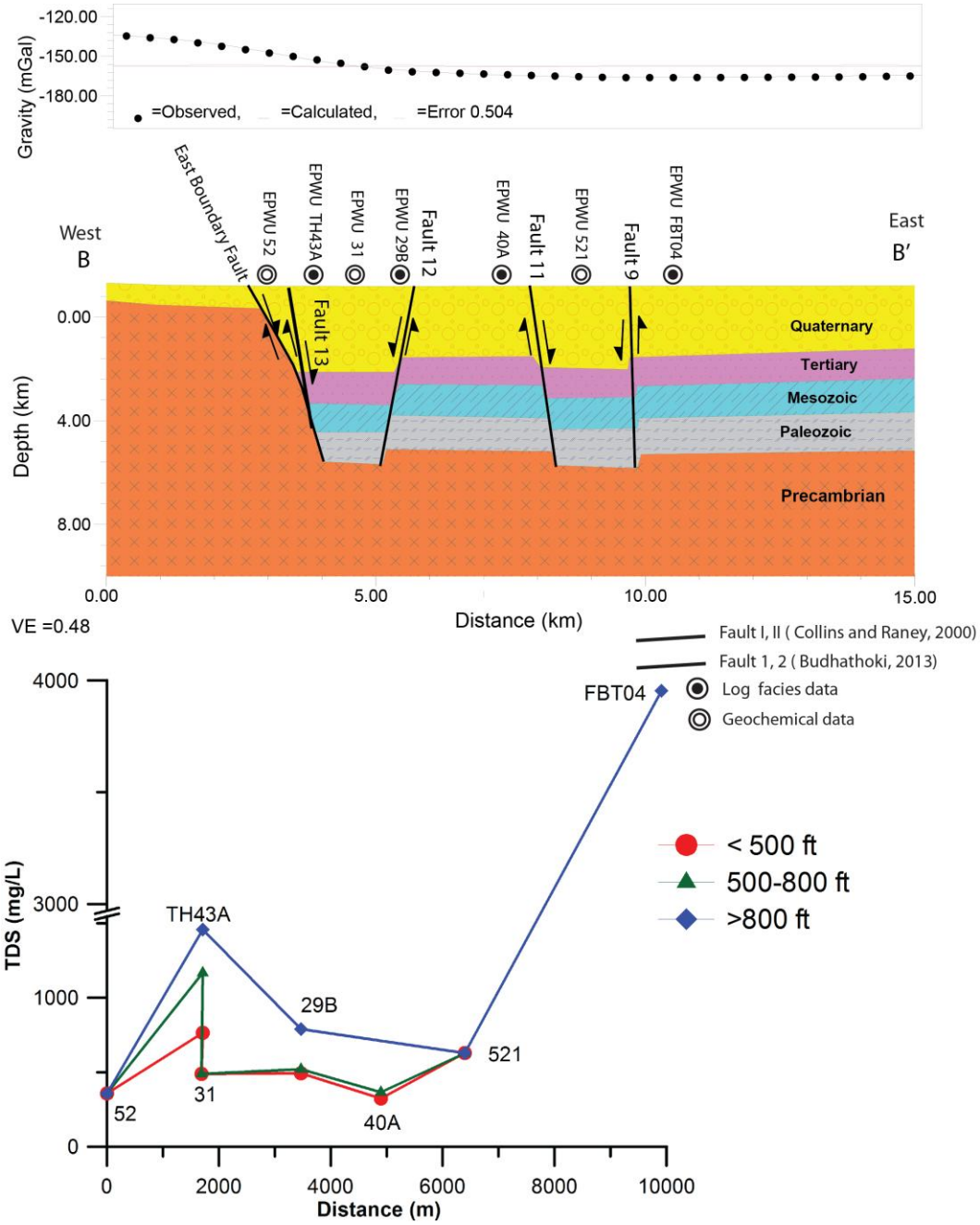

Figure 3.18(A): Gravity profile based on gravity modeling from Avila (2011). Note that the two values of TDS from the two aquifers taping the water at 500ft and 500-800ft in well TH43A.

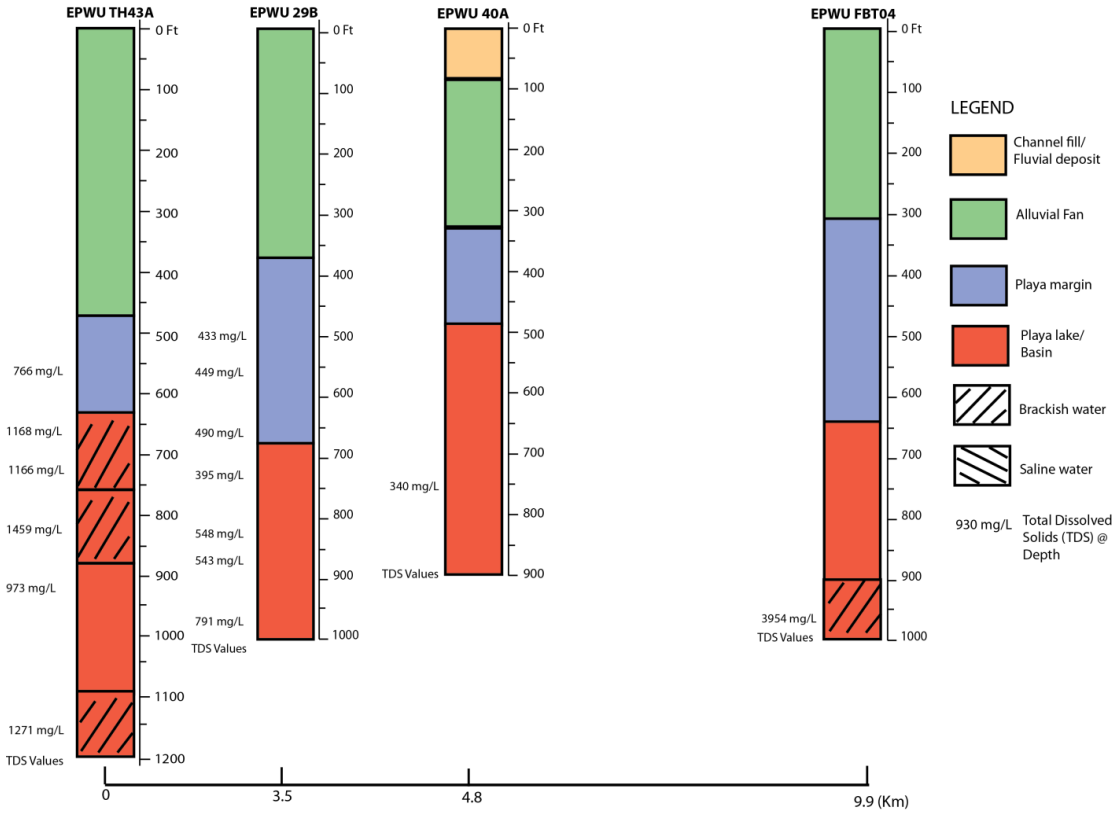

Figure 18(B): Facies determined from well log analysis by Budhathoki (2013 and this study. Note that TDS values are averaged over depth.

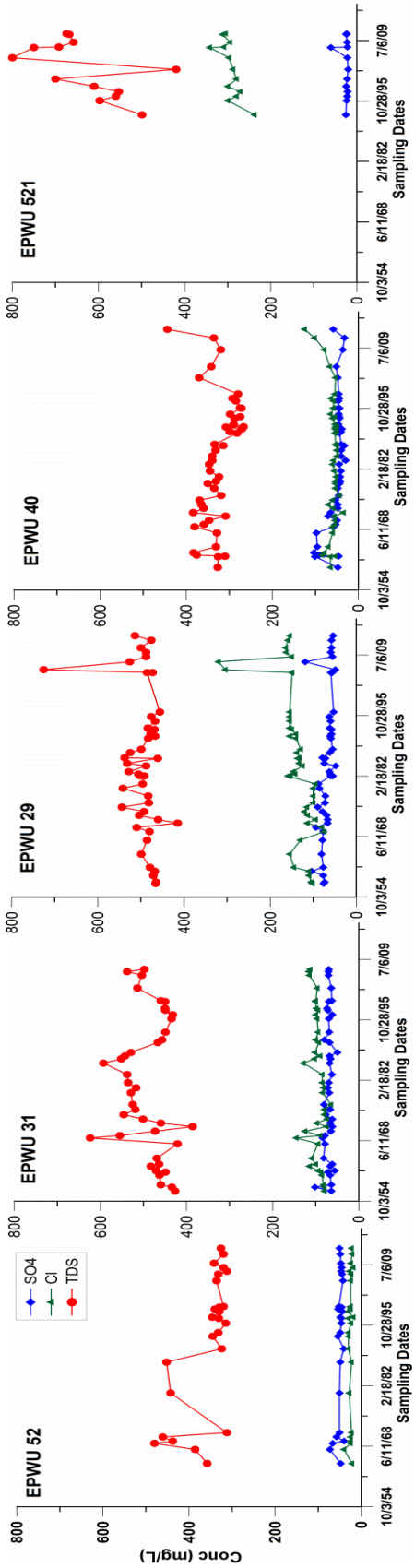

Figure 3.18(C): Geochemical profiles (this study) indicating the change in water chemistry over

the past ~50 years. The values are averaged over the certain depth and time periods as data provided by El Paso Water Utilities in Appendix table A1..

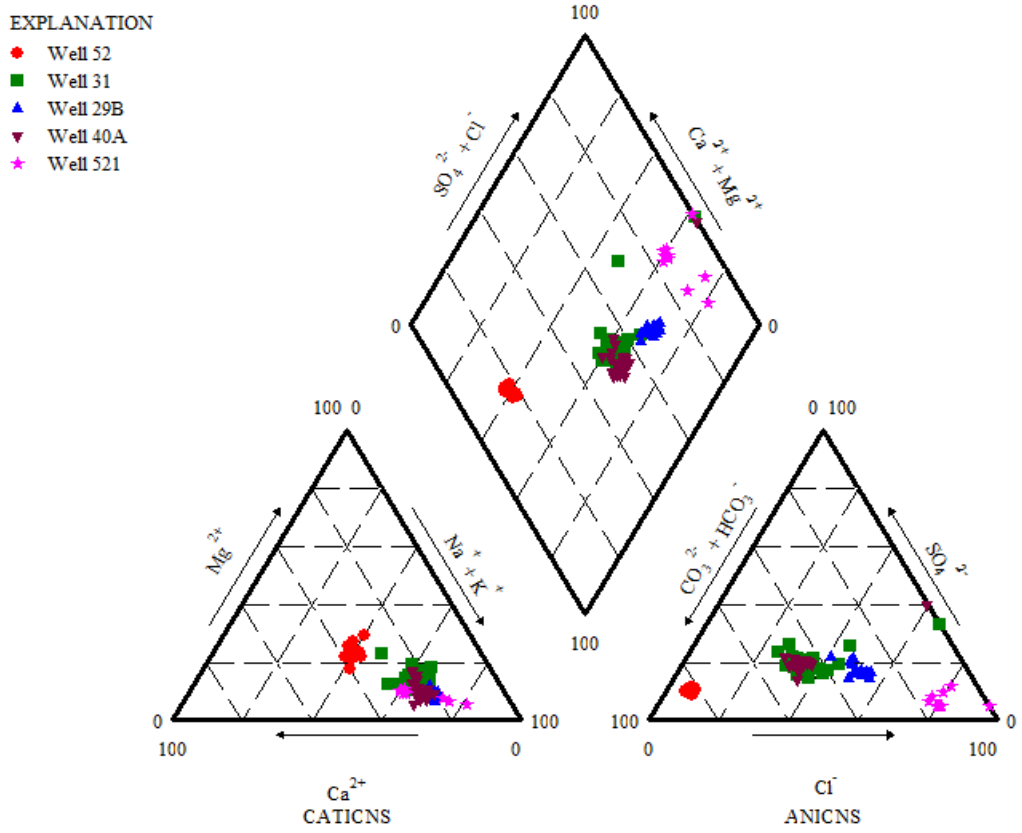

Figure 3.19: Piper diagram representation of hydrochemical data of Profile C-C'. Each well data are averaged over the depth of aquifer from where El Paso Water Utilities tap the water (Appendix Table A1).

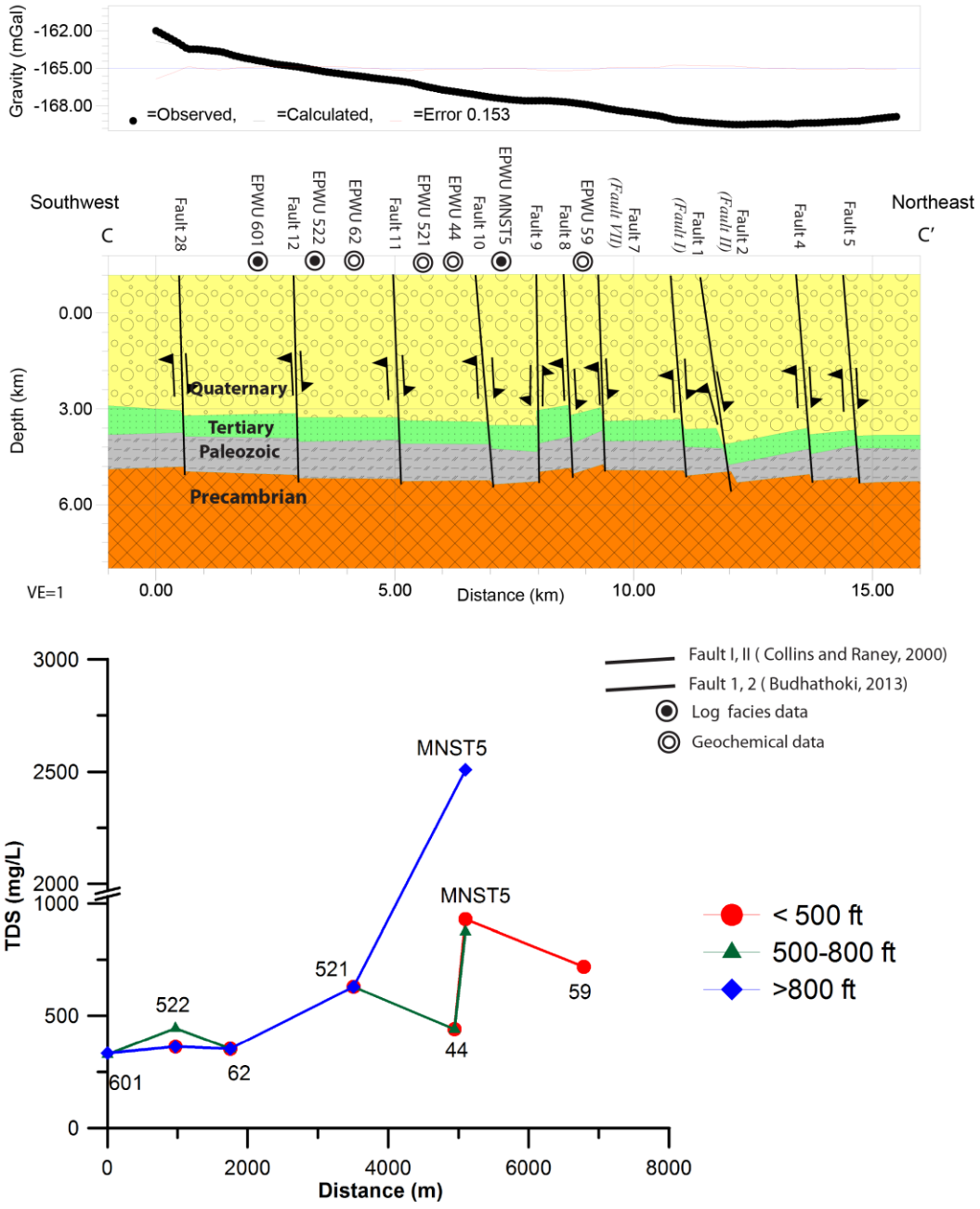

Figure 3.20(A): Gravity profile based on gravity modeling from Budhathoki (2013). Note that the two values of TDS from the two aquifers taping the water at <500ft in well MNST5.

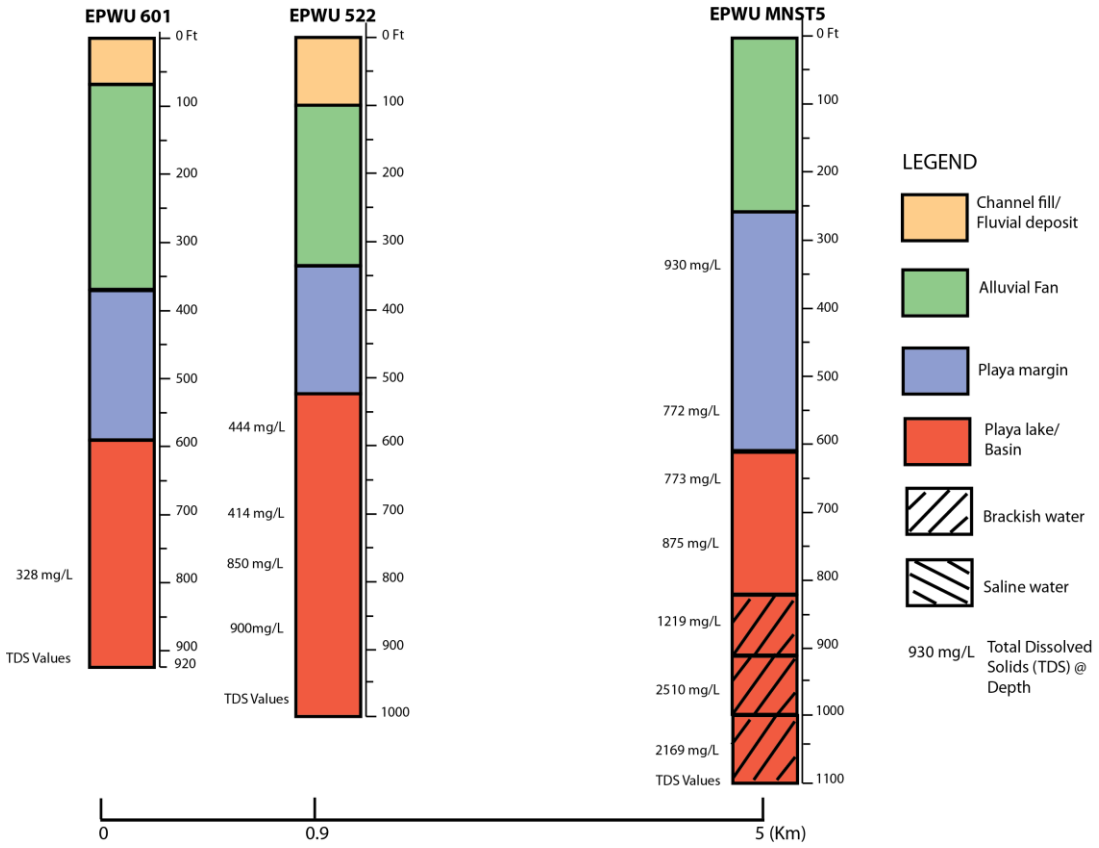

Figure 3.20(B): Facies determined from well log analysis by Budhathoki (2013 and this study). Note that TDS values are averaged over depth.

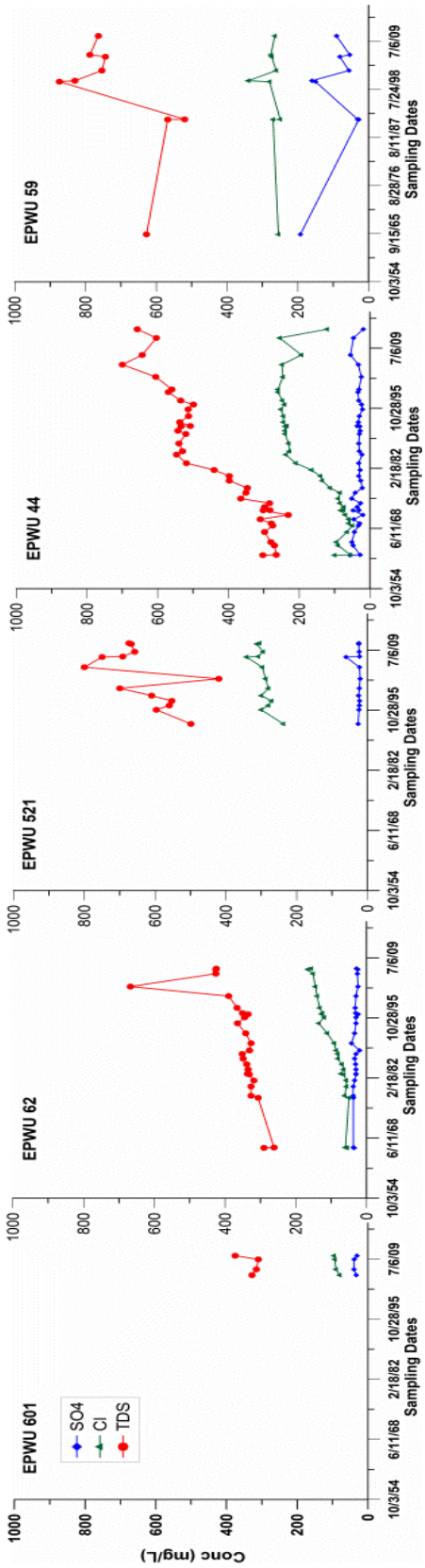

Figure 3.20(C): Geochemical profile (this study) indicating the change in water chemistry over

the past ~50 years. The values are averaged over the certain depth and time periods as data provided by El Paso Water Utilities in Appendix table A1.

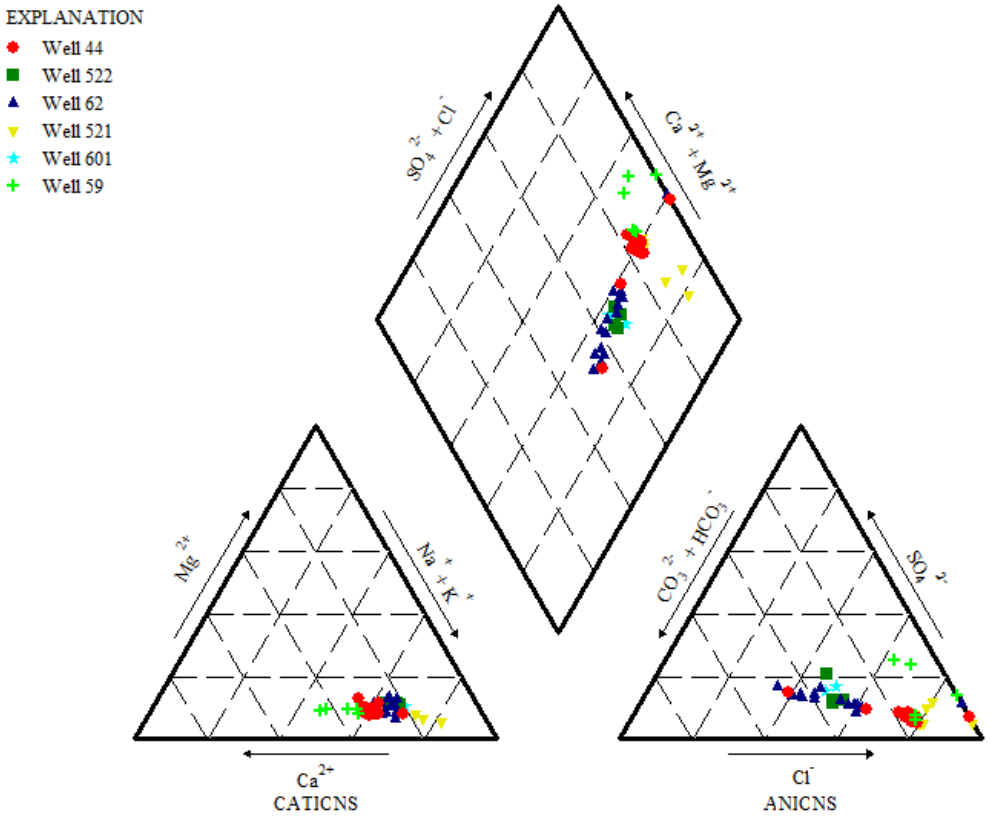

Figure 3.21: Piper diagram representation of hydrochemical data of Profile Y-Y'. Each well data are averaged over the depth of aquifer from where El Paso Water Utilities tap the water (Appendix Table A1).

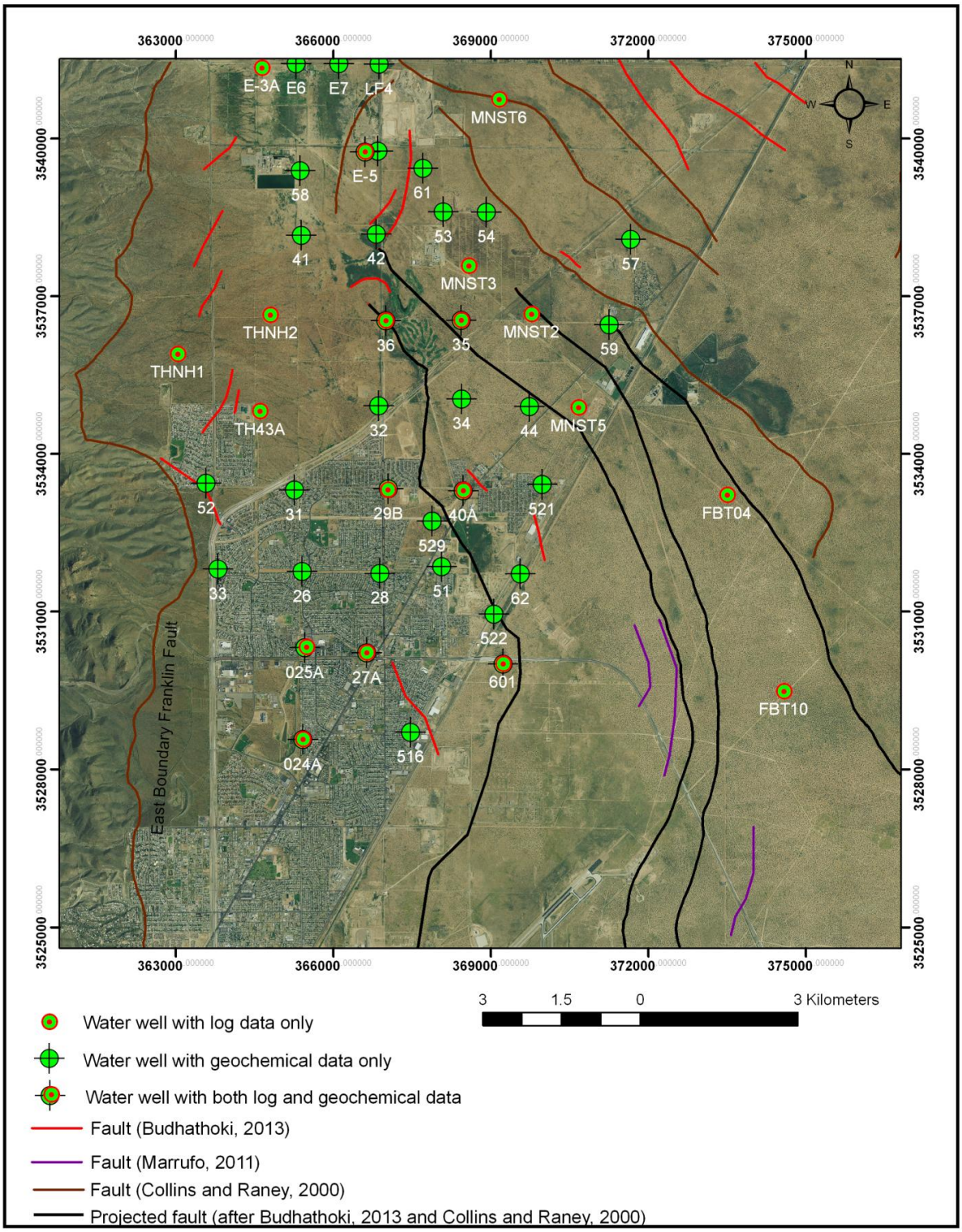

Figure 3.22: Fault model developed from connecting major and minor fault after this detailed study in Western HBA.

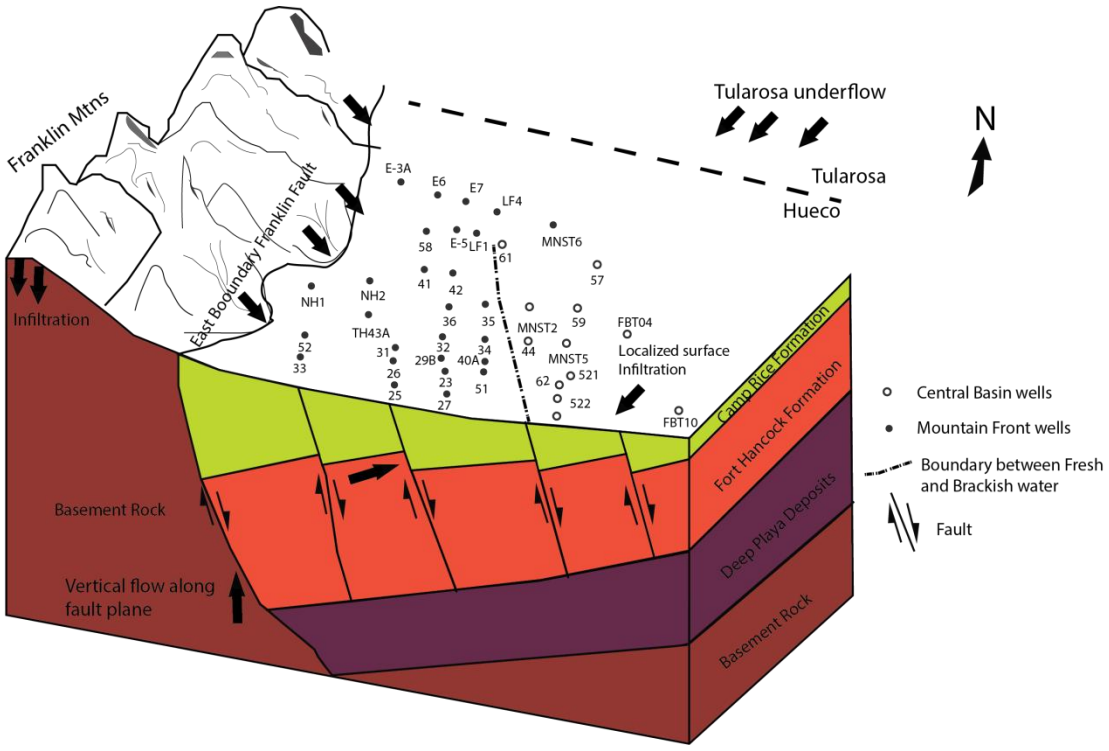

Figure 3.23: Conceptual groundwater flow model of Western Hueco Bolson Aquifer.

SECTION 4

Appendix

Table A1: Vertical Variation of Total Dissolved Solids (TDS) with three different depth interval as shown in Figures 10, 11, 12 (as described in the discussion section)

	State No	Well No	Lat	Long	Sampling Dates	Sampling Interval	Ca	Na	Cl	SO4	TDS	pH	Depth for Maps
1	JL-4905-321	LF1	31.9860759	-106.4094379	1988-2009	300-500	76.95	250.26	178.89	435.58	1224.83	7.65	500
2	JL-4905-325	LF4	32.0010117	-106.4094148	1989-2013	300-500	24.75	52.81	29.09	47.88	258.37	8.02	500
3	JL-4905-305	E5	31.9859446	-106.4119439	1965-2010	374-499	30.21	78.27	87.03	48.04	347.91	7.98	500
	JL-4905-305	E5	31.9859446	-106.4119439	n/a	n/a	n/a	n/a	n/a	n/a	814.00	n/a	500-800
	JL-4905-305	E5	31.9859446	-106.4119439	n/a	n/a	n/a	n/a	n/a	n/a	3899.00	n/a	800-1000
4	JL-4905-212	E6	32.0009504	-106.4260956	1974-2013	463-839	42.60	101.87	157.27	41.63	459.40	7.97	500
	JL-4905-212	E6	32.0009504	-106.4260956	1974-2013	463-839	42.60	101.87	157.27	41.63	459.40	7.97	500-800
5	JL-4905-213	E7	32.0009911	-106.4175455	1975-2008	445-875	49.77	160.19	271.50	41.34	643.27	7.92	500
	JL-4905-213	E7	32.0009911	-106.4175455	1975-2009	445-875	49.77	160.19	271.50	41.34	643.27	7.92	500-800
6	n/a	E3A	32.000096	-106.432976	n/a	n/a	n/a	n/a	n/a	n/a	631.00	n/a	500-800
	n/a	E3A	32.000096	-106.432976	n/a	n/a	n/a	n/a	n/a	n/a	663.00	n/a	800-1000
7	JL_4905-804	24	31.8849374	-106.4229338	1952-2002	301-788	49.03	64.37	65.57	60.51	416.38	7.90	500
	JL-4905-811	024A	31.8849374	-106.4229338	2004-2013	650-885	53.53	91.09	82.30	73.46	454.29	7.59	500-800
8	JL-4905-803	025A	31.9007561	-106.4224575	1953-2013	318-428	48.13	91.40	95.21	73.73	492.25	7.80	500
9	JL-4905-802	26	31.9130000	-106.4240000	1953-2012	360-820	46.27	112.20	129.31	81.07	555.67	7.87	500
	JL-4905-802	26	31.913	-106.424	1953-2012	360-820	46.27	112.20	129.31	81.07	555.67	7.87	500-800
10	JL-4905-902	27	31.8999356	-106.4103269	1955-1990	360-832	34.58	141.97	132.67	89.23	548.61	7.95	500.00
	JL-4905-902	27A	31.8999356	-106.4103269	2002-2013	680-700	81.73	281.64	456.74	95.23	1138.14	7.74	500-800
	JL-4905-902	27A	31.8999356	-106.4103269	2002-2013	680-800	n/a	n/a	n/a	n/a	1330.00	n/a	800
	JL-4905-902	27A	31.8999356	-106.4103269	2002-2013	880-1000	n/a	n/a	n/a	n/a	3040.00	n/a	1000
11	JL-4905-901	28	31.9136241	-106.4078754	1956-2013	348-727	32.66	110.28	89.06	81.96	475.42	8.03	500
	JL-4905-901	28	31.9136241	-106.4078754	1956-2013	348-727	32.66	110.28	89.06	81.96	475.42	8.03	500-800
12	JL-4905-606	29	31.9281490	-106.4064247	1956-1980	310-766	32.05	123.52	114.76	82.19	493.86	8.09	500

	JL-4905-615	29A	31.928149	-106.4064247	1982-1996	557-920	33.16	121.79	144.95	60.95	491.95	8.01	500-800
	JL-4905-615	29B	31.928149	-106.4064247	2005-2013	550-1020	36.48	131.89	190.56	63.17	519.67	7.79	500-800
	JL-4905-615	29B	31.9281490	-106.4064247	2005-2013	550-1020	36.48	131.89	190.56	63.17	519.67	7.79	800
	JL-4905-615	29B	31.9281490	-106.4064247	2005-2013	550-1020	n/a	n/a	n/a	n/a	791.00	n/a	1000
13	JL-4905-501	31	31.9277453	-106.4253123	1957-2007	319-730	35.83	110.98	96.07	69.71	489.25	7.90	500
	JL-4905-501	31	31.9277453	-106.4253123	1957-2007	319-730	35.83	110.98	96.07	69.71	489.25	7.90	500-800
14	JL-4905-603	32	31.9423855	-106.4085982	1957-2010	335-657	32.45	106.42	95.69	72.83	450.79	8.00	500
	JL-4905-603	32	31.9423855	-106.4085982	1957-2010	335-657	32.45	106.42	95.69	72.83	450.79	8.00	500-800
15	JL-4905-801	33	31.9140088	-106.4405387	1957-2013	418-1125	37.13	68.39	36.35	44.16	368.44	7.76	500
	JL-4905-801	33	31.9140088	-106.4405387	1957-2013	418-1125	37.13	68.39	36.35	44.16	368.44	7.76	500-800
	JL-4905-801	33	31.9140088	-106.4405387	1957-2013	418-1125	37.13	68.39	36.35	44.16	368.44	7.76	800
16	JL-4905-604	34	31.9437615	-106.3918717	1958-2007	325-802	55.07	100.98	153.20	82.41	512.63	8.07	500
	JL-4905-604	34	31.9437615	-106.3918717	1958-2007	325-802	55.07	100.98	153.20	82.41	512.63	8.07	500-800
17	JL-4905-602	35	31.9572486	-106.3921736	1958-2009	354-699	119.05	165.49	317.00	169.15	942.55	7.82	500
	JL-4905-602	35	31.9572486	-106.3921736	1958-2009	354-699	119.05	165.49	317.00	169.15	942.55	7.82	500-800
18	JL-4905-601	36A	31.9569721	-106.4073405	1958-2007	350-690	43.00	106.14	109.12	94.24	502.35	7.94	500
	JL-4905-601	36A	31.9569721	-106.4073405	1958-2007	350-690	43.00	106.14	109.12	94.24	502.35	7.94	500-800
	JL-4905-601	36A	31.9569721	-106.4073405	n/a	n/a	n/a	n/a	n/a	n/a	1128.00	n/a	800-1000
19	JL_4905-607	40	31.9280174	-106.3912856	1959-2005	308-826	23.06	74.98	57.67	52.31	324.70	8.11	500
	JL-4905-637	40A	31.9280174	-106.3912856	1999-2013	650-885	31.87	84.27	102.27	42.67	366.67	7.47	500-800
20	JL-4905-204	41	31.9715078	-106.4246224	1959-2005	359-515	34.39	127.90	132.43	79.86	507.35	7.94	500
	JL-4905-301	42	31.9718547	-106.4095069	1958-2007	320-671	31.19	85.48	84.83	51.14	375.07	8.05	500
	JL-4905-301	42	31.9718547	-106.4095069	1958-2007	320-671	31.19	85.48	84.83	51.14	375.07	8.05	500-800
21	JL-4905-605	44	31.9426038	-106.3782061	1960-2013	324-769	41.25	100.13	208.08	46.70	440.03	8.06	500
	JL-4905-605	44	31.9426038	-106.3782061	1960-2013	324-769	41.25	100.13	208.08	46.70	440.03	8.06	500-800
22	JL-4905-903	51	31.9149178	-106.3954912	1963-2013	269-1037	26.80	88.86	68.60	63.92	382.00	8.04	500
	JL-4905-903	51	31.9149178	-106.3954912	1963-2013	269-1037	26.80	88.86	68.60	63.92	382.00	8.04	500-800
	JL-4905-903	51	31.9149178	-106.3954912	1963-2013	269-1037	26.80	88.86	68.60	63.92	382.00	8.04	800
23	JL-4905-504	52	31.9287016	-106.4431667	1961-2013	481-1152	44.50	54.26	25.68	49.94	357.24	7.72	500
	JL-4905-504	52	31.9287016	-106.4431667	1961-2013	481-1152	44.50	54.26	25.68	49.94	357.24	7.72	500-800
	JL-4905-504	52	31.9287016	-106.4431667	1961-2013	481-1152	44.50	54.26	25.68	49.94	357.24	7.72	800
24	JL-4905-303	53	31.9758277	-106.3960251	1955-2000	380-860	78.17	229.20	447.03	52.73	909.67	7.91	500

	JL-4905-303	53	31.9758277	-106.3960251	1955-2000	380-860	78.17	229.20	447.03	52.73	909.67	7.91	500-800
25	JL-4905-304	54	31.9758730	-106.3873375	1955-1974	377-746	77.94	276.25	523.94	58.06	1066.69	7.88	500
	JL-4905-304	54	31.9758730	-106.3873375	1955-1974	377-746	77.94	276.25	523.94	58.06	1066.69	7.88	500-800
26	JL-4906-101	57	31.9714886	-106.3581841	1965	n/a	115.60	245.80	465.00	151.20	1060.20	7.54	500
27	JL-4905-214	58	31.9825992	-106.4250553	1996-2006	276-685	58.64	145.10	211.10	102.13	632.00	7.90	500
	JL-4905-214	58	31.9825992	-106.4250553	1996-2006	276-685	58.64	145.10	211.10	102.13	632.00	7.90	500-800
28	JL-4906-401	59	31.9568417	-106.3622977	1965-2010	348-451	80.42	137.67	274.56	93.58	718.89	7.81	500
29	JL-4905-306	61	31.9832761	-106.4002868	2000-2006	391-603	89.67	186.67	345.17	109.29	972.83	7.82	500
	JL-4905-306	61	31.9832761	-106.4002868	2000-2006	391-603	89.67	186.67	345.17	109.29	972.83	7.82	500-800
30	JL-4905-906	62	31.9138642	-106.3795951	1966-2007	330-950	29.18	80.16	98.72	31.34	352.12	8.07	500
	JL-4905-906	62	31.9138642	-106.3795951	1966-2007	330-950	29.18	80.16	98.72	31.34	352.12	8.07	500-800
	JL-4905-906	62	31.9138642	-106.3795951	1966-2007	330-950	29.18	80.16	98.72	31.34	352.12	8.07	800
31	JL-4905-914	516	31.8864275	-106.4012598	1992-2012	371-935	27.26	102.64	98.87	72.37	390.19	7.93	500
	JL-4905-914	516	31.8864275	-106.4012598	1992-2012	371-935	27.26	102.64	98.87	72.37	390.19	7.93	500-800
	JL-4905-914	516	31.8864275	-106.4012598	1992-2012	371-935	27.26	102.64	98.87	72.37	390.19	7.93	800
32	JL-4905-635	521	31.9292332	-106.3753919	1992-2011	380-965	57.66	139.23	293.62	26.20	629.31	7.89	500
	JL-4905-635	521	31.9292332	-106.3753919	1992-2011	380-965	57.66	139.23	293.62	26.20	629.31	7.89	500-800
	JL-4905-635	521	31.9292332	106.3753919	1992-2011	380-965	57.66	139.23	293.62	26.20	629.31	7.89	800
33	JL-4905-921	522	31.9069127	-106.3847870	2005-2012	550-1020	25.55	78.18	108.08	32.16	361.75	8.06	500
	JL-4905-921	522	31.9069127	-106.3847870	2005-2012	550-1020	25.55	78.18	108.08	32.16	444.00	8.06	500-800
	JL-4905-921	522	31.9069127	-106.3847870	2005-2012	550-1020	25.55	78.18	108.08	32.16	361.75	8.06	800
34	n/a	529	31.9227087	-106.3975305	n/a	n/a	24.63	78.85	90.43	35.85	332.50	7.98	500
35	JL-4905-922	601	31.8983330	-106.3828330	2005-2010	700-931	24.63	78.85	90.43	35.85	328.00	7.98	500-800
	JL-4905-922	601	31.8983330	-106.3828330	n/a	n/a	24.63	78.85	90.43	35.85	332.50	7.98	800
36	n/a	FBT10	31.8942253	-106.3262368	n/a	n/a	n/a	n/a	n/a	n/a	1146.00	n/a	500-800
	n/a	FBT10	31.8942253	-106.3262368	n/a	n/a	n/a	n/a	n/a	n/a	1481.00	n/a	800-1000
37	n/a	FBT05	31.9407930	-106.2862043	n/a	n/a	n/a	n/a	n/a	n/a	1207.00	n/a	500
	n/a	FBT05	31.9407930	-106.2862043	n/a	n/a	n/a	n/a	n/a	n/a	1469.00	n/a	500-800
	n/a	FBT05	31.9407930	-106.2862043	n/a	n/a	n/a	n/a	n/a	n/a	1731.00	n/a	800-1000
38	n/a	FBT04	31.927807	-106.338157	n/a	n/a	n/a	n/a	n/a	n/a	3954.00	n/a	800-1000
39	n/a	MNST02	31.958452	-106.378051	n/a	n/a	n/a	n/a	n/a	n/a	953.00	n/a	500
	n/a	MNST02	31.958452	-106.378051	n/a	n/a	n/a	n/a	n/a	n/a	1311.00	n/a	500-800

	n/a	MNST02	31.958452	-106.378051	n/a	n/a	n/a	n/a	n/a	n/a	2127.00	n/a	800-1000
40	n/a	MNST03	31.966587	-106.390805	n/a	n/a	n/a	n/a	n/a	n/a	940.00	n/a	500
	n/a	MNST03	31.966587	-106.390805	n/a	n/a	n/a	n/a	n/a	n/a	986.00	n/a	500-800
	n/a	MNST03	31.966587	-106.390805	n/a	n/a	n/a	n/a	n/a	n/a	2340.00	n/a	800-1000
41	n/a	MNST06	31.995182	-106.385088	n/a	n/a	n/a	n/a	n/a	n/a	3905.00	n/a	500
	n/a	MNST06	31.995182	-106.385088	n/a	n/a	n/a	n/a	n/a	n/a	3412.00	n/a	500-800
	n/a	MNST06	31.995182	-106.385088	n/a	n/a	n/a	n/a	n/a	n/a	12078.00	n/a	800-1000
42	n/a	MNST05	31.942494	-106.368275	n/a	n/a	n/a	n/a	n/a	n/a	930.00	n/a	500
	n/a	MNST05	31.942494	-106.368275	n/a	n/a	n/a	n/a	n/a	n/a	875.00	n/a	500-800
	n/a	MNST05	31.942494	-106.368275	n/a	n/a	n/a	n/a	n/a	n/a	1219.00	n/a	800-1000
43	n/a	NH1	31.950801	-106.449208	n/a	n/a	n/a	n/a	n/a	n/a	2389.00	n/a	500-800
	n/a	NH1	31.950801	-106.449208	n/a	n/a	n/a	n/a	n/a	n/a	3174.00	n/a	800-1000
44	n/a	NH2	31.957727	-106.430704	n/a	n/a	n/a	n/a	n/a	n/a	5501.00	n/a	500-800
	n/a	NH2	31.957727	-106.430704	n/a	n/a	n/a	n/a	n/a	n/a	10562.00	n/a	800-1000

Note that the TDS values are separated in three depth ranges to see the vertical variation. These contour maps at three different depths are based on the TDS values obtained from different sampling interval or at one particular depth shown here as data provided by EPWU. In some cases, the sampling interval is divided into three depth ranges. The average data for these depth ranges are reported here.

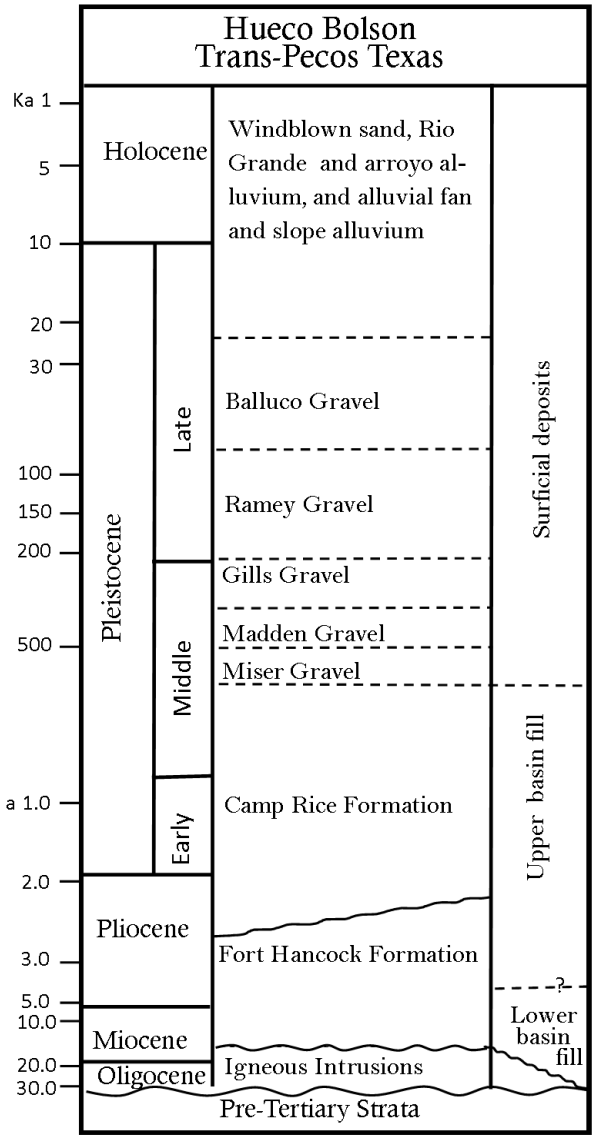

Figure S1 Hueco bolson stratigraphy (Modified after Collins and Raney, 2000)

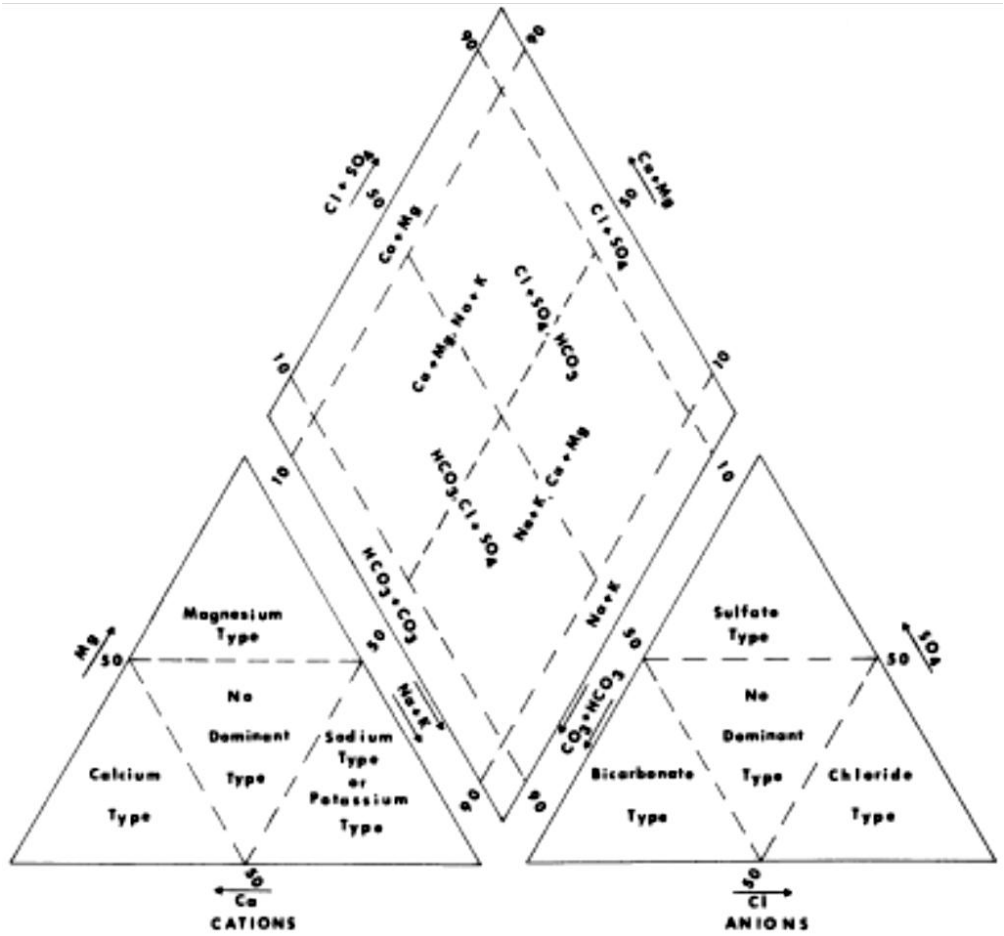

Figure S2: Hydrochemical facies of water analysis diagram, in percent of total equivalents per million. The diamond shaped upper part of Piper diagram is divided into six hydrochemical facies classes such as 1) Ca-HCO_3 type, 2) Na-Cl type, 3) Mixed Ca-Na-HCO_3 type, 4) Mixed Ca-Mg-Cl, 5) Ca-Cl type, and 6) Ca-Na-HCO_3 type

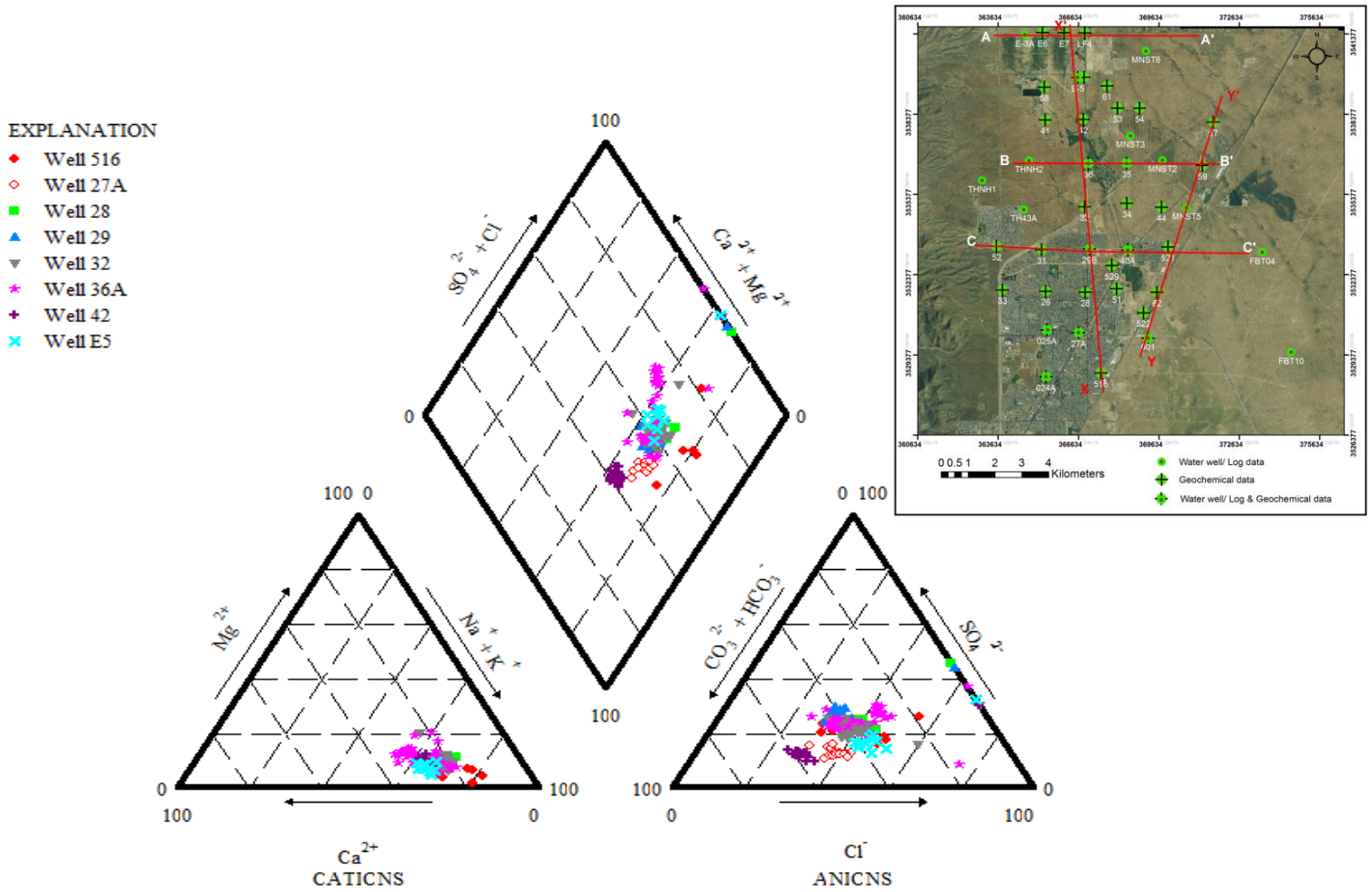

Figure S3 Piper diagram representation of hydrochemical data of wells that lie in the center of study area (XX' in inset figure)

Vita

Anita Thapalia is daughter of Bodha Raj Thapalia and Sita Thapalia born in Koshidekha, Kavre, Nepal. She is the first generation to obtain PhD degree in her family. Anita earned her Bachelor of Science degree in Geology in 2001 and Master of Science degree in Geology in 2005 from Tribhuvan University, Nepal. After graduation she started teaching in University and working as a geologist, and during those days she realized to pursue her dream of higher studies aboard. In 2007 she joined the Masters Program in Geology at UTEP. After obtaining her second MS degree in 2009, she started her doctorate degree.

She has published three papers and presented her research in several meetings. She has been the recipient of numerous scholarships including a Vernon and Joy Hunt, Frank B. Cotton Memorial, George A. Krutilek Memorial, American Association of Petroleum Geologists (AAPG) Southwest Section, and a West Texas Geological Society (WTGS) E Russell Lloyd. Moreover, she was the recipient of a Norman H. Foster Memorial AAPG Research Grant, Geological Society of America (GSA) research grant and an Elsevier Research Grant from International Association of Geochemistry.

While pursuing her degree, she worked as a Research Associate and Head Teaching Assistant for the Department of Geological Sciences as well as she is a proud mother. She has interned with ExxonMobil Exploration, BP America, Hess Corporation, and TRER Corporation. After graduation, she is planning to excel her geoscientist career with Encana Corporation, Denver, Colorado.

She participated in several extracurricular activities; Co-Chair of the 25th Annual Geological Sciences Colloquium, vice-president of AAPG, and secretary of Society of Exploration Geophysicists (SEG) UTEP chapter. In recognition of her outstanding contribution, she was awarded a Bruce Davidson Memorial Student Award in the Geology Department and an SEG/ExxonMobil Student Education Program Travel Grant. Her dissertation: *Geochemical studies of backfill aggregates, lake sediment cores and the Hueco Bolson Aquifer* were supervised by Dr. David Borrok and Dr. Diane Doser.

Permanent address: 78/31 Anmol Galli-33
Kathmandu, Nepal

This dissertation was typed by Anita Thapalia.